Università degli Studi di Ferrara

DOTTORATO DI RICERCA IN
SCIENZE DELL'INGEGNERIA

CICLO XXI

COORDINATORE Prof. Trillo Stefano

STUDY OF THE EFFECT OF THIN HARD COATINGS ON THE RESISTANCE OF HIGH STRENGTH-TO-MASS RATIO COMPONENTS

Settore Scientifico Disciplinare ING-IND/14

Dottorando
Dott. Tordini Federico

Tutore
Prof. Baragetti Sergio

Anni 2006/2008

Università degli Studi di Ferrara

DOTTORATO DI RICERCA IN
SCIENZE DELL'INGEGNERIA

CICLO XXI

COORDINATORE Prof. Trillo Stefano

STUDY OF THE EFFECT OF THIN HARD COATINGS ON THE RESISTANCE OF HIGH STRENGTH-TO-MASS RATIO COMPONENTS

Settore Scientifico Disciplinare ING-IND/14

Dottorando
Dott. Tordini Federico

Tutore
Prof. Baragetti Sergio

Anni 2006/2008

Acknowledgments

I wish to thank prof. Sergio Baragetti for his guidance and precious suggestions during these three years of doctoral research activity.

A particular thanks to my family for supporting me in every moment.

Many thanks to all my friends, of whom a special thanks goes to Michela and Rosalba.

Contents

1 Introduction and aim of the research activity

The rising need of lightening mechanical components by means of broader and broader use of light alloys is becoming crucial for the coming future. In the automotive and aerospace industries, for example, the request for more power with lower gas polluting emissions is expected to acquire more and more importance. The fatigue behaviour of light alloys, however, is often worse than the one of traditional construction steels. The wear resistance, surface hardness and load bearing capacity can represent weak points for the former materials too. As a result, suitable surface treatments – such as thin hard coating deposition – can be decisive for improving their properties and make such properties be at least similar to the ones shown by the steels. The effects induced on both steel and light alloy specimens or components by thin hard coating deposition had already been studied when the present doctoral research activity started, in 2006. Nevertheless, further research developments were necessary, especially with regard to the fatigue and contact/rolling contact fatigue behaviour of coated components. Therefore, the main goal of the present research activity was to widen, by means of suitable experimental, theoretical, numerical and statistical methods, the knowledge of the effects on the strength of components, with particular attention to light base materials, induced by thin hard coating deposition.

Thin hard coatings deposited by means of physical vapor deposition (PVD) and chemical vapor deposition (CVD) techniques (see chapter 2 for more details) are, for the time being, wide spread in an increasing number of technological applications. Starting from the consolidated field of cutting and machining tools, a few decades ago, many other fields such as oil, aerospace, transports, optics, electronics, chemistry and biomedical ones

have been showing remarkable interest in them. This broad use of thin hard coatings is mainly due to the improvements achieved in the tribological and corrosion behaviour of the coated components and has concurred to consolidate the deposition techniques and justify the growing interest of research studies. PVD- and CVD-deposited thin hard films constitute examples of surface deposition treatments in which the coating thickness is very often lower than 10 μm. Hence these surface deposits are usually referred to as "thin films". Recent research studies, both experimental and numerical, have also demonstrated that thin hard coatings can prove effective in increasing the fatigue resistance of mechanical components and machine elements. From this point of view, on account of the high temperatures reached during CVD deposition processes which may compromise the surface characteristics of the base material, PVD is preferable between the two families of coating deposition techniques. The application of such coatings gives rise to surface modifications in the substrate which are responsible for the improvement of the corrosion and wear resistance and the surface hardness. The increasing diffusion of the nanoindentation technique has concurred to characterize the mechanical properties of the thin hard coatings with better and better accuracy.

With regard to the fatigue resistance, in case of compressive residual stresses induced by the deposition process in correspondence of the surface layers of the base material, an increase of the fatigue limit, therefore of the number of load cycles until failure, is possible. By contrast, if such residual stresses were tensile a significant detrimental effect on the fatigue behaviour could be produced. It is also worth underlining that the fatigue behaviour is improved, even though in a less remarkable way than the one from surface residual compressive stresses, also by the good surface finishing guaranteed by the current deposition techniques, which are practically able to preserve the one of the substrate. Also, machining and surface treatments other than coating deposition, if any, represent further factors influencing the distribution of surface residual stresses which have hence to be accurately taken into account.

As previously stated, a number of research studies about the wear, corrosion and mechanical characterization of thin hard coatings are available in the literature [1.1-1.9]. A few studies have also shown that the fatigue resistance of mechanical components can be increased by some coatings [1.10-1.17]. As well known, fatigue is a localized phenomenon

which is strictly related to the stress level at the component surface. Therefore, the high surface compressive residual stresses induced in some cases by the coating deposition process may prove beneficial for preventing or retarding fatigue crack initiation, provided that the coating is uncracked and free from defects. In the literature, numerical models simulating the presence of surface coatings are available [1.18-1.21]. Nevertheless, most of the studies concerning the analysis of coated components are focused on the coating characterization and only a few on the crack simulation by means of numerical methods. As a result, further developments are required in the field of crack nucleation and growth simulation in thin hard-coated components in order to develop powerful and more and more reliable procedures for fatigue life prediction. Furthermore, proper models able to predict the number of cycles necessary for damage initiation in the presence of contact or rolling contact fatigue for coated components are even fewer in the literature. A thorough review of studies on the contact and rolling contact fatigue behaviour in presence of thin hard coatings was provided by Stewart et al. in [1.11]. References dealing with the prediction of the number of load cycles until fatigue damage initiation or with the crack growth simulation in mechanical components such as meshing gears are available in the literature [1.22, 1.23], but no enough efforts have been made to develop numerical or theoretical-numerical models to study the fatigue damage initiation in the presence of thin coatings.

Bearing the previous considerations in mind, it has been tried to go in depth through the fatigue and contact/rolling contact fatigue behaviour of thin hard-coated mechanical components. In the three years of doctoral research activity, experimental, numerical and statistical methods were used to study different bulk materials and coatings. Particular attention has been paid to those applications where increasing the fatigue limit of mechanical components can represent a decisive factor for performance elevation. For example, the opportunity of lightening mechanical components of endothermic motors for competition applications by means of effectively coated aluminium or titanium alloys has been carefully considered. Also, theoretical-numerical models enabling a designer to foresee the performance of a coated component under fatigue and contact/rolling contact fatigue conditions were applied and proposed with good results. These procedures enable reliable fatigue life prediction of thin hard-coated components and were applied, in particular, to gears. The coatings addressed to the experimental tests were deposited by

Lafer SpA and MOMA srl and, as regards the previsional models for PVD-coated gears, the research has been carried out in collaboration with DUCATI CORSE srl, which provided gears used in competitions and data. The work developed has also allowed to publish on international journals such as the *International Journal of Fatigue*, *Key Engineering Materials* and *Structural Durability & Health Monitoring* and present at international conferences such as the "International Conference on Fatigue Damage of Structural Materials", in 2006, and the "International Conference on Fracture and Damage Mechanics", in 2007 and 2008, and at the Imperial College of London in 2008. The presentations have collected remarkable interest from the audience, conference organizers and delegates.

The number of cycles necessary to achieve specified crack depths, until final failure, in coated and uncoated steel and titanium transmission spur gears was evaluated with one of the aforementioned previsional procedures. CrN and TiN coatings PVD-deposited on, respectively, steel and titanium base material were analyzed in this case and measurements of surface micro-hardness and residual stress fields were used in the theoretical-numerical calculations. As far as the fatigue tests on coated and uncoated specimens, several rotating bending experiments were carried out on both steel and light alloys [1.24-1.27]. Different PVD and CVD coatings were deposited and the fatigue behaviour of the coated base materials was compared with the one shown without coating. Thin SiO_x coating was deposited on both steel and aluminium alloy, WC/C and DLC on aluminium alloy and TiN on titanium alloy. SiO_x coatings, deposited with the PE-CVD (Plasma Enhanced-CVD) technique, are suitable for many base materials and are currently used in applications requiring a high resistance to scratches and corrosion or a barrier for gas permeation, at both high and low temperatures. PVD-deposited WC/C coatings usually show good adhesion and low friction coefficient and can be used for a number of different materials and structural applications. DLC films were deposited with the PA-CVD (Plasma Assisted-CVD) technique. Such films prove effective for their extremely low friction coefficient and high wear resistance. Up to now, the attention of researchers has been paid to the tribological and mechanical characterization of SiO_x, WC/C and DLC coatings but not on their influence on the fatigue behaviour of aluminium or steel substrates. As regards TiN, the fatigue behaviour of PVD-coated titanium alloy specimens was studied both

numerically and experimentally and the influence of the presence of both coating and a notch was also taken into account. The contact and rolling contact fatigue behaviour of coated components was investigated with experimental, numerical and statistical methods [1.28, 1.29]. CrN PVD-coated and uncoated case hardened automotive transmission spur gears were investigated by means of numerical models and experimental contact fatigue tests [1.28]. A suitable theoretical-numerical procedure able to predict the number of cycles necessary to promote initial fatigue damage at the contact area was developed and the results were compared with the experimental ones. Furthermore, this procedure was used to collect the data necessary to apply an advanced statistical method – namely Design and Analysis of Computer Experiments [1.30, 1.31] – to achieve the optimization of parameters, related to both coating and base material, influencing the fatigue and the rolling contact fatigue behaviour of coated components. The presence of the self-equilibrated residual stresses induced by the coating deposition process was accurately simulated in the numerical model.

References

[1.1] Merlo AM. The contribution of surface engineering to the product performance in the automotive industry. *Surf Coat Technol* 2003; 174-175:21-26.

[1.2] Vetter J, Barbezat G, Crummenauer J, Avissar J. Surface treatment selections for automotive applications. *Surf Coat Technol* 2005; 200:1962-1968.

[1.3] Mendibide C, Steyer P, Fontaine J, Goudeau P. Improvement of the tribological behaviour of PVD nanostratified TiN/CrN coatings – An explanation. *Surf Coat Technol* 2006; 201:4119-4124.

[1.4] Guu YH, Hocheng H. Improvement of fatigue life of electrical discharge machined AISI D2 tool steel by TiN coating. *Mater Sci Eng* 2001; A318:155-162.

[1.5] PalDey S, Deevi SC. Single layer and multilayer wear resistant coatings of (Ti,Al)N: a review. *Mater Sci Eng* 2003; A342:58-79.

[1.6] Pharr GM, Oliver WC. Measurement of Thin Film Mechanical Properties Using Nanoindentation. *MRS Bulletin* 1992; 17:28-33.

[1.7] Brotzen FR. Mechanical Testing of Thin Films. *Int Mater Reviews* 1994; 39(1):24-45.

[1.8] Sinnott SB, Colton RJ, White CT, Shenderova OA, Brenner DW, Harrison JA. Atomistic Simulations of the Nanometer-Scale Indentation of Amorphous Carbon Thin Films. *J Vac Sci Technol A* 1997, 15(3):936-940.

[1.9] Shojaei OR, Karimi A. Comparison of mechanical properties of TiN thin films using nanoindentation and bulge test. *Thin Solid Films* 1998; 332:202-208.

[1.10] Kim KR, Suh CM, Murakami RI, Chung CW. Effect of intrinsic properties of ceramic coatings on fatigue behavior of Cr-Mo-V steels. *Surf Coat Technol* 2003; 171:15-23.

[1.11] Stewart S, Ahmed R. Rolling contact fatigue of surface coatings - A review. *Wear* 2002; 235:1132-1144.

[1.12] Inoue K, Lyu S, Deng G, Kato M. Fracture mechanics based evaluation of the effect of the surface treatments on the strength of carburized gears. *Proc VDI Berichte* 1996; 1320:357-369.

[1.13] Baragetti S, La Vecchia GM, Terranova A. Fatigue behaviour and FEM modelling of thin-coated components. *Int J Fat* 2003; 25:1229-1238.

[1.14] Baragetti S, La Vecchia GM, Terranova A. Variables affecting the fatigue resistance of PVD-coated components. *Int J Fat* 2005; 27(10-12):1541-1550.

[1.15] Baragetti S, Fatigue resistance of steel and titanium PVD coated spur gears, *Int J Fat* 2007; 29:1893-1903.

[1.16] Baragetti S, La Vecchia GM, Terranova A. Analysis of fatigue crack propagation in nickel-plated components. *Int J Fat* 2001; 23:S395-S404.

[1.17] Su YL, Yao SH, Wei CS, Wu CT, Kao WH. Evaluation on wear, tension and fatigue behaviour of various PVD coated materials. *Materials Letters* 1998; 35:255-260.

[1.18] Moinereau D, Brochard J, Guichard D, Bhandari S, Sherry A, France C. Local approach of cleavage fracture applied to a vessel with subclad flaw. A benchmark on computational simulation. *ASME Publ PVP* 1996; 324:267-76.

[1.19] Smith RW. Computer simulation of intergranular stress corrosion cracking via hydrogen embrittlement. Modelling and simulation in materials science and engineering. *Mater Sci Eng* 2000; 8(4):629-648.

[1.20] Dejun M, Kewei X, Jiawen H. Numerical simulation for determining the mechanical properties of thin metal films using depth-sensing indentation technique. *Thin Solid Films* 1998; 323:183-187.

[1.21] Souza RM, Mustoe GGW, Moore JJ. Finite-element modeling of the stress and fracture during the indentation of hard elastic films on elastic-plastic aluminum substrates. *Thin Solid Films* 1999; 355-356:303-310.

[1.22] Šraml M, Flašker J. Computational approach to contact fatigue damage initiation analysis of gear teeth flanks. *Int J Adv Manuf Technol* 2007; 31:1066-1075.

[1.23] Glodež S, Aberšek B, Flašker J, Ren Z. Evaluation of the service life of gears in regard to surface pitting. *Engng Fract Mech* 2004; 71:429-438.

[1.24] Baragetti S, Tordini F. Fatigue Resistance of PECVD Coated Steel Alloy. *Int J Fat* 2007; 29:1832-1838.

[1.25] Baragetti S, Lusvarghi L, Bolelli G, Tordini F. Fatigue behaviour of a 2011-T6 aluminium alloy coated with PVD WC/C, CVD DLC and PECVD SiO_x coatings. Submitted to *Surf Coat Technol*.

[1.26] Baragetti S, Lusvarghi L, Pighetti Mantini F, Tordini F. Fatigue Behaviour of Notched PVD-coated Titanium Components. *Key Engineering Materials* 2007; 348-

349:313-316.

[1.27] Baragetti S, Tordini F. A Numerical Study of the Fatigue Behaviour of Notched PVD-coated Ti-6Al-4V. *Structural Durability & Health Monitoring* 2007; 3(3):165-176.

[1.28] Baragetti S, Terranova A, Tordini F. Contact Fatigue Behaviour of PVD-coated Spur Gears. *Key Engineering Materials* 2008; 385-387:57-60.

[1.29] Baragetti S, Tordini F. Variables affecting the fatigue and rolling contact fatigue resistance of PVD-coated spur gears. Submitted to *Int J Fat*.

[1.30] Condra LW. *Reliability Improvement with Design of Experiments*. New York: Marcel Dekker Inc.; 1993.

[1.31] Montgomery DC. *Design and Analysis of Experiments*, 4th ed. New York: John Wiley & Sons; 1997.

2 Thin hard coatings: deposition, applications and properties

The deposition of thin hard coatings makes it possible to apply ceramic layers (or multilayers) on substrate surfaces. Coating thicknesses of few microns are involved in this category, while thick films are intended to be at least tens of microns thick. The main benefits in using thin hard coatings versus thick hard coatings and soft coatings may be summarized in the following points:

- high hardness and wear resistance without affecting the dimensional tolerances of the coated components;
- suitability for coating small components;
- good wear protection of particular geometries (e.g. sharp edges);
- process capability to coat complex-shaped components.

PVD (Physical Vapor Deposition) and CVD (Chemical Vapor Deposition) are the two main families of techniques used to deposit a solid material from a gaseous phase to form suitable thin coatings on component surfaces. In a PVD process the material addressed to deposition (precursor) is vaporised in vacuum from a solid target and condensed onto the substrate to form the thin coating. CVD differs in that the precursors are deposited from the gaseous state and chemical reactions take place both in the gaseous phase and on the substrate surface. By means of such techniques it is possible to deposit thin hard coatings on a wide range of materials and for a number of applications, from the less sophisticated (e.g. decorative) to the most advanced ones (microelectronics, semi-conductor devices, optical, biomedical, etc.). The use of vacuum environment to perform the deposition shows

some important advantages such as the cleanness of the deposited layers, the low polluting impact, the low oxidation of the treated materials, an adequate free mean path of the vaporised materials to reach the substrate. Electron beam deposition, sputter deposition, cathodic arc deposition, pulsed laser deposition are some of the most popular PVD techniques. Conventional "thermal" CVD has variants such as PE-CVD (Plasma Enhanced-CVD) and PA-CVD (Plasma Assisted-CVD), which are, respectively, supported and activated by plasma. Some of the aforementioned deposition techniques will be detailed in the following.

2.1 Physical vapor deposition

PVD thin hard coatings are used in a very large number of different applications, e.g. medical implants, cutting tools, decorative fittings, competition racing parts, etc. Particularly, in the field of the machining tools PVD coatings are widely used to increase the life and productivity of tools, since coated tools can work faster showing less wear. Also, PVD coatings reduce the need for cutting fluids, hence enabling considerable cost reduction, since they can work dry or with very low amount of fluid. As far as the machine components are concerned, low friction coatings make it possible to reduce energy losses and the need for lubricant. Competition motor sport applications widely use hard, wear resistant and low friction PVD coatings to eliminate or limit the need for lubricant oil.

Table 2.1 Typical properties of some PVD coatings.

	TiN	CrN	TiCN	ZrN	AlTiN
Hardness, HV	2200-2500	1800-2200	3000-4000	2300	2400-3000
Thickness, μm	1-5	4-20	1-4	1-4	1-4
Max work. temp., °C	600	700	400	600	800
Friction coefficient	0.2-0.6	0.05-0.9	0.5	0.5	0.6
Coating structure	monolayer	monolayer	multilayer	monolayer	monolayer
Color	gold	silver	blue-gray	pale yellow	violet

PVD is now the most spread way to deposit thin hard coatings such as titanium nitride

(TiN), titanium carbonitride (TiCN), aluminum titanium nitride (AlTiN), chromium nitride (CrN), zirconium nitride (ZrN) and so on. It has been being used for few decades and was initially focused on the cutting tool and die industry. Dies and machining tools are usually made from special alloys to work under highly severe contact pressures and often at very high working temperatures at the contact area. The high surface hardness achieved with film deposition makes it possible to enhance wear resistance and hence to extend tool and die life. Such coatings can be applied on metallic components only, since the processes require conductive substrates. Also, the high temperatures (up to the order of 400°C) often involved in the deposition process may induce structural or chemical-physical modifications in the base material which thus has to be properly chosen. Nevertheless, the latest progresses made by the current technique enable to deposit new kinds of coatings at lower temperature (e.g. WC/C coatings). Table 2.1 collects the main properties of some of the most popular PVD coatings.

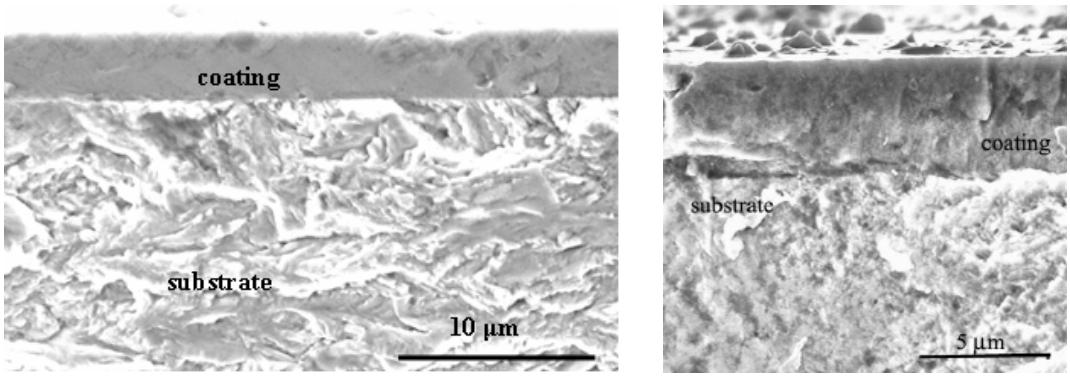

Figure 2.1 High magnifications of PVD coatings.

Predictably, as regards the wear resistance, such coatings can be deposited only on hard or hardened substrates, otherwise the substrate itself would collapse under concentrated pressure without giving the necessary support to the coating. Surface hardness measurements after deposition are carried out at an indentation depth of 0.05 mm, since the coatings have thicknesses in the order of microns. Figure 2.1 shows high magnifications of PVD coatings. Some of the most important applications of the PVD coatings are listed below:

- deposition of thin and thick single layer and multilayer coatings;

- deposition of graded-layer and multiphase coatings having different characteristics from the external surface to the film-substrate interface;
- enhancing wear and corrosion resistance of mass production automotive industry;
- Al-based anticorrosion coatings on fuel cells for aerospace applications;
- anticorrosion and decorative coatings for the automotive field;
- decorative coatings for mass production items (glasses, watches, etc.);
- biomedical applications (e.g. Ti-based films);
- low deposition temperature applications (e.g. DLC-based coatings for optics or mechanics);
- modification of reflection and transmission properties in optical applications;
- shape memory coatings (e.g. Ti-Ni-based ones).

It is worth underlining that the target workpiece with the growing coating is often subjected to intense ionic bombardment due to collisions among ions of the process gases. Such a bombardment proves effective in enhancing the coating properties: it removes not well adherent molecules from the substrate and compacts the coating giving rise to a defects- and pores-free film and preventing it from delaminating. In fact, the energetic ions allow the deposition of dense, hard films by supplying the sputtered neutrals with sufficient energy to find a suitable nucleation site on the substrate surface and inducing high compressive stresses. The combination of thermal stresses – arising from differences in thermal expansion coefficients between coating and substrate – and intrinsic stresses – resulting from the energy transferred by the ionic and the atomic flow during deposition – can generate high residual stresses in both coating and substrate surface layers [2.1-2.3]. Such stress distributions have clearly to be self-equilibrated. As already mentioned, having residual compressive stresses at the external surface can help to increase the fatigue resistance of the substrate and, due to the fact that PVD coatings has been observed to be more effective than CVD coatings from this point of view, more details will be provided about the former ones in the following.

2.1.1 PVD coating applications

The main industrial fields concerned about PVD thin hard coatings are optical, electronics, mechanics, chemistry, decorative, biomaterials. The most popular applications for these coatings will be discussed in the next paragraphs.

2.1.1.1 PVD in the cutting tool industry

The introduction of PVD coatings for cutting tools in the metal cutting industry took place about thirty years ago and since then their success has kept on increasing. The first PVD coating material which found commercial application on cutting tools was TiN in the early 1980s and, from then on, PVD coatings have been applied on most cutting tools, particularly in applications where having sharp edges – e.g. threading, grooving, end-milling, etc. – or a tough cutting edge – e.g. drilling – is fundamental. The TiAlN coating is currently the most widely deposited PVD coating for cutting tools but other coatings such as TiCN and CrN offer better solutions in certain applications.

The deposition of PVD coatings enables the coated cutting tools to work faster, hence allowing the production of more components in less time. As far as the wear damage is concerned, in the metal cutting different wear processes may take place depending on the workpiece material. PVD coatings are resistant to all forms of wear resulting in a considerable increase in the life of cutting tools. Also, many coatings allow to work in unlubricated condition, enabling companies to save money for cutting fluids, which cost them a considerable amount of their total production costs. As a matter of fact, the high speed cutting or dry machining involves extremely high working temperatures at the cutting edge and PVD coatings – e.g. TiAlN – have great thermal stability, hardness and oxidation resistance, hence enabling their use without or with a very limited amount of cutting fluid. Materials having very high hardness – e.g. 63 HRC – can be cut by means of PVD hard-coated tools. Coatings having hardness in the range 1000-4000 HV – i.e. approximately five times the hardness of the high speed steels – and very low friction coefficient can be deposited with PVD.

2.1.1.2 PVD in the automotive industry

Due to the current growing importance of the need of saving fuel consumption, the automotive industry is strongly concentrating on the reduction of weight and energy loss for friction. General mass production is affected by these problems, but motorsport competitions are particularly influenced by them. The use of suitably PVD-coated components as a solution has therefore gained popularity first in applications such as Formula 1 or motorcycle world championship. For instance, wear reduction for fork rods or other components of competition motorcycles (Figure 2.2) is achieved with PVD thin hard coating deposition using TiN or TiAlN, which enables a remarkable increase in the steel rod surface hardness.

Among the main sources of friction losses in internal combustion engines, the valve train system is responsible for a consistent amount of such losses, and piston liner assembly as well as engine bearings contribute too. For the time being, lots of components of valve trains are coated with low friction PVD coatings in order to reduce the energy losses. On top of the much lower friction offered by certain coatings with respect to the traditional oil lubrication, a higher wear resistance is guaranteed too. The traditional carbon steel or cast iron materials used for automotive components are expected to be more and more replaced with lighter materials such as aluminium, titanium or magnesium alloys. However, despite the good strength of these materials, their tribological performances are poor if compared to the ones of steels and they also tend to stick to the countersurface giving rise to excessive plastic deformation or abrasive and adhesive wear – hence increasing friction. The use of proper low friction PVD coatings can solve of these problems reducing wear and energy losses from friction for light alloys.

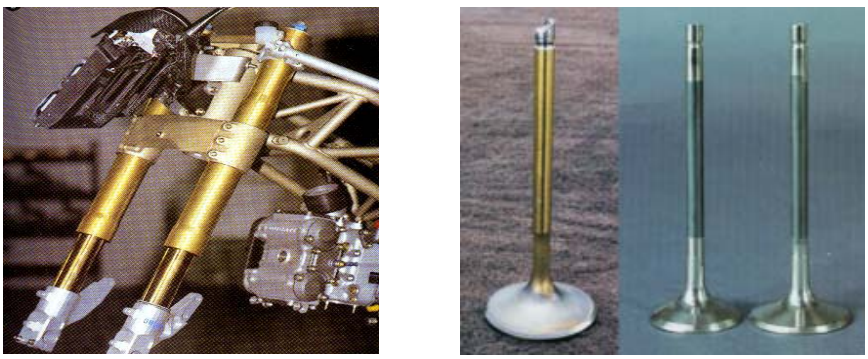

Figure 2.2 PVD hard-coated motorcycle components.

2.1.1.3 PVD in the decorative industry

The high quality and the long time duration of the surface finish obtained with some PVD coatings has attracted many manufacturers of the decorative industry in the last decade. A wide colour range is available by the deposition of PVD coatings and metals used as target materials are titanium, chromium, zirconium, niobium and titanium-aluminum alloys. The selected colour is obtained, regardless of the substrate, by tuning the deposition parameters and the composition of the deposited materials. Ceramic coatings PVD-deposited proves better than traditional electroplated coatings since they show higher hardness and wear resistance and good anti-corrosive properties, do not lose colour and are not affected by UV radiation. In case of deposition of very thin thicknesses, PVD coatings can not act as a corrosion barrier and therefore are applied upon a corrosion resistant layer such as a nickel or a nickel-chromium electroplated coating.

2.1.1.4 PVD for optical applications

Glass is widely used for optical applications, e.g. in architecture and in communication technologies. Nevertheless, it shows weakness, for instance, in its low reflectance of the room temperature radiation and high transmission of the solar radiation resulting in low thermal efficiency for buildings which increases the energy necessary for cooling buildings or in its excessive reflection which can not be allowed for optical lens applications. On account of these problems, PVD coating deposition on architectural and automotive glass, screens and lenses has been increasing continuously in recent times. Due to the reproducibility and uniformity over large areas required by such applications, magnetron sputtering (see in the following) is the mostly used technology for the time being. As regards spectacles and sun glasses, anti-reflection coatings are thoroughly applied and magnetron sputtering has gained most popularity even in this field as it enables the deposition of denser and more durable optical coatings than the ones from conventional electron beam evaporation process (see in the following).

2.1.2 PVD techniques

Among the PVD deposition techniques, in this section details about the wide spread electron beam, (magnetron) sputtering and cathodic arc evaporation processes will be provided. Magnetron sputtering represents the current technique displaying suitability for the majority of applications.

2.1.2.1 Sputtering deposition

A sputtering PVD process consists in film deposition by ejecting material from a solid target (source) onto a substrate. The removal of atomised material from the solid target (cathode) takes place by means of energetic bombardment of its surface with gaseous ions or neutral particles produced with electric discharges between the cathode and the anode (chamber). The collisions between the gas ions and the cathode generate the ejection of atoms and molecules. Such vapor particles then migrate towards the substrate and condense on it creating the coating. For the time being, the most spread sputter deposition technique is magnetron sputtering, which is very powerful and flexible and could be used to coat practically any component and a large range of materials, from metal alloys to compounds. Furthermore, it has enabled a considerable sputter rate enhancement, even though other techniques show higher performances from this point of view. Before the sputtering takes place, a vacuum of at least 10^{-7} atm is achieved in the process chamber so as to produce a reproducible coating having the needed coating composition. A strictly controlled flow of an inert gas is then introduced and gives rise to a pressure increase up to the minimum needed to work, namely in the range 10^{-5}-10^{-6} atm. Magnetron sputtering also enables the deposition of coatings following the exact surface roughness of the substrate material, hence it proves very effective for high precision applications.

Magnetrons are special devices having permanents magnets (Figure 2.3) which are used to generate strong electric and magnetic fields to trap electrons close to the surface of the target. When power is supplied to a magnetron, a negative voltage is applied to the target which attracts positive ions to its surface at high speed. If the energy transferred with a collision is enough – i.e. approximately equal to the heat of sublimation – target atoms can be sputtered. Voltages are in the order of thousands of volts using traditional cathodes,

while they are less than 1000 volts with magnetrons. The sputter process shows nearly no limitations in the choice of target materials, ranging from pure metals to semiconductors and isolators. In the presence of metals a DC power supply can be used, while semiconductors and isolators require a RF or pulsed DC power supply. The deposition process can be carried out in either non reactive (inert gas only) such as argon or reactive (inert and reactive gas) atmospheres and using single or multi-elemental targets. Besides atom sputtering, another important phenomenon is the emission of secondary electrons from the target surface. If a suitable magnetic field is used to trap such secondary electrons close to the target, the helical paths followed by them around the magnetic field lines improves the ionisation of the plasma near the target making it possible to get a higher sputter rate. The atoms sputtered have a neutral charge, thus they are unaffected by the magnetic trap.

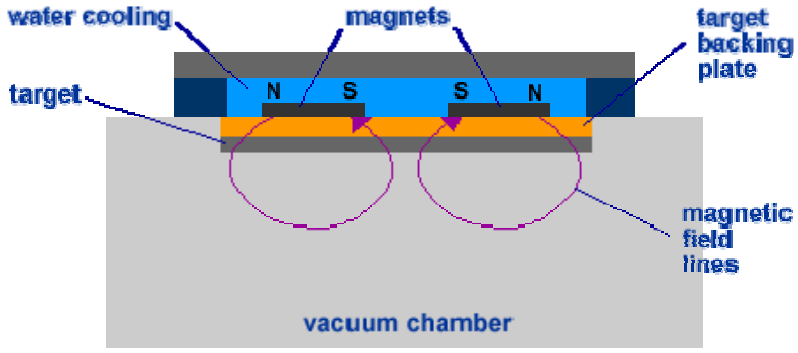

Figure 2.3 Schematic sketch of a magnetron cathode [2.4].

Typical sputtering deposition applications are in the semiconductor industry or the deposition of antireflection coatings on glass for optics. Important advantages of sputter deposition are that even the highest melting point materials are easily sputtered and that the deposited films have a composition close to that of the source material. The film adhesion guaranteed by sputtering is better than the one by evaporation techniques.

2.1.2.2 Electron beam deposition

In an electron beam PVD process, intense flows of electrons given off by charged tungsten filaments are used to vaporize a target material (anode) in high vacuum – in the

order of 10^{-5} mbar. The electrons provide the necessary energy by the conversion of their kinetic energy into thermal one at the bombarded surface of the target material. The surface temperature of the target increases resulting in a liquid melt formation, then target atoms evaporate under vacuum and precipitate into solid form to create the thin film on the substrate. The power of the electronic flow is adjusted so as to make the target achieve a temperature at which its vapor pressure is sufficient to maintain the necessary evaporation rate. Electronic flows are typically in the order of hundreds of mA with energy of a few keV. Suitable copper crucibles cooled with water circulation are adopted to hold the target. The material of the melting pot must not reach its evaporation temperature and the use of copper is therefore convenient for its good both thermal and electric conductivity.

To run the process, a filament is kept under a negative voltage of hundreds of kV and at a high temperature from the passage of an intense current. As a result, electrons are emitted from the filament and then addressed to the melting pot through suitable electromagnets. The current in the electromagnets is set to comply with the deflection of the electron flow needed to reach the target so as to prevent the filament degradation – resulting in non-uniform evaporation rate – from vaporised material deposition. The power of the electronic flow has to be kept continuously adjusted to maintain as much constant as possible the vaporization rate by monitoring the film growth rate during the whole process. The deposition rate in an electron beam process can vary from 1 nm to few micrometers per minute depending on the material to deposit. In presence of complex-shaped workpieces to coat, the substrates need to be properly moved during the deposition in order to let the flow of vaporised material reach all the surfaces – anyhow, inner surfaces cannot be coated by means of an electron beam process. A suitable manipulator shaft attached to the substrate holder translates and rotates to adjust the distance between the vapor source and the substrate and to obtain a uniformly deposited film. A negative voltage of hundreds of volts is applied to the substrate. Additional ion sources can also be used to bombard the substrate surface for etching and cleaning or controlling its microstructure and for sputtering the target material. Furthermore, such ion beams can be used to bombard the coated surface modifying the film microstructure and changing possible residual tensile stresses into compressive ones. The very high deposition rate makes this process be convenient for depositing wear resistant and thermal barrier coatings for the aerospace industry, hard

coatings for machining tools and optical films for semiconductor applications.

2.1.2.3 Cathodic arc deposition

Cathodic arc PVD deposition is extensively and typically adopted to deposit extremely hard films on the surface of cutting tools. A broad range of thin hard coatings – e.g. TiN, TiAlN, CrN – can be applied by means of this technique. An arc PVD process begins with an electric discharge of a high current between a cathode (the vapor source) and an anode (the walls of the process vacuum chamber) resulting in a small area, called "cathode spot", of few square microns emanating a high amount of energy – i.e. millions of amperes per square millimetre. The extremely high local temperature achieved in this area – thousands of Celsius degrees – gives rise to a high speed plasma flow of vaporised and highly ionized material from the cathode. As a result, a crater on the cathode surface is left behind such a flow. Due to the intense flows of ions that can be obtained, the PVD arc technique has one of the highest deposition rates among the ones available on the market. Also, the cathode spot tends to rapidly self-extinguish and move in a new area close to the previous one, enabling a good use and uniform erosion of the cathode material.

By controlled introduction of a reactive gas during this evaporation process, ionization and excitation can take place from the interaction with the flow of ions and a suitable compound is deposited on a substrate kept under negative voltage to accelerate positive ions so as to generate an intense ion bombardment onto it. In this way, this deposition technique is also one of the less sensitive to the target workpiece geometry. On top of charged ions, the plasma flow contains also neutral particles and larger clusters of atoms and molecules (droplets). A proper magnetic field is applied to uniformly move the cathode spot preventing it from staying at the same evaporative point for too long and hence ejecting a too large amount of droplets – detrimental to the quality of the deposited coating. TiN deposition on mechanical components is a typical example of application of PVD arc process.

2.1.3 PVD thin hard coatings

PVD thin hard coatings are typically made of ceramic materials such as carbides, nitrides, borides or silicides. Because of their high hardness, they are particularly suitable for applications in which wear resistant properties are needed. Single metal nitrides – e.g. TiN, CrN – were first developed for cutting applications due to the higher hardness than the one of high speed steel or cemented carbide, and, for the time being, they are still the best solution for many applications. With regard to high temperature applications such as high speed machining, their thermal resistance may be insufficient. Improvements have then been studied in recent times to increase the coating temperature resistance. For instance, by introducing suitable elements – e.g. Al into the TiN lattice to form TiAlN – an improvement in the oxidation resistance has been achieved. Further improvement has been from the development of multilayers and superlattices, which are deposited by alternating two different components to form layered films on the substrate surface, whereas PVD nanocomposite coatings constitute the most recent research result. Some details of some important PVD hard coatings are provided below.

2.1.3.1 TiN

TiN is still the most popular PVD hard coating and was the first to be used with success in industrial applications. Its typical gold colour made this ceramic coating attractive even for decorative purposes. As the deposition temperature is below 500°C, the first application was for coating high speed steel tools – in fact, 500°C is the temperature at which such a material starts to soften. In the middle 1980s TiN PVD-coated cemented carbide cutting tool inserts were first introduced for milling applications. The high resistance to wear enables the use of TiN hard films in a large number of applications. Moreover, its low friction coefficient helps cutting operations: chip flow is easier, building up of workpiece material at the tool edge is prevented and cutting forces and tool temperature are reduced. TiN coating is therefore used for machining tools, dies, moulds, punches, and a wide range of metal stamping and forming tools. As previously stated, due to its colour such a coating can replace gold plating on decorative components.

2.1.3.2 TiAlN

TiAlN coating has replaced TiN in lots of applications so far, as it often offers better performances. The colour of the coating can range from black to bronze depending on the Ti-to-Al ratio. In fact, as regards machining applications, the formation of aluminium oxide – from the addition of aluminium to TiN – on the surface of the coated tool results in an increase of the maximum working temperature of the coating up to 800°C. Aluminium oxide forms for the heating in air during service and protects the coating from further oxidation resulting in better hot hardness than most other coatings. In recent times, the addition of vanadium or chromium and yttrium has even increased the maximum working temperature up to more than 900°C. TiAlN coating is suitable for dry machining or cutting operations at high temperature with minimum use of lubricant. Analogously, TiAlN is also suitable to protect dies and moulds operating at high temperatures – e.g. those used in hot forging and extrusion industries.

2.1.3.3 TiCN

TiCN coating is harder and has a lower friction coefficient than TiN does but it is suitable only for certain cutting, punching or wear applications, where moderate temperatures are generated during service. TiCN colour ranges from pink to blue-grey depending on the Ti-to-C ratio. Good diffusion has been achieved by this coating in applications requiring the deposition on end mills, hobs, taps, reamers, drills, carbide inserts.

2.1.3.4 CrN

CrN shows high hardness, good oxidation resistance and low friction coefficient and it is very effective for applications such as metal and plastic forming. Its corrosion resistant and toughness are greater than TiN and the possibility of replacing electroplated hard chromium coatings with less environmentally harmful PVD CrN deposits constitutes another strong point. The colour of CrN coating is similar to silver.

2.2 Chemical vapor deposition

Chemical vapor deposition allows to deposit thin solid layers having high purity and showing remarkable performances. The semiconductor industry is one of the most involved application fields for these thin film deposition techniques. In a CVD process the substrate is exposed to one or more volatile precursors, which react and/or decompose on its surface to form the desired layer. In case gaseous by-products are produced during the process, they are removed by the passage of a gas flow through the reaction chamber. The applications concerned in CVD coatings are different from the ones cited for PVD, for example those ones making broad use of micro-fabrication processes. In this case, films are deposited in various forms, including mono- and poly-crystalline and amorphous. Typical coating materials are silicon, carbon fibers, silicon dioxide, silicon nitride or oxynitride, silicon-germanium, silicon carbide, tungsten, titanium nitride. CVD is also used to produce synthetic diamonds or very hard diamond-like coatings such as DLC (Diamond Like Carbon).

2.2.1 CVD: generalities

Generally speaking, the way CVD processes take place is that precursor gases, which are often diluted in carrier gases, are introduced into the reaction chamber at about room temperature and, once they come into contact with heated substrate, they will react and/or decompose giving rise to a solid deposit onto its surface. Furthermore, the substrate temperature is a critical parameter and has a great influence on what reactions are expected to occur. CVD makes it possible to deposit fine grained coatings having high purity and greater hardness than the one of similar hard ceramic materials produced with conventional fabrication techniques. Nearly any metallic or ceramic compound may be deposited by means of CVD techniques, including metals and metal alloys, intermetallic compounds, nitrides, carbides, oxides, borides. The deposition rate is usually low – in the range of a few hundred microns per hour – and coating thicknesses are in the order of a few microns.

A typical CVD apparatus consists of a number of basic elements. A gas delivery system is needed for delivering precursor gases into the reactor chamber, which is the place

where deposition actually takes place, whereas a suitable energy source is necessary to make the precursors react and/or decompose. The required heating for CVD processes can be obtained with energy sources such as resistive (e.g. tube furnaces), radiant (e.g. halogen lamps), radio frequency (e.g. induction heating) ones and also with lasers. As coating materials are deposited starting from the gaseous phase, precursors have necessarily to be volatile and, at the same time, stable enough to enable their delivery to the reactor. Precursor compounds may provide the deposited material with a single element or even more than one, hence simplifying the delivery system, as the number of the reactants required would be reduced. There is a number of categories of precursor gases and details about them are available in the literature [2.5]. A suitable system for introducing and removing substrates and a process control equipment, including alarms and safety devices, for monitoring process parameters such as pressure, temperature and time are always present. The required vacuum level is achieved by means of a vacuum system able to remove all the gases other than the process ones. Exhaust and exhaust treatment systems are used, respectively, to remove volatile by-products from the reaction chamber and, in case exhaust gases cannot be released into the atmosphere, to properly treat or convert such harmful gases into harmless compounds. In fact, gaseous CVD by-products may be toxic, flammable or corrosive and therefore must be treated carefully and with proper procedures.

2.2.2 CVD techniques

Several options of CVD deposition technique are available on the market and a number of research studies has been keeping on developing the various issues concerning these processes. Some of the main CVD processes – more details are reported, for instance, in [2.5] – available on the market are listed below:

- Low Pressure CVD (LP-CVD) and Ultrahigh Vacuum CVD (UHV-CVD): by using low pressures, film uniformity may be improved from the reduction of unwanted gas-phase reactions;
- Aerosol Assisted CVD (AA-CVD): the precursors are delivered to the substrate by means of a liquid or gaseous aerosol;

- Direct Liquid Injection CVD (DLI-CVD): the precursors are in liquid form, or solid dissolved in a suitable solvent, and are injected in the vacuum chamber through injectors; high growth rates can be achieved with this technique;
- Plasma Assisted CVD (PA-CVD) and Plasma Enhanced CVD (PE-CVD): such techniques utilize plasma to activate and enhance, respectively, the precursor chemical reaction rates; PE-CVD enables low deposition temperatures (see also the following chapter) and this is very important for semiconductor manufacturing;
- Atomic Layer CVD (AL-CVD): successive layers of different materials can be deposited to obtain multilayer crystalline films;
- Hot Wire CVD (HW-CVD): gaseous precursors are chemically decomposed with a hot filament;
- Metal-organic CVD (MO-CVD): metal-organic precursors are employed;
- Rapid Thermal CVD (RT-CVD): heating lamps or other methods are used to rapidly heat the substrate without heating the gas or the chamber walls in order to reduce certain gas phase reactions giving rise to particle formation.

2.2.3 CVD applications

Thin coatings CVD-deposited find application in a wide range of industrial fields. Applications requiring high resistance to wear, erosion, corrosion, high temperatures have achieved good results using these deposits. Semiconductors, integrated circuits and sensors or optical fibres for telecommunications constitute other important applications for CVD coatings. As regards composites, ceramic matrix composites such as carbon-carbon, carbon-silicon carbide and silicon carbide-silicon carbide may be produced and in this case CVD is also called CVI (Chemical Vapor Infiltration). Also, thin walled dense structural parts, hard to produce with conventional fabrication techniques, may be produced using CVD process. Further applications are the production of powders and fibres and in the field of catalysts and of nanotechnologies.

References

[2.1] Pauleau Y. Generation and evolution of residual stresses in physical vapour-deposited thin films. *Vacuum* 2001; 61:175-181.

[2.2] Knuyt G., Lauwerens W., Stals L.M. A unified theoretical model for tensile and compressive residual film stress. *Thin Solid Films* 2000; 370:232-237.

[2.3] Bemporad E., Sebastiani M., De Felicis D., Carassiti F., Valle R., Casadei F. Production and characterization of duplex coatings (HVOF and PVD) on Ti-6Al-4V substrate. *Thin Solid Films* 2006; 515:186-194.

[2.4] www.pvd-coatings.co.uk.

[2.5] *Manuale di trattamenti e finiture*. Milano: Tecniche Nuove; 2003.

3 Experimental tests

In this chapter the results collected through experimental fatigue and contact fatigue tests carried out on both specimens and components are reported and commented. Standard specimens made of steel, aluminium and titanium alloys were tested under rotating bending, while case hardened steel alloy transmission spur gears under contact fatigue. The tests were performed on both coated and uncoated samples and components to evaluate and characterize any possible variation induced by the presence of the coatings. The tests allowed the evaluation of the performance of each coating with respect to the specific substrate on which it was deposited.

3.1 Fatigue tests on SiO_x-coated and uncoated 39NiCrMo3 steel alloy

As reported in the previous chapters, PVD and CVD techniques have been used for a long time in industry. It was also said that thin hard coatings can improve the tribological and corrosion-resistant properties of the substrate [3.1-3.3] and that the compressive residual stresses which may arise in the surface layers from some deposition processes can increase, especially in case of PVD, the fatigue limit of the coated components [3.4-3.12]. Thin hard coatings are widely used in the aeronautical and automotive industries [3.13, 3.14], and for cutting tools and dies [3.15].

A few references dealing with the benefits of PVD coatings on the fatigue behaviour of

coated components are available in the literature [3.4, 3.7-3.10]. However, no significant studies have been made on SiO_x thin coatings deposited by means of the Plasma Enhanced CVD (PE-CVD) technique for fatigue applications. For the time being, thin film deposition by means of this technique constitutes one of the most popular industrial applications of plasmas. A PE-CVD deposition process utilizes cold plasma, which is obtained at extremely low pressures – i.e. ranging from a few hundred to ten thousand times lower than ambient pressure – and at low temperatures – a few tens of Celsius degrees. Therefore, PE-CVD allows to coat a broad range of different materials preventing them from thermal degradation. SiO_x coatings are particularly suitable for applications requiring high resistance to scratches and corrosion or a barrier against gas permeation, at both high and low temperatures. PE-CVD coatings are very dense and thin, hence enabling the reduction of the process time, as with a compact film there is no need of a thick layer for corrosion resistance [3.16-3.19], and guaranteeing good film elasticity.

There had not been any evidence, until this study, that PE-CVD SiO_x thin coatings could not be used on steels addressed to applications involving significant fatigue loads. Bearing this in mind, it was decided to evaluate if the coating deposition could determine the same or a higher fatigue limit than the one of the uncoated material with, furthermore, the benefit of a good scratch and corrosion resistance [3.16-3.19]. Contact fatigue was not taken into account in this case. Standard hourglass-shaped specimens were then machined from quenched and tempered 39NiCrMo3 steel alloy and both coated and uncoated series of such specimens were tested under rotating bending. Cleaning operations were carried out on the surface of the specimens to remove contaminants like dusts, grease and oxides before coating deposition so as to guarantee uniformity and good adhesion of the film. In fact, physical and mechanical discontinuities make the coating-substrate interface an extremely critical area and, as a result, if the surface is not prepared properly, the coating may delaminate with cracks. Some technological parameters of the deposition process used to coat a series of specimens are listed in Table 3.1.

The tests performed allowed to calculate the fatigue limit for the coated and the uncoated samples by analyzing the data collected with a suitable statistical method – i.e. Stair-case [3.20]. The experimental results did not evidence any improvement in the fatigue behaviour but, however, they were evaluated rather encouraging for further possible

developments. The fracture surfaces of the specimens were examined using an SEM to point out possible differences in the mechanisms of fatigue damage and propagation between the coated and the uncoated samples. Scratch tests were also performed on coated plane samples to evaluate SiO_x adhesion to the steel substrate.

Table 3.1 Parameters of the PE-CVD SiO_x deposition process used to coat the specimens [3.21].

Polymeric product deposited	SiO_x
Plasma generation frequency	13.56 MHz (radiofrequency)
Reagents	O_2 + HMDSO (hexamethyldisiloxane)
Thickness deposited (estimation)	≤ 1 μm
Deposition temperature	room

The results of this study were published on the *International Journal of Fatigue*, Vol. 29, in 2007 [3.21] and presented at the "International Conference on Fatigue Damage of Structural Materials VI", Sheraton Hyannis Resort, Hyannis, Massachusetts, USA, 17-22 September 2006.

3.1.1 The rotating bending test machine

The rotating bending tests were carried out with the computer-controlled testing machine (Italsigma X2TM412, Forlì, Italy) shown in Figure 3.1. A worm gear screwjack enables the application of the bending moment and while tests are running the load is constantly kept under control by means of a load cell. A feedback control system with automatic correction of the applied bending moment is also available and allows real time test monitoring and automatic test suspension in case of significant variation in the applied bending moment value. A computer equipped with a data acquisition card with a serial communication port and a suitable electric control panel enables one to control the machine by monitoring all the test parameters during each test. In Figure 3.2 a sketch of the test machine with the indication of its main components is depicted. Two mandrel holder supports (2, 3) are mounted on a rigid steel platform (1) and are connected to the corresponding mandrels (4, 5) with two journals having the axes of rotation perpendicular

to the longitudinal-vertical plane. The autoalignment of the specimen (6) during the assembly is guaranteed with this arrangement. A 200-watts brushless motor (11) transmits the main rotary motion to one of the two mandrels (4) which then drives the specimen as well as the other mandrel. Two coaxial collets (12) allow to hold specimens having circular cross section. The rotation of the mandrels around the journals enables the specimen to be subjected to a uniform bending moment over its whole length. A worm gear screwjack (10) is used to impose and adjust the value of the bending moment to apply during a test and is controlled by a load cell (9). Moreover, specimens with gage lengths ranging from 30 to 90 mm can be tested by changing the position of the slide (7) and therefore translating the corresponding driven mandrel (5). Two levers (8) constitute the blocking system of the slide at the base of the support (3) of the driven mandrel.

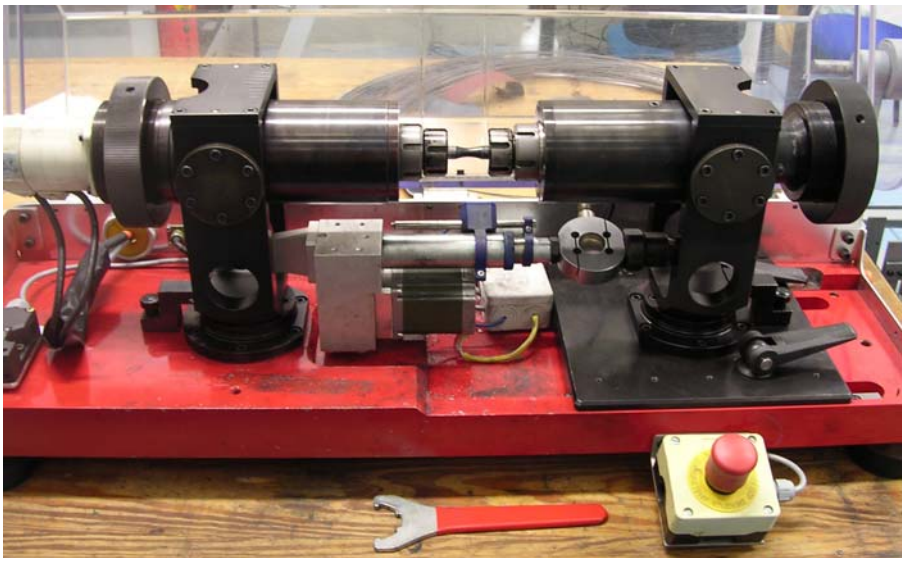

Figure 3.1 Rotating bending test machine.

A maximum bending moment of 75 Nm and a maximum speed of rotation of 3000 rpm can be applied with the test machine. The applied bending moment is recorded with the data acquisition system at each time interval through the load cell. In case of variations beyond a set threshold occur, the control software will immediately stop the test. Also, the bending moment can be kept at the preset value with very low oscillations by means of the automatic load correction. Periodic strain gage tests showed a very low (0.2%) average error for the preset bending moment with respect to the value given by the load cell

feedback.

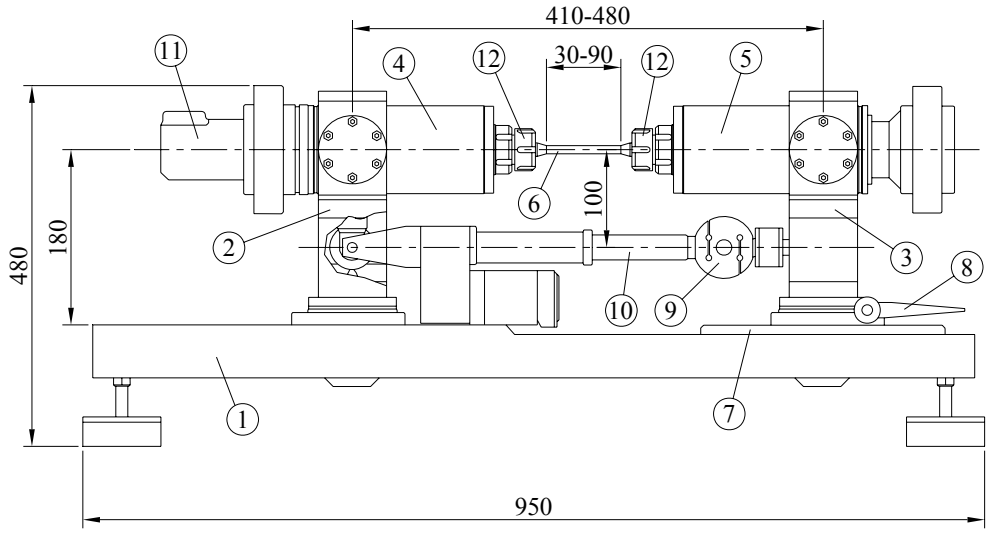

Figure 3.2 Rotating bending test machine: sketch showing the fundamental components [3.21].

3.1.2 Base material characterization

The chemical composition and the microstructure of the steel alloy used as base material were analyzed and the mechanical properties were determined prior to the fatigue tests. Tensile tests were executed on standard cylindrical specimens according to UNI EN 10002-1 standard and ultimate and yield strength values of, respectively, 1050 and 910 MPa resulted. The measured Vickers hardness average value – i.e. 322 HV_5 – was in good agreement with these material resistance data and, furthermore, similar hardness values were observed at the core and on the surface. Therefore, the absence of any previous surface treatment on the steel alloy under examination was pointed out. Metallographic analyses using nital (96% ethyl alcohol and 4% HNO_3) etching solution on polished specimens allowed to observe a tempered martensitic microstructure, with very fine grains and a high level of carbides (Figure 3.3), resulting from the quenching and tempering process which the material was subjected to. The steel alloy chemical composition (wt%) determined with a wet-chemical analysis according to ASTM E350-95 standard was: 0.395 C, 0.700 Mn, 0.240 Si, 0.018 P, 0.031 S, 0.740 Cr, 0.880 Ni, 0.190 Mo and Fe bal. This

composition confirmed that the material was a quenched and tempered 39NiCrMo3 steel alloy (UNI EN 10083-1:1993).

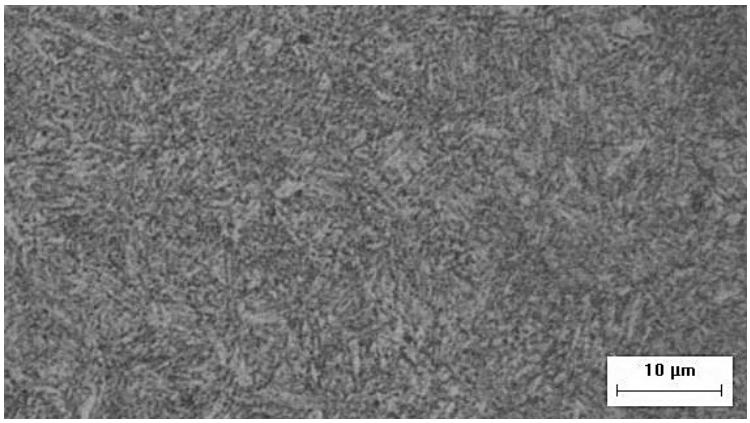

Figure 3.3 Optical microstructure of the quenched and tempered 39NiCrMo3 steel alloy [3.21].

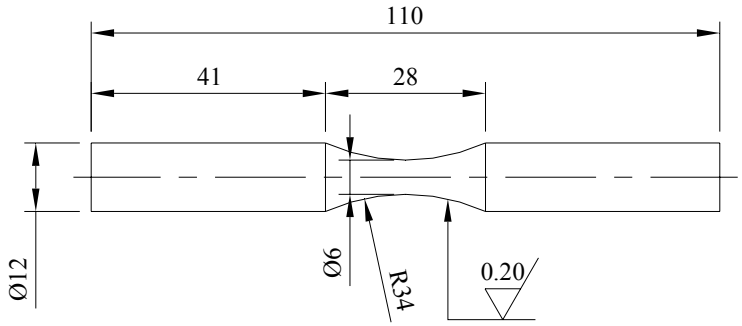

Figure 3.4 Dimensions of the specimens used in the fatigue tests [3.21].

3.1.3 Fatigue tests

Rotating bending tests (R = -1) were carried out following the procedures prescribed by applicable standards (UNI 3964 and ISO 1143). Standard hourglass-shaped specimens – characterised by a wide fillet radius and smooth surface finishing in the gage length – were machined according to ISO 1143 standard. Figure 3.4 shows the specimen dimensions. Accurate polishing allowed to keep the average surface roughness below the value of 0.25 µm and the final operations were performed lengthwise leaving no scratches along the circumferential direction to prevent or limit the presence of possible micro-notches lying on the most critical – with respect to the way the load was applied – plane. The average

roughness value was about 0.20 μm.

Load ranges of 400-560 MPa and of 480-560 MPa were used for the uncoated and the coated specimens, respectively. The upper limit for the fatigue life was set at 10 million load cycles and the pitch selected for the load variation was 40 MPa. The tests were performed at 2000 rpm, which falls within the limits prescribed by the applicable standards. The Stair-case method [3.20] was used as statistical analysis procedure to calculate the average value of the fatigue limit for each series of samples, in terms of level of imposed bending stress withstood at the aforesaid reference number of load cycles. Such a method guarantees a reliability of 50%. Even though each test should be repeated with at least 15 specimens, due to the smaller number of available samples and to the regularity shown by the trend of the numerical data resulting from the tests a reduced Stair-case method [3.20] was applied. Tables 3.2 and 3.3 collect each experimental observation for the uncoated and the coated specimens, respectively.

Table 3.2 Fatigue test results for the uncoated 39NiCrMo3 specimens [3.21].

Test no.	Bending stress, MPa	Cycles to failure
1	400	$> 10^7$
2	440	$> 10^7$
3	480	$> 10^7$
4	520	$> 10^7$
5	560	875000
6	520	$> 10^7$
7	560	1194000
8	520	$> 10^7$
9	560	676000
10	520	$> 10^7$
11	560	526000

Based on the experimental data, an average fatigue limit of 538 MPa with a standard error of 21 MPa was calculated for the uncoated specimens, whereas 503 MPa and 23 MPa were the same parameters for the coated ones. Figure 3.5 also shows the tests results and approximated S-N curves for the two series of samples. The data evidenced a limited difference between the coated and the uncoated specimens – i.e. less than 10% between the

average values of the fatigue limit. Hence the fatigue behaviour was not significantly affected by the presence of the chosen PE-CVD SiO_x coating.

Table 3.3 Fatigue test results for the coated 39NiCrMo3 specimens [3.21].

Test no.	Bending stress, MPa	Cycles to failure
1	560	$< 10^7$ (*)
2	520	227000
3	480	10^7
4	520	269000
5	480	10^7
6	520	319000
7	480	10^7
8	520	286000

(*) Not recorded value, in any case lower than 10^7 cycles

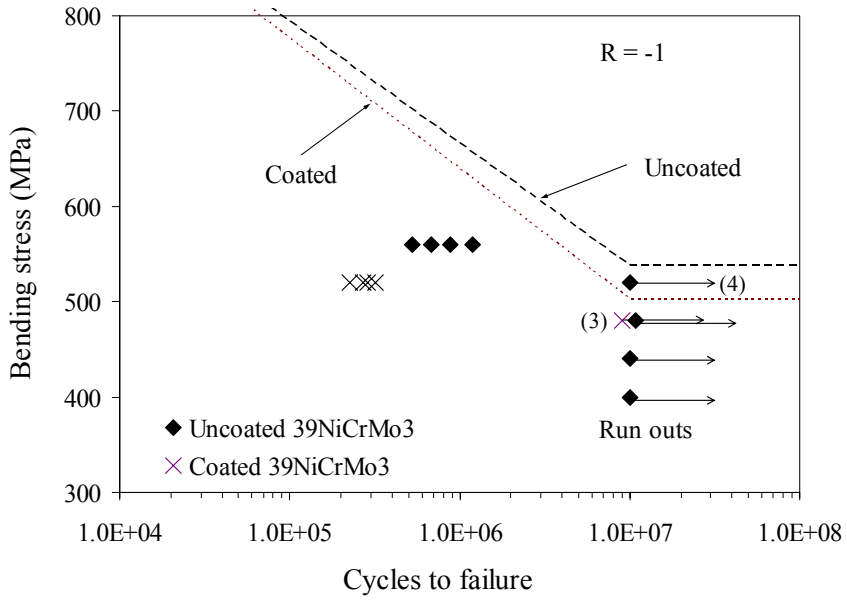

Figure 3.5 Bending stress vs. Cycles to failure for the coated and the uncoated 39NiCrMo3 specimens [3.21].

3.1.4 Laboratory analyses and discussion

Scratch tests were executed with a Rockwell indenter (Micro-Combi Tester, CSM Instruments, Peseux, Switzerland) on suitable coated flat samples in order to test the

adhesion of the coating to the substrate steel alloy. A Rockwell indenter having a radius of 0.8 mm was first used to test coated samples applying incremental loads from 0.1 to 10 N and, subsequently, from 0.1 to 20 N and no damage was observed in both cases. The tests were then repeated with an indenter radius of 0.2 mm and failure of the coating occurred for both load ranges. Figure 3.6 shows two traces made with the 0.2-mm indenter. Some elasticity and rather uniform behaviour of the SiO_x coating were observed during the tests and the adhesion to the substrate was assessed to be reasonable with first and complete delamination loads up to 4.4 and 7.3 N (Table 3.4).

Table 3.4 Results of the scratch tests using a Rockwell indenter having a radius of 0.2 mm [3.21].

Incremental load, N		I test	II test
0.1-10	First delamination, N	3.0	4.2
	Complete delamination, N	5.5	7.3
0.1-20	First delamination, N	4.4	4.0
	Complete delamination, N	5.0	5.2

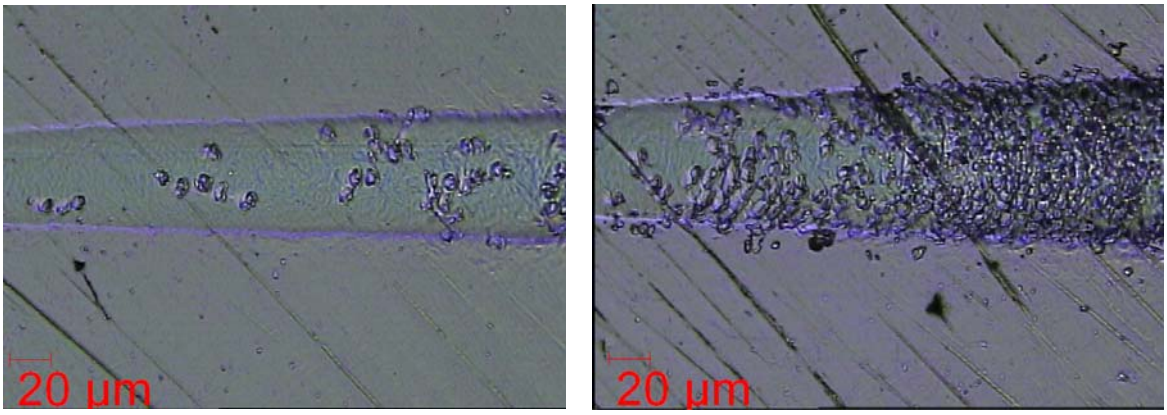

(a) **(b)**

Figure 3.6 Scratch test traces on coated samples (indenter radius 0.2 mm, load 0.1-10 N): (a) first and (b) complete delamination [3.21].

All the fracture surfaces of the specimens led to failure throughout the fatigue tests were observed under scanning electron microscope. Attention was paid to the assessment of the possible differences between the fatigue crack propagation mechanisms of the coated and the uncoated specimens, verifying whether the PE-CVD coating had affected the crack initiation phase. Figure 3.7 shows an overview and a detail of the fracture surface of one of

the uncoated specimens, on which the classic stable crack propagation area, as fatigue cycles repeat, and the overload final failure one are visible on the left and on the right side, respectively. In the specific case of the specimen shown in Figure 3.7, the coalescence of two cracks was also observed. Their initiations were located in the areas marked with the letters A and C and, by propagating, a "step" was generated in B because of the offset between the two crack planes.

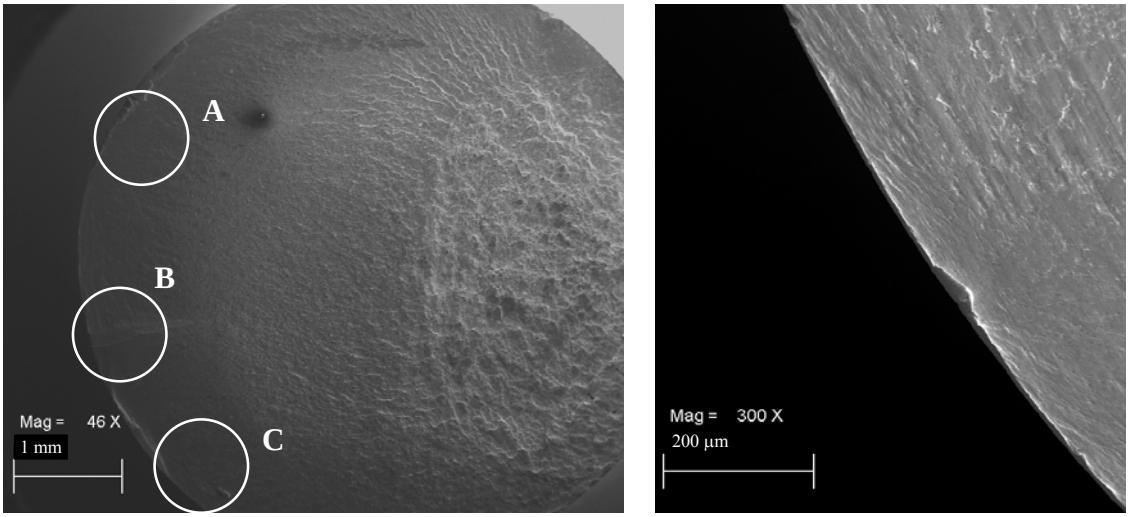

Figure 3.7 (a) Fracture surface overview of an uncoated specimen and (b) higher magnification of C [3.21].

By observing the fracture surfaces of the coated specimens, it was noted that both crack nucleation and propagation were comparable with the ones of the uncoated specimens, suggesting that the presence of the thin coating had not significantly affected the fatigue behaviour of the base material. The fracture surface of one of the coated specimens is shown in Figure 3.8, with the direction of crack propagation indicated by the arrow depicted. The depths – more than 10 μm – of the surface defects from which fatigue cracks initiated were deeper than the coating thickness – namely less than 1 μm. Therefore, eventual defects present in the coating did not affect crack initiation and one of the reasons for the similar behaviour between the coated and the uncoated specimens could be due to this fact. From SEM observations, both the initiation points and the propagation phase of the coated and the uncoated samples were considered to be superimposable.

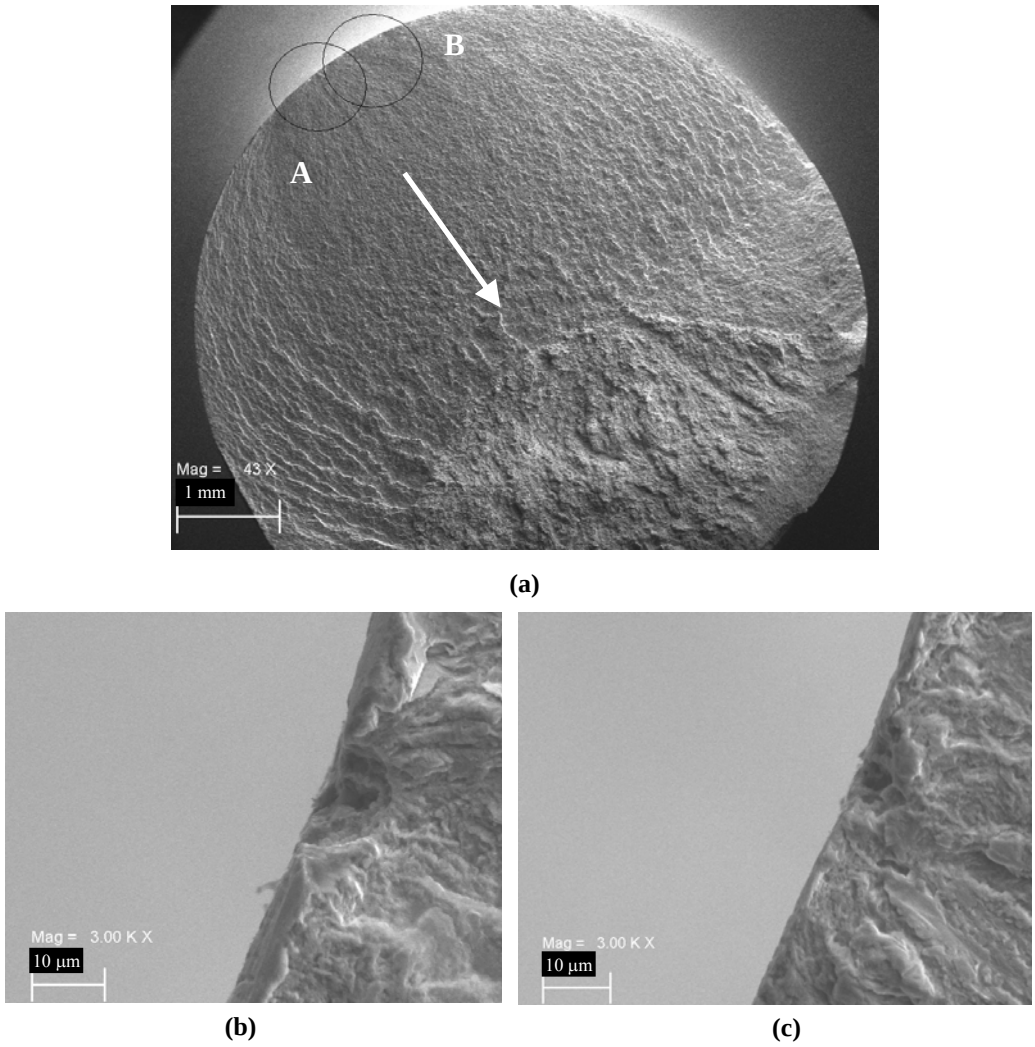

Figure 3.8 (a) Fracture surface overview of a coated specimen and higher magnifications of possible crack initiation areas (b) B and (c) A [3.21].

3.1.5 Conclusions

Based on the experimental evidence, it is worth underlining that the PE-CVD SiO_x coating did not significantly affect the fatigue behaviour of the base material, with a decrease of less than 10% in the average value of the fatigue limit of the coated steel alloy specimens with respect to the uncoated ones. Furthermore, fracture surface observations emphasized that the fatigue crack propagation mechanism in the coated samples was similar to the one occurring in the uncoated ones.

It was argued that, due to the low temperature used in the coating deposition process,

significant surface residual stresses should not have been induced in the substrate and the absence of surface compressive stresses was evaluated as a concrete reason for the unbeneficial contribute of the SiO_x thin coating to the fatigue behaviour. Anyway, considering the limited decrease in the coated steel fatigue resistance, in all the applications requiring good resistance to scratches and corrosion and that must withstand high fatigue stresses, the choice of a coating like the one analyzed could lead to interesting developments. In fact, the opportunity of coupling the advantages from using PE-CVD SiO_x coatings in applications where the environment is rather corrosive with acceptable fatigue behaviour for the coated components could be taken into account conveniently.

3.2 Fatigue tests on coated and uncoated 2011-T6 aluminium alloy

The possibility of lightening mechanical components and machine elements by broad use of light alloys is expected to become more and more essential in the next future. In the automotive and aerospace industries, the request for more power with lower gas polluting emissions is indeed gaining popularity very quickly. However, the fatigue behaviour, as well as the wear resistance, surface hardness and load bearing capacity of light alloys, such as aluminium ones, are often worse than those of steels. As a matter of fact, the capability shown by thin hard coatings deposited with PVD or CVD techniques of enhancing the wear and corrosion resistance of structural mechanical components can be beneficial to these base materials. Electrical conductors, automotive and aircraft, packaging, building and architecture are some of the most popular applications for aluminium alloys. Therefore, the improvement in the fatigue resistance of coated components would represent another good reason for accelerating the enlargement of the use of light alloys in structural applications, as coated light alloys with similar or even better performances than the ones of the traditional construction steels would be highly useful and favourable in many fields. However, the choice of the most suitable coatings for a certain substrate is very critical and not trivial, since requirements other than the pure fatigue resistance could be fundamental –

e.g. wear and corrosion resistance.

For the time being, the study of coated aluminium bulk material has been focused on tribological aspects [3.22, 3.23] and not on the influence of PVD and CVD thin hard coatings on its fatigue behaviour. Only in a few references the effect of the residual stresses from surface treatments on the fatigue resistance of coated aluminium alloys was studied. In [3.24] the beneficial effect of shot peening on the fatigue resistance of chromium electroplated 7050-T7451 aluminium alloy was pointed out, whereas in [3.25] it was demonstrated that such a mechanical pre-treatment can increase the fatigue limit and the micro-hardness of 2024-T351 alloy coated with a ceramic coating by plasma-electrolytic oxidation. Good results were found in [3.26] in the fatigue and corrosion-fatigue behaviour of 7075-T6 alloy coated with an electroless deposit. The beneficial effect of surface compressive residual stresses was emphasized in the reference [3.27], in which an enhancement in the fatigue resistance of 6082-T6 aluminium alloy coated with Al_2O_3 deposited with fluidized bed processing was observed.

Aluminium alloys included in the 2xxx series are suitable for low temperatures and, due to their high strength-to-weight ratio, they prove effective for the automotive and aircraft industries. However, their poor corrosion resistance with respect to other aluminium alloys may require the use of proper protection treatments such as anodizing, cladding, painting, coating deposition. Furthermore, the high temperatures used in several deposition processes could be detrimental to the mechanical properties of such bulk materials and hence the choice of the coating has to be made carefully. The 2011 alloy is widespread in many and common applications – e.g. adapters, pipe stems, machine parts, clock parts and gears, meter shafts and gears, nozzles, pipe stems and filters, etc. – as it guarantees good machinability and mechanical properties.

In this section the study of the fatigue behaviour of 2011-T6 aluminium alloy coated with PVD WC/C, PA-CVD DLC and PE-CVD SiO_x thin hard coatings is reported. Both coated and uncoated specimens were tested under rotating bending in order to evaluate the changes occurring in the fatigue limit at 10^7 load cycles in the coating presence. The fracture surfaces were examined under scanning electron microscope and the adhesion of each thin film to the bulk material was assessed by means of suitable scratch tests. The selection of the mentioned coatings was accurately made in order to keep the deposition

temperature below 200°C so as to prevent the substrate from the risk of compromising its strength. As regards PVD WC/C coatings, they usually show good adhesion to the base material and are particularly effective for reducing friction. Such coatings can be used for structural applications, machining tools and dies [3.28-3.31] and, due to their low deposition temperature (180°C), can be deposited on many substrates. For the time being, the tribological and the mechanical characterization of WC/C coatings have already been studied [3.32-3.34], but their influence on the fatigue behaviour of the bulk material and the use of aluminium as a substrate have not been developed enough yet. In the reference [3.35] a beneficial effect of a WC/C coating on the wear resistance in the presence of high residual compressive stresses was observed. DLC thin hard coatings show extremely low friction coefficient and good wear resistance. Since the PA-CVD technique allows deposition temperatures as low as 90-130°C and also enables the deposition of the coating on internal surfaces, the number of applications in which DLC coatings are used and the range of substrate materials are larger than it is with PVD. Similarly to WC/C, references reporting studies on tribological aspects of DLC thin coatings are mainly available [3.36-3.38]. The last coating under investigation was SiO_x PE-CVD-deposited. Even in this case no significant researches have been carried out to study its effects on the fatigue resistance of aluminium alloys. As the deposition of SiO_x takes place at very low temperatures (see above), the risk of thermal degradation of aluminium substrate is prevented.

This study allowed to record important results on the suitability of coating aluminium alloys in the presence of fatigue. Furthermore, coated aluminium with fatigue limit close to or even higher than the one of the uncoated material would make it possible to couple good structural behaviour to the aforementioned benefits on the wear and corrosion resistance from the presence of the coating. A paper reporting the results was submitted to *Surface and Coatings Technology* for publication [3.39].

3.2.1 Experimental technique

The following chemical composition (wt%) certified by the dealer was for the 2011-T6 aluminium alloy base material analyzed: 5.00-6.00 Cu, 0.20-0.60 Pb, 0.20-0.60 Bi, 0.40 Fe, 0.20 Si, 0.10 Zn, 0.05 Mg, 0.05 Mn and Al bal. Tensile tests (Galdabini Sun 5, Italy) were

performed using cylindrical specimens according to UNI EN 10002-1 standard in order to determine the strength of the base material. A Remet HX-1000 Vickers micro-indenter was utilized to measure its Vickers micro-hardness with an indentation load of 300 gf and five indentations for each sample. The micro-hardness tests were carried out on suitable samples before and after the deposition processes to verify whether the mechanical properties had been affected by the deposition temperature. Standard (ISO 1143) hourglass-shaped specimens for fatigue testing were produced from round bars: the minimum diameter was 8 mm and the fillet radius of the gage length was 30 mm (Figure 3.9). The average value of the surface roughness within the gage length was reduced below the value of 0.25 μm by polishing.

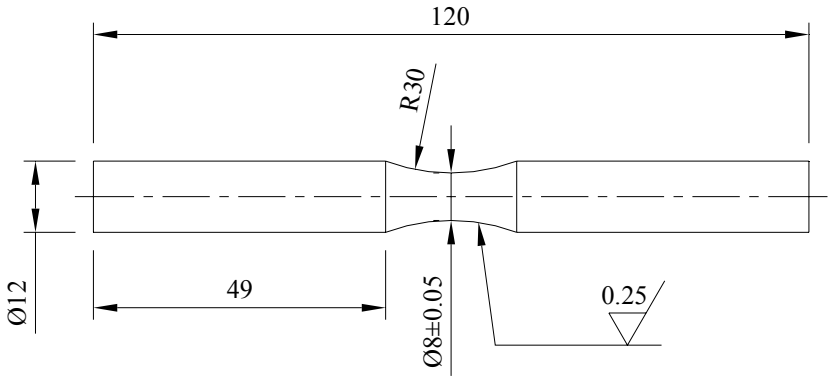

Figure 3.9 Dimensions of the 2011-T6 aluminium alloy specimens tested under rotating bending [3.39].

Besides a series of uncoated samples, three series including 15 samples coated with WC/C, 15 with DLC and 5 with SiO_x were addressed to the fatigue tests. The limited number of specimens of the last series made it possible to point out only a possible trend for the fatigue behaviour in the presence of a SiO_x coating, without the same statistical confidence of the other two series of coated samples. As usual, the surface of the specimens was accurately cleaned prior to coating deposition in order to remove contaminants like dust, grease and oxides to guarantee uniform and well adherent films. Commercial magnetron sputtering PVD and PA-CVD deposition processes were executed at LAFER Spa, Piacenza, Italy, to deposit, respectively, the WC/C and DLC coatings. A nominal temperature of 180°C was for the PVD process and the average thickness of the WC/C film was about 1 μm, as confirmed by SEM micrographs. A lower temperature – i.e. in the range

90-130°C – was used during the PA-CVD process and in this case the average thickness of the DLC coating was 3.2 μm. A PE-CVD process was carried out at MOMA srl, Dalmine, Bergamo, Italy, at room temperature to apply a SiO_x coating having a thickness estimated in the order of 1 μm. Figure 3.10 shows high magnifications of fracture surfaces which enable one to distinguish the deposited WC/C and DLC coatings.

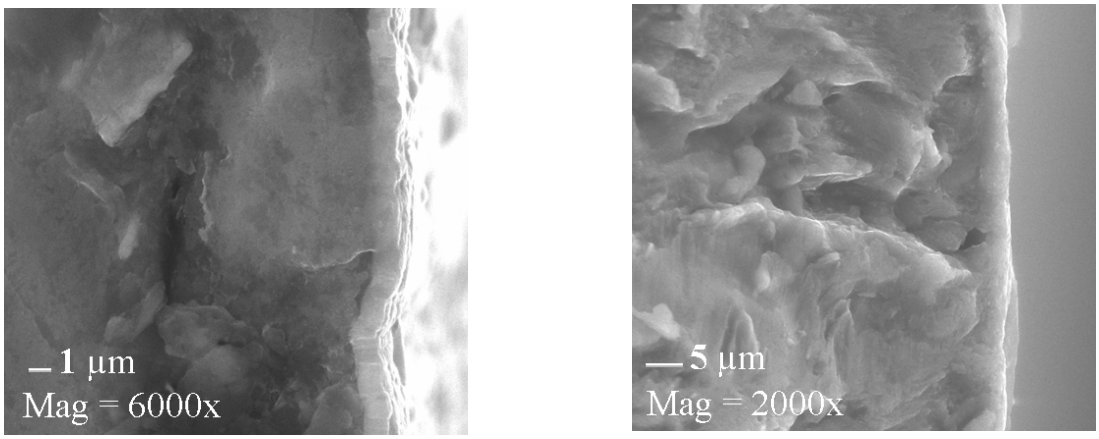

(a) **(b)**

Figure 3.10 High magnifications of fracture surfaces of (a) WC/C- and (b) DLC-coated samples [3.39].

Depth-sensing Berkovich nano-indentation (Nano-Indentation Tester, CSM Instruments, Peseux, Switzerland) was used to measure the nano-hardness of the coatings on suitable coated plane samples. Scratch tests (Micro-Combi Tester, CSM Instruments, Peseux, Switzerland) allowed to evaluate the coating-substrate interface delamination by determining the cracking load (L_{C1}), the coating spallation at the side of the scratch groove load (L_{C2}) and the coating spallation inside the groove load (L_{C3}) [3.39, 3.40] with the application of an incremental load from 0 to 30 N (5 N/min with a scratch length of 4 mm).

The rotating bending tests were carried out (Italsigma X2TM412, Forlì, Italy) at a frequency of 50 Hz (3000 rpm) in laboratory air and at room temperature. The tests allowed to evaluate, by means of the Stair-case method, the average value of the fatigue limit at 10^7 load cycles for the coated and the uncoated specimens. A load step of 12 MPa was chosen and the uncoated base material was loaded at maximum bending stress values included in the range 90-162 MPa, while the WC/C-, the DLC- and the SiO_x-coated specimens were loaded, respectively, within 142-190 MPa, 154-178 MPa and 154-166 MPa. After the

fatigue tests the fracture surfaces of both the coated and the uncoated specimens were observed by means of an SEM (FEI Quanta-200, Eindhoven, The Netherlands) to detect the crack initiation sites and assess possible modes and directions of propagation and the coating integrity at the crack initiation sites.

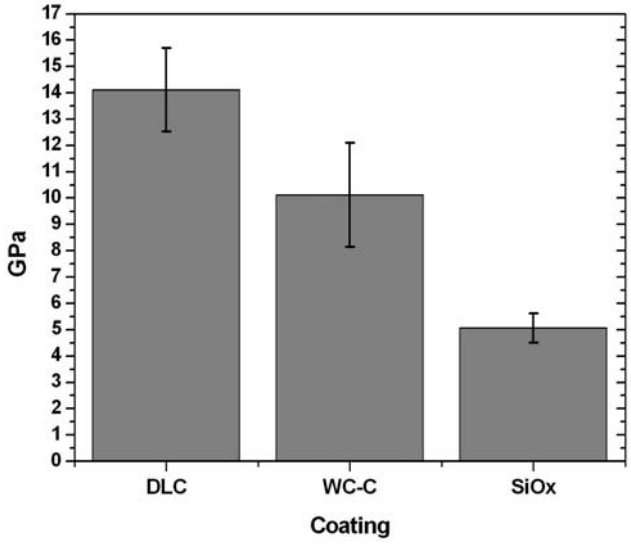

Figure 3.11 Berkovich nano-hardness of the tested films on 2011-T6 alloy [3.39].

3.2.2 Test results and discussion

The ultimate tensile strength, the yield strength and the deformation at rupture of the uncoated aluminium alloy were, respectively, 370 MPa, 272 MPa and 27%. The hardness of the uncoated bulk material was measured to be 124±4 $HV_{0.3}$ and, predictably, its value was not modified at all by the deposition temperature of the SiO_x coating. Negligible variations were observed on WC/C- and DLC-coated samples: 123±4 and 124±5 $HV_{0.3}$, respectively. Therefore, film deposition had not produced significant changes in the substrate hardness and it was inferred that, due to the low deposition temperatures, the mechanical properties of the aluminium substrate had remained substantially unaffected. Figure 3.11 shows the Berkovich nano-hardness value of each coating. The value for the DLC one was higher than both WC/C and SiO_x confirming its higher wear resistance – which is also expected to be coupled with very low friction coefficient.

The critical load values collected through the scratch tests are reported in Table 3.5.

Poor adhesion of the DLC film was evidenced and presumably due to the presence of a much softer substrate, while the tests performed on the WC/C-coated samples showed higher critical load values. Due to the extremely brittle behaviour, the critical load values of the SiO_x film were the lowest ones. Furthermore, as the SiO_x coating started fragmenting at very low loads, it was not possible to distinguish the L_{C2} load from the L_{C3} one. Both the DLC and the SiO_x coatings were not able to follow the deformation of the substrate during the scratch test indentations.

Table 3.5 Critical loads of the three coatings from the scratch tests. Values expressed in N [3.39].

Coating	L_{C1}	L_{C2}	L_{C3}
DLC	2.3 ± 0.3	3.1 ± 0.6	3.5 ± 0.4
WC/C	5.6 ± 0.1	9.6 ± 0.4	9.6 ± 0.4
SiO_x	0.9 ± 0.2	2.8 ± 0.9	2.8 ± 0.9

Table 3.6 Uncoated specimens: fatigue test results [3.39].

Test no.	Maximum bending stress, MPa	Number of cycles
1	90	10^7
2	102	10^7
3	114	10^7
4	126	10^7
5	138	10^7
6	150	10^7
7	162	5148680
8	150	10^7
9	162	5621700
10	150	3915405
11	138	10^7
12	150	10^7
13	162	7164235
14	150	10^7
15	162	1644153
Fatigue limit, MPa	154	
Standard error, MPa	6	

The fatigue resistance of the bulk material was influenced by the presence of each coating, although limited variations were observed. The highest load levels were possible in

the case of WC/C-coated aluminium alloy specimens (see above). Tables 3.6 to 3.9 report the experimental data as well as the average value and the corresponding standard error of the fatigue limit at 10^7 load cycles for each series of specimens.

Table 3.9 WC/C-coated specimens: fatigue test results [3.39].

Test no.	Maximum bending stress, MPa	Number of cycles
1	166	4655359
2	154	2957634
3	142	10^7
4	154	10^7
5	166	10^7
6	178	10^7
7	190	890178
8	178	1271863
9	166	10^7
10	178	1566452
11	166	10^7
12	178	2643692
13	166	10^7
14	178	9446361
15	166	10^7
Fatigue limit, MPa	169	
Standard error, MPa	15	

The fatigue limit average value for the uncoated specimens was 154 MPa with a standard error of 6 MPa (Table 3.6). The following values of the same parameters were calculated for the coated specimens: an average fatigue limit of 169 MPa and a standard error of 15 MPa were for the WC/C-coated ones (Table 3.7), 162 MPa and 6 MPa for the DLC-coated ones (Table 3.8) and 162 MPa and 7 MPa in the presence of the SiO_x coating (Table 3.9). Therefore, the presence of each coating increased the average value of the fatigue limit with respect to the uncoated specimens, suggesting that the thin hard films investigated could be beneficial to the fatigue resistance of 2011 aluminium alloy. The best enhancement – about 10 % – was produced by the WC/C coating, whereas 5% was the improvement in the case of both DLC and SiO_x coatings. Hence, with regard to the fatigue resistance, the WC/C coating proved more effective than the other ones, even though the

corresponding standard deviations could make one consider the actual improvement to be less interesting. Anyway, the coatings analyzed could result highly beneficial in all applications requiring both good tribological and mechanical properties, since the fatigue limit is expected to be increased or at least not altered by such coatings.

Table 3.8 DLC-coated specimens: fatigue test results [3.39].

Test no.	Maximum bending stress, MPa	Number of cycles
1	178	486736
2	166	10^7
3	178	350028
4	166	10^7
5	178	1179351
6	166	5224174
7	154	10^7
8	166	1921049
9	154	10^7
10	166	627000
11	154	10^7
12	166	2317399
13	154	10^7
14	178	486736
15	166	10^7
Fatigue limit, MPa	162	
Standard error, MPa	6	

Table 3.9 SiO_x-coated specimens: fatigue test results [3.39].

Test no.	Maximum bending stress, MPa	Number of cycles
1	154	10^7
2	166	2183594
3	154	10^7
4	166	8965245
5	154	10^7
Fatigue limit, MPa	162	
Standard error, MPa	7	

Figure 3.12 shows the diagram including the experimental observations collected throughout the fatigue tests for the uncoated, the WC/C- and the DLC-coated specimens as well as the approximated S/N curves plotted by linking the boundary of quasi-static failure

– i.e. 10^3 load cycles – to the fatigue limit evaluated at 10^7 load cycles.

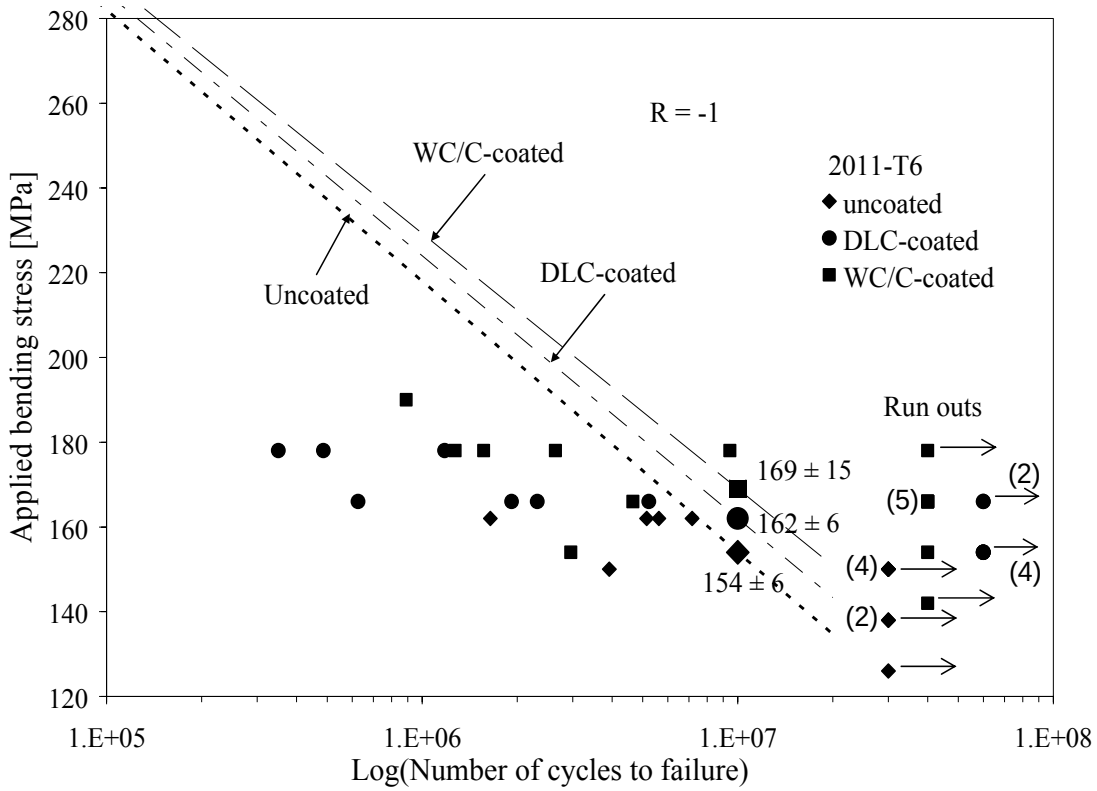

Figure 3.12 Bending stress vs. Number of cycles until failure diagram [3.39].

The SEM observations of the fracture surfaces of both the coated and the uncoated specimens allowed to evaluate the influence of each coating on the fatigue crack nucleation and propagation mechanisms. A single fatigue crack initiation site was detected in almost all the failed samples at or close to the external surface of the base material. The cracks propagated following directions emanated from the initiation points towards the core of the specimens until the final ductile failure pointed out with the SEM analysis. Furthermore, in the WC/C-coated samples cracks nucleated at a depth range of 10-50 μm below the substrate surface (Figure 3.13). Possible surface compressive stresses induced by the PVD coating deposition process could have produced such a shift from the external surface as well as the improvement of the aluminium alloy fatigue resistance. The DLC-coated samples showed crack nucleation closer to the substrate external surface – i.e. at a depth less than 10 μm (Figures 3.14(a) and (b)). The cracks nucleated close to or at the external

surface in the SiO_x-coated specimens (Figures 3.14(c) and (d)). The lower increase in the fatigue limit produced in the presence of DLC and SiO_x could hence be placed in the less or almost null amount of residual surface compressive stresses.

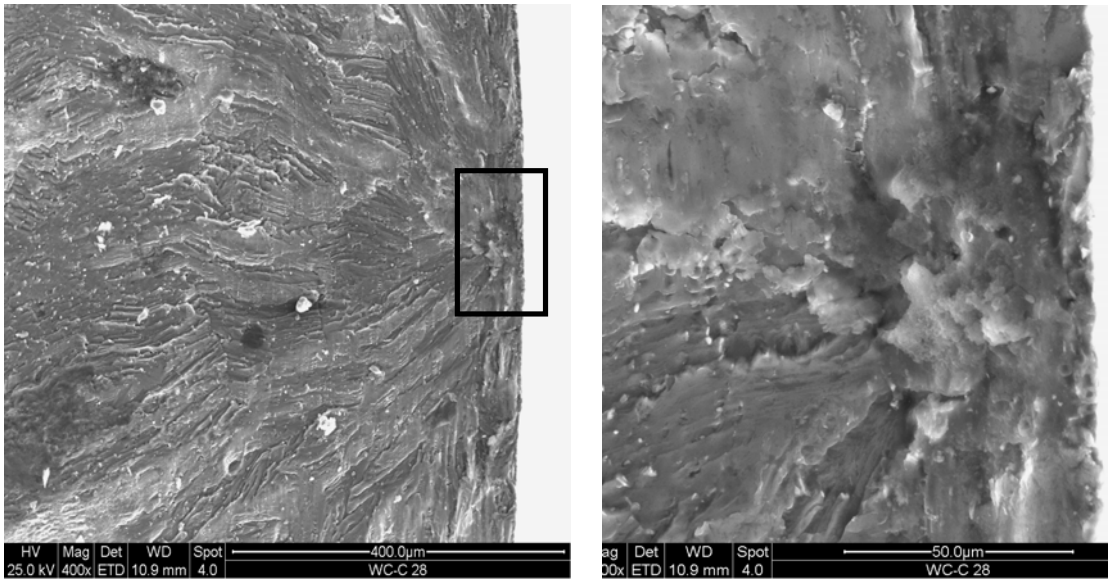

(a) **(b)**

Figure 3.13 SEM micrographs of a WC/C-coated sample fracture surface: (a) indication of the crack nucleation site and (b) higher magnification of this area. The crack initiation is located below the surface.

It was argued that, in the case of the WC/C-coated samples, compressive stresses could have had an extent not higher than 35-40 μm from the external surface – so as to comply with the position of the crack nucleation sites. Some references dealing with PVD-coated components [3.7, 3.8, 3.41] also confirm such depth orders. In addition, the observations pointed out no WC/C coating delamination during the fatigue tests (Figure 3.15(a)), according to the scratch test evidence which emphasized the best behaviour of the WC/C coating (see above). Such good adhesion of the WC/C coating is – together with the possible surface compressive stresses – clearly beneficial to the fatigue resistance of the base material. By contrast, based on the experimental evidence one can argue that the DLC and SiO_x coatings should have induced lower or even negligible compressive stresses in the aluminium base material, as the improvement in the fatigue limit was lower than the one with the WC/C coating. SEM high magnifications of the fracture surfaces showed that the DLC (Figure 3.15(b)) coating was subjected to delamination and detachments from the

substrate surface.

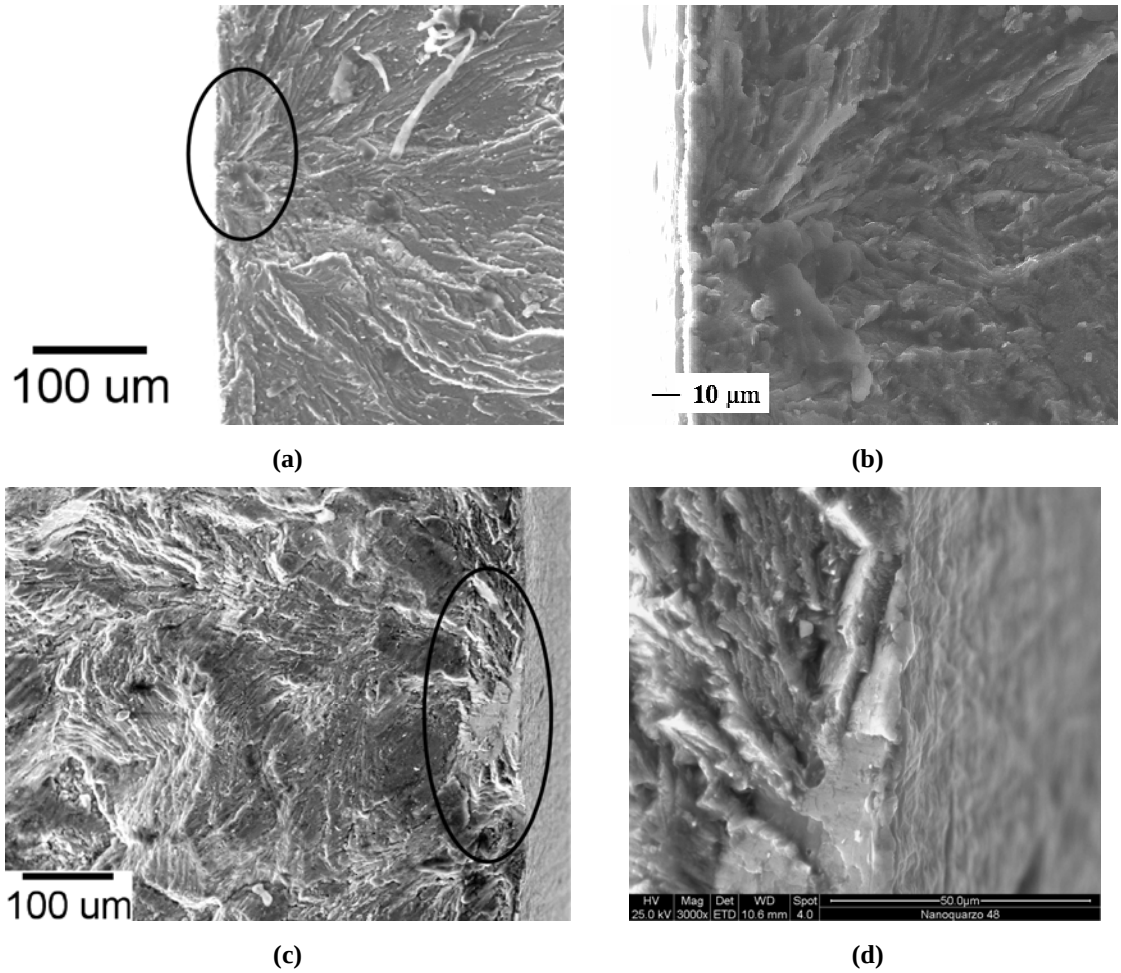

Figure 3.14 SEM micrographs of a DLC-coated sample fracture surface: (a) indication of the crack nucleation site and (b) higher magnification of this area. SEM micrographs of a SiO_x-coated sample fracture surface: (c) indication of the crack nucleation site and (d) higher magnification of this area. The crack initiations are close to or at the external surface.

A coating showing poor adhesion can hardly prove effective in enhancing the fatigue resistance of the substrate, since a relaxation of the beneficial compressive stress distributions could take place in the surface layers – i.e. the most critical area with regard to the fatigue behaviour. As a matter of fact, both the CVD deposition processes did not produce remarkable effects on the substrate fatigue resistance with respect to the PVD one.

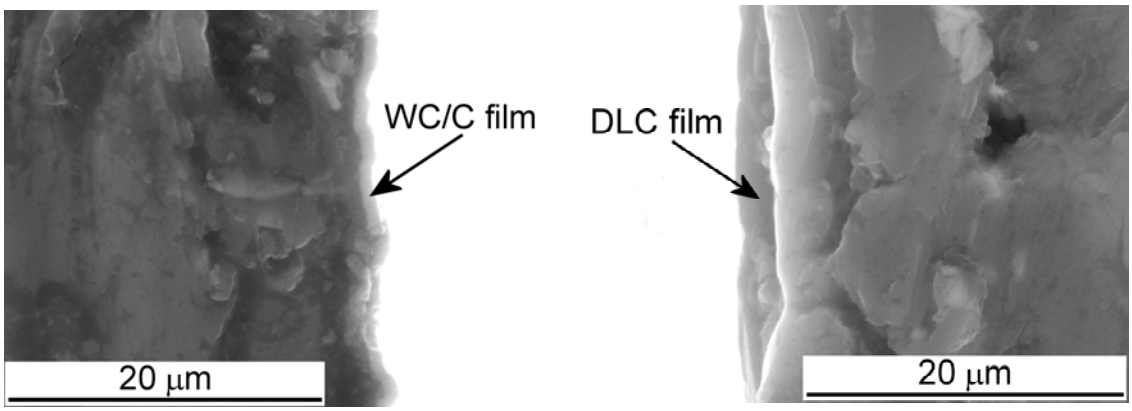

(a) **(b)**

Figure 3.15 High magnifications of the fracture surfaces of (a) a WC/C- and of (b) a DLC-coated sample: DLC delaminated from the substrate [3.39].

3.2.3 Conclusions

The fatigue tests allowed to observe that the PA-CVD DLC and PE-CVD SiO_x coatings did not significantly increase the fatigue behaviour of 2011-T6 aluminium alloy, whereas the PVD WC/C one proved more effective. An improvement of about 10% in the fatigue limit with respect to the uncoated material was produced by the WC/C thin hard coating. SEM observations showed a crack nucleation shift within the range 10-50 μm below the substrate surface in the presence of this film. A probable compressive stress field induced by the WC/C PVD deposition process at the surface layers – beneficial to the substrate fatigue resistance – was supposed to be responsible for such a crack initiation shift. This complied with the attitude shown by the WC/C coating not to delaminate and be detached from the substrate surface during the fatigue tests pointed out with the microscope analyses and the scratch tests [3.39].

The DLC and SiO_x coatings proved less effective in increasing the substrate fatigue limit and the fatigue cracks were observed to nucleate close to or at the substrate surface. Therefore, less significant surface residual compressive stresses were presumably generated by the CVD processes. With regard to DLC, the delamination during the tests could also have relieved any possible beneficial residual compressive stress field in the substrate.

The results of this study allowed to strengthen the idea that the use of opportunely coated light alloys would make it possible to couple the benefits in the wear-, friction- and

corrosion-resistant properties with a good fatigue behaviour.

3.3 Fatigue tests on coated and uncoated Ti-6Al-4V titanium alloy

Bearing in mind that, as previously stated, few references deal with the influence of thin hard coatings on the fatigue behaviour of light alloys, the fatigue behaviour of Ti-6Al-4V alloy coated with a PVD arc-deposited TiN film was also studied. The results of the study are reported in this section. Rotating bending tests were carried out in laboratory air and at room temperature on both conventional and notched hourglass specimens to evaluate the fatigue limit at 200000 load cycles. Both coated and uncoated specimens were tested to investigate the effect of the coating on the fatigue limit of the titanium alloy, with and without the presence of a surface sharp notch. Fracture surfaces were observed, as usual, by means of SEM.

The results of this study were published on *Key Engineering Materials*, Vols. 348-349, pp. 313-316, in 2007 [3.42] and on *Structural Durability & Health Monitoring*, Vol. 3, No. 3, pp. 165-176, in 2007 [3.43] and presented at the "6th International Conference on Fracture and Damage Mechanics", Madeira, Portugal, 17-19 July 2007.

3.3.1 Experimental technique and material

The base material was Ti-6Al-4V ELI ASTM F136 titanium alloy having the following composition (wt%): 0.006 C, 3.800 V, 6.000 Al, 0.120 Fe, 0.099 O, 0.003 H, 0.009 N and Ti bal. Its ultimate tensile and yield strength were, respectively, 895 and 829 MPa, as certified by the dealer. Standard (ISO 1143) hourglass-shaped specimens for fatigue tests were produced from bars having diameter equal to 12 mm. The minimum cross section diameter was 8 mm and the fillet radius of the gage length was 40 mm (Figure 3.16). Accurate surface finishing within the gage length by proper mechanical polishing made it possible to keep the average surface roughness below 0.20 μm and, as usual,

circumferential notches were prevented with final lengthwise polishing. The 120° V-shaped surface notches were machined transversally to the specimen axis at the minimum cross section and were 0.2 mm deep (Figure 3.16). The notch size was very small if compared to the specimen cross section, hence the nominal bending stress for the notched specimens was approximated to the one calculated without the presence of the notch. Some of the notched and smooth samples were coated with a commercial TiN PVD arc-deposited thin hard film: the nominal deposition temperature was 420°C and the average deposited thickness was 3.9 μm. The bulk material Vickers micro-hardness was measured (Remet HX-1000 Vickers microindenter) before and after the deposition process to verify if the mechanical properties had been affected by the deposition process temperature.

Four series of rotating bending tests were then carried out (Italsigma X2TM412, Forlì, Italy) at room temperature and a frequency of 50 Hz. Each series – smooth-uncoated, smooth-coated, notched-uncoated and notched-coated – included 15 samples. The Stair-case method with a 20-MPa load step was used to determine, as aforesaid, the fatigue limit at 200000 load cycles. The smooth-uncoated samples were loaded at maximum bending stresses included in the range 600-720 MPa, the smooth-coated ones in the range 540-640 MPa, the notched-uncoated ones within 300-360 MPa and the notched-coated ones within 260-300 MPa. All the fracture surfaces were investigated under SEM (FEI Quanta-200, Eindhoven, The Netherlands) paying particular attention to the study of the crack initiation sites.

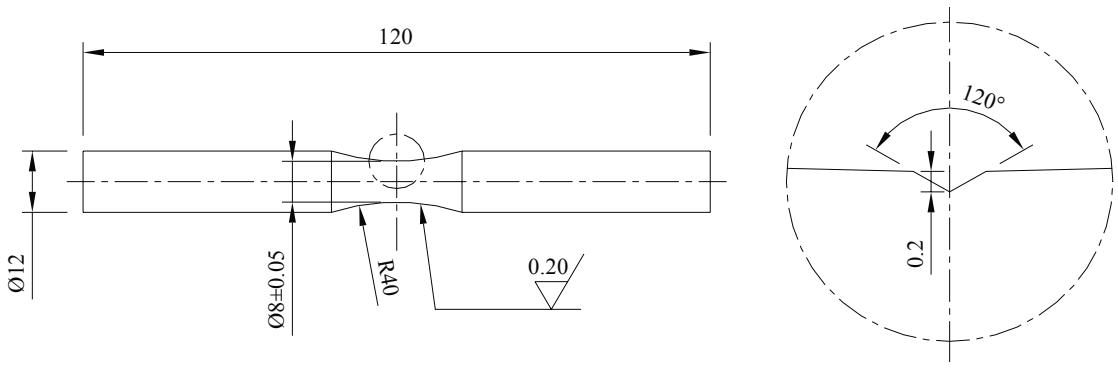

Figure 3.16 Standard specimen dimensions and a particular of the V-notch [3.43].

3.3.2 Test results and discussion

The deposition process did not significantly affect the surface hardness of the titanium alloy, as it resulted 271±4 $HV_{0.5}$ before the deposition and 286±4 $HV_{0.5}$ afterwards. The diagram shown in Figure 3.17 includes each experimental observation from the fatigue tests and the approximated S/N curves matching the data collected are also depicted in the finite life region of the Wöhler diagram. As regards the smooth specimens, the average values of the fatigue limit were 646 and 574 MPa for the uncoated and for the coated ones, respectively, and the value of the standard error was 45 MPa for both the two series. In the presence of the notch, 327 MPa and 14 MPa were the values of the average fatigue limit and of the standard error for the uncoated specimens, while 281 MPa and 9 MPa were the same parameters for the coated ones.

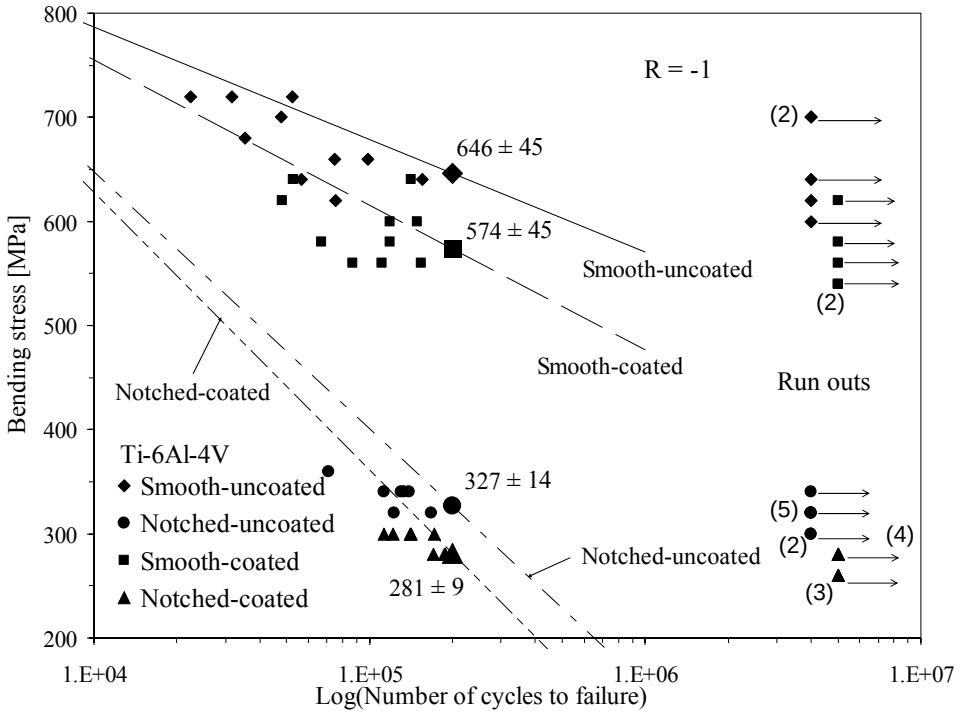

Figure 3.17 Bending stress vs. Cycles to failure diagram for the Ti-6Al-4V specimens [3.42].

As far as the smooth specimens are concerned, a certain scattering of the fatigue test results was observed. By contrast, the experimental observations collected for the notched specimens presented a much lower dispersion, suggesting that the notch had acted as a

dominant stress concentrator with respect to any other possible defect in the base material. Nevertheless, data available in the literature [3.44] confirmed the reliability of the experimental results for the smooth specimens. The coating produced a decrease in the fatigue limit of the smooth and of the notched specimens less than 12% and 14%, respectively. Therefore, regardless of the presence of the notch, the coating seemed to have a similar influence on the fatigue behaviour of the two types of titanium alloy specimens. Only few references report data on the fatigue behaviour of TiN-coated Ti-6Al-4V and, from this point of view, no significant alteration with respect to the uncoated material was pointed out [3.45].

The reduction of the imposable bending stress was also quantified by a fatigue stress intensification factor K_f – calculated for a fatigue life of 200000 cycles – defined as the ratio between the average values of the fatigue limit at 200000 cycles of, respectively, the smooth and the notched specimens. It resulted 1.98 for the uncoated samples and 2.04 for the coated ones. Furthermore, by means of a preliminary finite element linear elastic analysis, a notch amplification stress coefficient equal to 3.70 was calculated. Therefore, by comparing this value to the lower K_f from the fatigue tests, it was inferred that the notch root plasticity due to the stress redistribution occurring at the notch tip could have represented one of the main parameters affecting the fatigue life of the notched specimens, at least as regards the uncoated ones [3.46, 3.47].

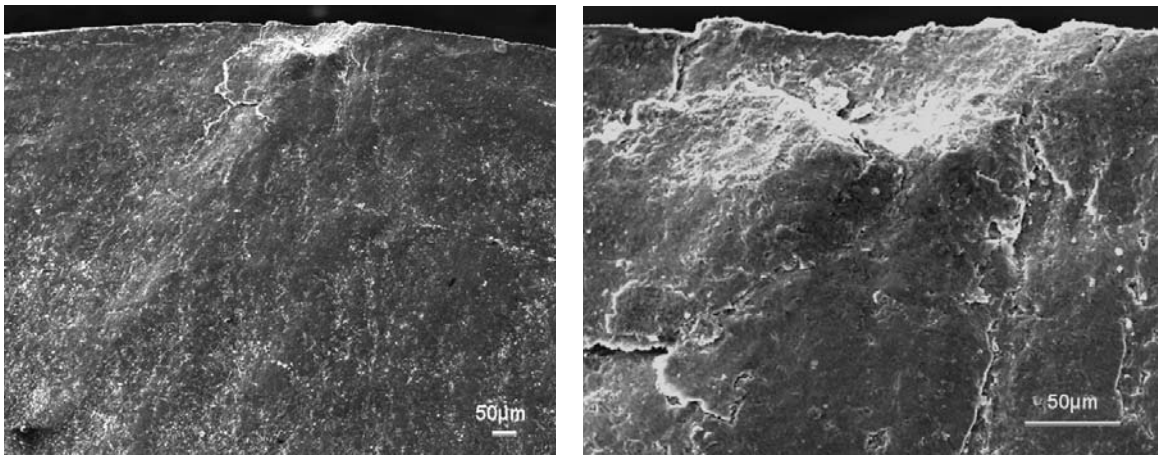

(a) **(b)**

Figure 3.18 SEM micrographs of a smooth-coated sample fracture surface: (a) overview and (b) high magnification of the crack initiation site [3.42].

The PVD process should have reasonably induced a surface residual stress field in the coated specimens. From this point of view, SEM observations showed that crack initiation points were located in the substrate, close to or on its external surface. Figure 3.18(b) shows a high magnification of the crack initiation site in a smooth-coated sample: the crack could have nucleated where the maximum residual tensile stresses took place (see also the next chapter). Figure 3.18(a) shows a lower magnification of the same area.

3.3.3 Conclusions

The fatigue test results pointed out that the TiN PVD coating analyzed was a few detrimental to the fatigue resistance of Ti-6Al-4V titanium alloy at 200000 cycles. The reduction for both the smooth and the 120° V-notched specimens was within the range 12-14%. In general, due to the brittle nature of thin hard coatings, in case of defects already present in the coating through-thickness cracks may be generated and then they would behave as severe micro-notches for the substrate [3.48, 3.49] and play an unbeneficial role in the fatigue resistance. The high tensile stresses arising in the coating after loading for the notch stress amplification would neither prevent coating fracture nor keep possible cracks closed. Coating fracture could also occur if the critical fracture strain was reached by load application – this is particularly critical for notched specimens. Therefore, fatigue tests at higher numbers of cycles, i.e. at lower load levels, could be useful to verify whether the coating analyzed, being subjected to a lower strain, is able to prove more effective. Furthermore, the subsurface tensile stresses from loading application would be reduced.

3.4 Summary of the rotating bending tests

Table 3.10 summarizes and enables one to make a comparison between the fatigue test results previously reported and commented. It is very clear how the choice of the most effective coatings for a certain substrate is not trivial and a large number of further tests and studies should be carried out to select the best treatments for each base material. Anyhow,

besides the tribological and corrosion-resistant properties, the data collected through the present researches and the ones already available in the literature [3.5, 3.7, 3.8] show that remarkable results, in terms of fatigue behaviour, can be achieved by means of coating deposition. Moreover, even when the experimental results are a few smaller than the expectations in the presence of a coating, they could be evaluated rather satisfying if the opportunity of coupling an acceptable fatigue resistance with the other good mentioned properties is considered. Based on the experimental observations and previous literature references, it was argued that the probable surface compressive residual stresses in the base material from the deposition process of the most effective coating – i.e. WC/C on aluminium alloy – gave an important contribution to the enhancement of the fatigue resistance.

Table 3.10 Comparison between the fatigue test results for the different coatings and base materials analyzed.

Base material	Fatigue Limit, MPa		Coating	Δ %	Ref.
	$2{\cdot}10^5$ cycles	10^7 cycles			
39NiCrMo3	-	538 ± 21	-		[3.21]
	-	503 ± 23	SiO_x	-10%	
2011-T6	-	154 ± 6	-		[3.42]
	-	169 ± 15	WC/C	+10%	
	-	162 ± 6	DLC	+5%	
	-	162 ± 7	SiO_x	+5%	
Ti-6Al-4V	646 ± 45	-	-		[3.45, 3.46]
	574 ± 45	-	TiN	-12%	
Ti-6Al-4V (notched)	327 ± 14	-	-		
	281 ± 9	-	TiN	-14%	

3.5 Contact fatigue tests on coated and uncoated gears

In order to study both the bending and the contact fatigue behaviour of components in the presence of thin hard coatings, suitable tests on CrN PVD-coated automotive

transmission spur gears were carried out [3.50, 3.51]. The device developed and assembled to perform both bending and contact (R = 0) fatigue tests on gear tooth flanks is shown in Figure 3.19. The introduction of a cylindrical roller – used for roller bearing applications – having a diameter of 8 mm between each couple of adjacent teeth, made it possible to apply loads normal to the tooth flanks. By means of the device the tested gears could be kept fixed while the pulsating load was being applied through the roller along the vertical direction. Tests on both CrN PVD-coated and uncoated gears were then performed.

The results of the study of the contact fatigue behaviour were published on *Key Engineering Materials*, Vols. 385-387, pp. 57-60, in 2008 [3.50] and presented at the "7th International Conference on Fracture and Damage Mechanics", Seoul, Korea, 9-11 September 2008.

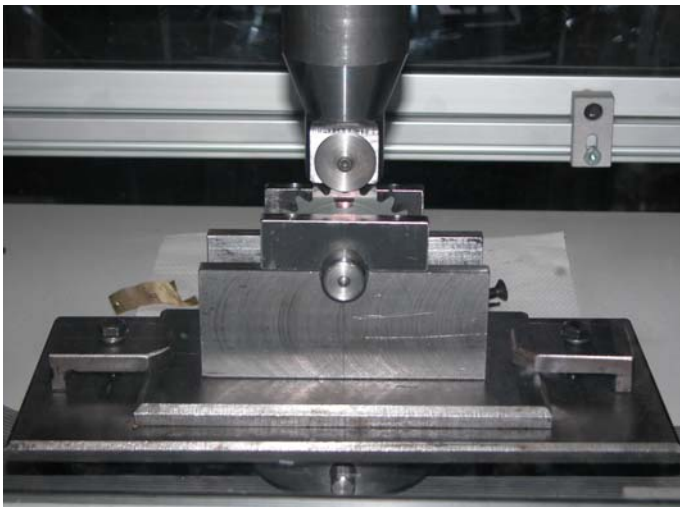

Figure 3.19 Picture of the device developed for bending and contact fatigue tests on spur gear teeth [3.51].

3.5.1 Experimental technique and material

Case hardened 18NiCrMo5 steel alloy gears, uncoated and coated with a CrN PVD arc-deposited coating having a thickness of about 10 μm, were addressed to the tests. An experimental evaluation of the influence of the coating on the base material fatigue damage was made and numerical models were developed (see the next chapter) to foresee the number of load cycles necessary for a surface crack located at the tooth base to propagate

from a certain depth to another and for the contact fatigue damage initiation to occur over the contact area. Optical (Leica MZ75) and scanning electron microscope (ZEISS EVO 40) observations of all the tested tooth flanks were also carried out to assess and quantify the contact fatigue damage. The damaged areas were measured – in terms of mm^2 – by means of optical observation of the integrity of each tooth flank after the tests. In order to evaluate the contact fatigue behaviour, the spur gears were tested, under unlubricated condition, on a computer-controlled universal testing machine (BRT VT250, Casei Gerola, Italy) at room temperature and at a test frequency of 20 Hz.

These tests were conceived, in particular, with the aim of setting up a suitable theoretical-numerical procedure able to predict the number of cycles under contact loading until the first damage appearance on tooth flanks. The bulk material mechanical properties were: yield strength equal to 690 MPa and ultimate tensile strength to 828 MPa. The surface hardness of the gears was 560 HV before deposition and 700 HV afterwards, whereas the case hardening penetration depth was in the interval 0.5-0.6 mm. The module of the gears was 2.95 mm, the number of teeth 24, the pitch diameter 70.80 mm and the tooth width about 13.34 mm.

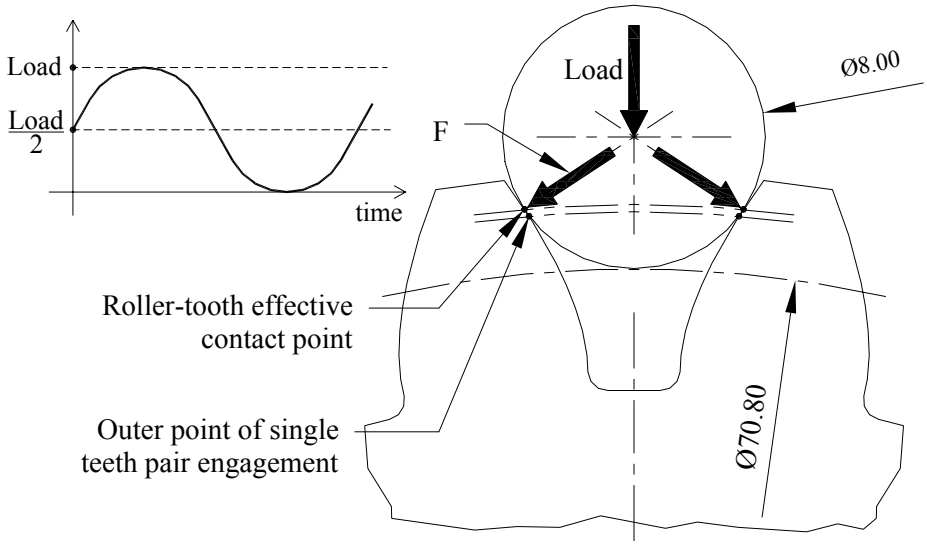

Figure 3.20 Load application scheme for the contact fatigue tests performed on steel alloy spur gears [3.50].

The choice of an 8-mm diameter for the cylindrical rollers used in the tests was made in order to produce a contact point with the tooth flanks very close to the outer point of

single teeth pair engagement, which falls in the most critical contact loading area during gear meshing. A sketch of the load application scheme is depicted in Figure 3.20, while Table 3.13 lists the six load levels – ranging from 0.625 to 15 kN – used in the tests with the resultant normal force on tooth flanks at each load level as well as the corresponding maximum contact Hertz's pressure in the case of steel-on-steel contact without friction. The material of the cylindrical rollers was hardened 100Cr6, hence showing much higher strength and hardness than the material of the gears – i.e. yield and ultimate strength equal to 1650 and to 1900 MPa, respectively, and hardness to 848 HV.

Table 3.13 Test loads on gear tooth flanks [3.50].

Load, kN	F, kN	p_{Hertz}, MPa
0.625	0.56	671
1.25	1.13	949
2.5	2.26	1343
5	4.51	1899
10	9.03	2685
15	13.54	3289

3.5.2 Test results and discussion

Wear, contact fatigue, coating rupture and/or delamination were believed to be the main sources of damage on tooth flanks. Figure 3.21 shows the extension of the damaged areas on the tooth flanks vs. the number of load cycles at a constant test load of 1.25 kN for both coated and uncoated gears, whereas Figure 3.22 depicts the damaged areas at constant numbers of cycles vs. the test load. By looking at these two diagrams it is evident that the coated gears showed a worse behaviour with respect to the uncoated ones. Certain linearity also resulted in the correlation between the damaged areas and both the number of cycles at constant load and the load level at constant number of cycles.

Large coating detachments were observed on the tooth flanks at the highest load levels, i.e. 10 and 15 kN, but coating damage and/or delamination occurred even at low loads and numbers of load cycles, confirming that lower thicknesses – i.e. not higher than 1 μm – or PVD coatings other than CrN could prove more effective under contact or rolling contact

fatigue [3.52]. It is worth underlining that the damaged areas in the coated gears were much wider than in the uncoated ones and this could have been due to possible extra quotas from pure coating failure. As regards the uncoated gears, negligible surface damage was detected on the tested tooth flanks after 10000 cycles only at 0.625 kN – i.e. the lowest load level.

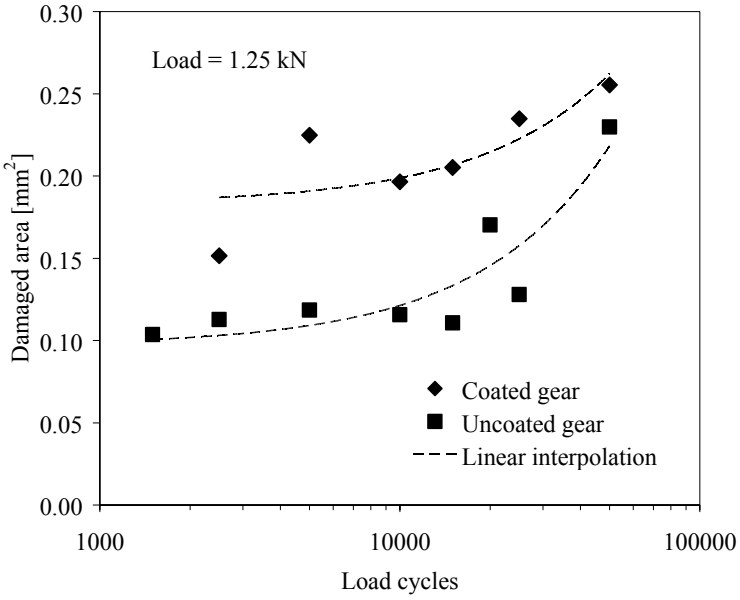

Figure 3.21 Damaged area vs. Number of cycles at constant load for CrN-coated and uncoated gears [3.50].

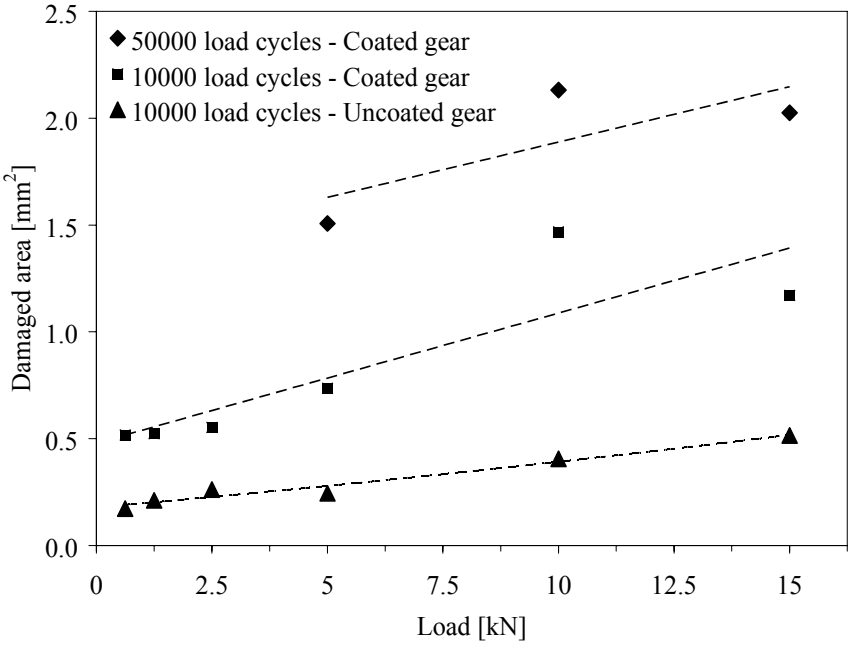

Figure 3.22 Damaged area vs. Load at constant numbers of cycles for CrN-coated and uncoated gears [3.50].

Due to the superior uniformity of the experimental correlation between tooth damage and load levels of the uncoated gears with respect to that of the coated ones (Figure 3.22), one may suppose that the high residual stresses induced by the PVD deposition process might have been detrimental. However, it is important to stress that, with regard to the higher loads, the coating could have failed even statically.

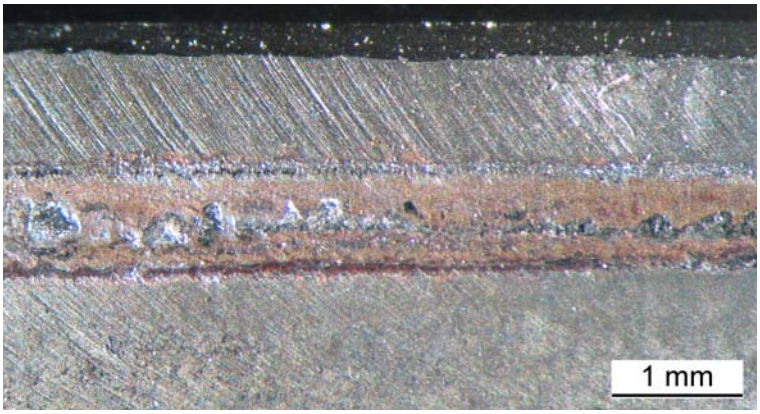

Figure 3.23 Optical magnification (2x) of a coated tooth flank tested at 10 kN and 50000 load cycles [3.50].

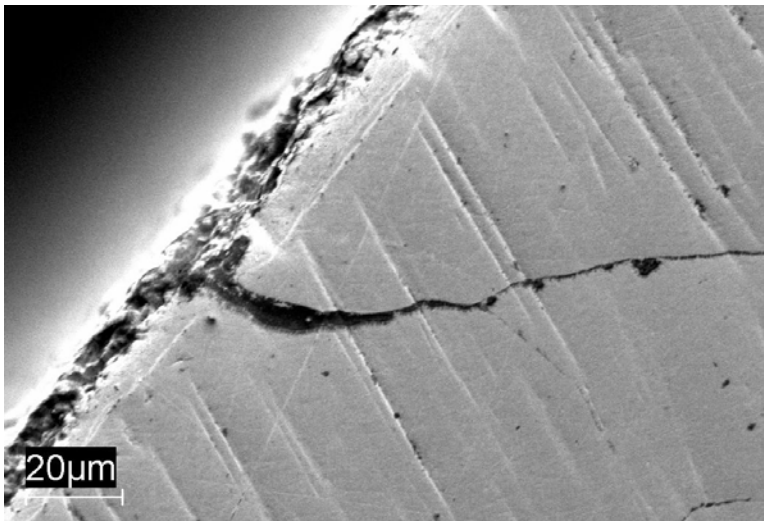

Figure 3.24 Incipient spall formation in a CrN-coated tooth tested at 1.25 kN and 50000 cycles [3.50].

Figure 3.23 shows the damaged area on a coated tooth flank tested under one of the most severe test conditions – namely at 10 kN and 50000 load cycles. Large coating delamination occurred on the tooth flank, with wide pieces of coating detached from the bulk material. Figure 3.24 shows a spall formation in a tooth flank of a coated gear tested at

1.25 kN and 50000 load cycles. From the inclination of this crack one can argue that the presence of the CrN coating should not have affected the typical damage mechanisms – pitting or spalling – which usually take place in uncoated gears from rolling contact fatigue [3.44, 3.53-3.55]. Furthermore, FEM analyses (see chapter 4) showed that the initial damage could have occurred at the external surface in the uncoated gears and at the coating-bulk material interface in the coated ones. This could have been due, in particular, to the high friction from the absence of lubrication during the tests.

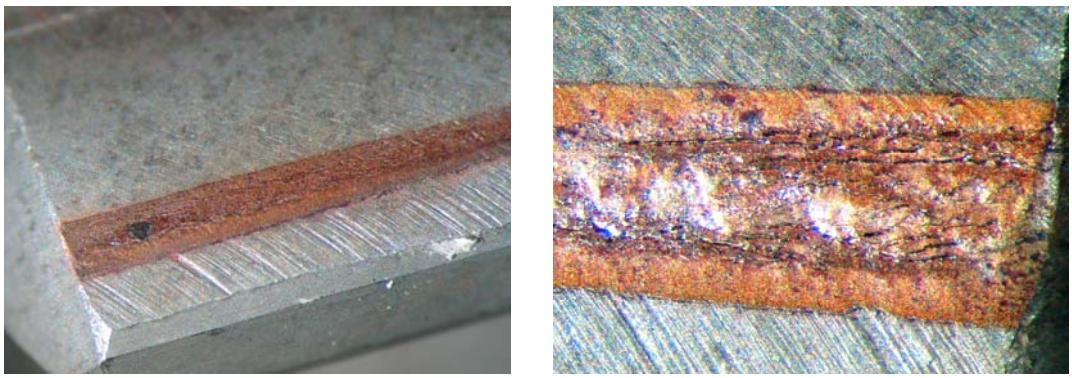

Figure 3.25 Appearance of the contact area of an uncoated steel spur gear tested under contact fatigue [3.51].

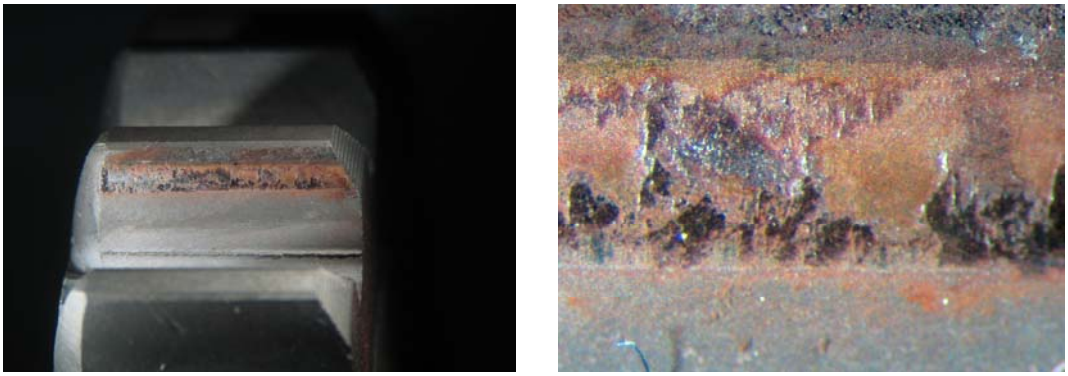

Figure 3.26 Appearance of the contact area of a CrN-coated steel spur gear tested under contact fatigue [3.51].

Microscopic examination and liquid penetrant inspection of gears tested under similar conditions to the ones just discussed emphasized that fatigue crack initiation and propagation did not occur at tooth base on both the uncoated and the coated gears [3.51]. The absence of initial cracks in that area was considered as a good explanation for this

evidence. A tooth flank of an uncoated gear after high load tests and a damaged surface of a CrN-coated gear are shown in Figures 3.25 and 3.26, respectively. Large coating delamination is visible on the tooth flanks and, due to probable lower oxidation, the damaged coated tooth flanks showed a darker colour.

References

[3.1] Baragetti S, Gelfi M, La Vecchia GM, Lecis N. Fatigue resistance of CrN thin films deposited by arc evaporation process on H11 tool steel and 2205 duplex stainless steel. *Fat Fract Engng Mater Struct* 2005; 28(7):615-621.

[3.2] Barata A, Cunha L, Moura C. Characterisation of chromium nitride films produced by PVD techniques. *Thin Solid Films* 2001; 398:501-506.

[3.3] Sathiyanarayanan S, Rajagopal G, Palaniswamy N, Raghavan M. Corrosion protection by chemical vapor deposition: A review. *Corrosion Reviews* 2005; 23(4-6):355-370.

[3.4] Kim KR, Suh CM, Murakami RI, Chung CW. Effect of intrinsic properties of ceramic coatings on fatigue behaviour of Cr-Mo-V steels. *Surf Coat Technol* 2003; 171:15-23.

[3.5] Baragetti S. Fatigue resistance of steel and titanium PVD coated spur gears, *Int J Fat* 2007; 29:1893-1903.

[3.6] Inoue K, Lyu S, Deng G, Kato M. Fracture mechanics based evaluation of the effects of the surface treatments on the strength of carburized gears. *Proc VDI Berichte* 1996; 1320:357-369.

[3.7] Baragetti S, La Vecchia GM, Terranova A. Fatigue behaviour and FEM modelling of thin-coated components. *Int J Fat* 2003; 25:1229-1238.

[3.8] Baragetti S, La Vecchia GM, Terranova A. Variables affecting the fatigue resistance of PVD-coated components. *Int J Fat* 2005; 27(10-12):1541-1550.

[3.9] Su YL, Yao SH, Wei CS, Wu CT, Kao WH. Evaluation on wear, tension and fatigue behaviour of various PVD coated materials. *Materials Letters* 1998; 35:255-260.

[3.10] Gelfi M, La Vecchia GM, Lecis N, Troglio S. Relationship between through thickness residual stress of CrN-PVD coatings and fatigue nucleation sites. *Surf Coat Technol* 2005; 192:263-268.

[3.11] Ejiri S, Sasaki T, Hirose Y. X-ray stress measurement for TiN films evaporated by PVD. *Thin Solid Films* 1997; 307:178-182.

[3.12] Murotani T, Hirose H, Sasaki T, Okazaki K. Study on stress measurement of PVD-coating layer. *Thin Solid Films* 2000; 377-378:617-620.

[3.13] Merlo AM. The contribution of surface engineering to the product performance in the automotive industry. *Surf Coat Technol* 2003; 174-175:21-26.

[3.14] Vetter J, Barbezat G, Crummenauer J, Avissar J. Surface treatment selections for automotive applications. *Surf Coat Technol* 2005; 200:1962-1968.

[3.15] Su YL, Yao SH, Wei CS, Kao WH, Wu CT. Comparison of wear, tensile, and fatigue properties of PVD coated materials. *Mater Sci Technol* 1999; 15(1):73-77.

[3.16] Angelini E, d'Agostino R, Fracassi F, Grassini S, Rosalbino F. Surface analysis of PECVD organosilicon films for corrosion protection of steel substrates. *Surf Interface Anal* 2002; 34:155-159.

[3.17] Angelini E, Grassini S, Rosalbino F, Fracassi F, Laera S, Palombo F. PECVD coatings: analysis of the interface with the metallic substrate. *Surf Interface Anal* 2006; 38:248-251.

[3.18] He JL, Chu CH, Wang HL, Hon MH. Corrosion protection by PECVD-SiO_x as a top coating on TiN-coated steel. *Surf Coat Technol* 1994; 63(1):15-23.

[3.19] Moretti G, Guidi F, Canton R, Battagliarin M, Rossetto G. Corrosion protection and mechanical performance of SiO_2 films deposited via PECVD on OT59 brass. *Anti-Corrosion Methods and Materials* 2005; 52(5):266-275.

[3.20] Dixon WJ, Massey Jr FJ. *Introduction to Statistical Analysis*. New York: McGraw-Hill, 1983, pp. 386-394.

[3.21] Baragetti S, Tordini F. Fatigue Resistance of PECVD Coated Steel Alloy. *Int J Fat* 2007; 29:1832-1838.

[3.22] Awad SH, Qian HC. Deposition of duplex Al_2O_3/TiN coatings on aluminium alloys for tribological applications using a combined microplasma oxidation (MPO) and arc ion plating (AIP). *Wear* 2006; 260:215-222.

[3.23] Carvalho ALM, Voorwald HJC. Influence of shot peening and hard chromium electroplating on the fatigue strength of 7050-T7451 aluminium alloy. *Int J Fat* 2007; 29:1282-1291.

[3.24] Asquith DT, Yerokhin AL, Yates JR, Matthews A. Effect of combined shot-peening and PEO treatment on fatigue life of 2024 Al alloy. *Thin Solid Films* 2006; 515:1187-1191.

[3.25] Puchi-Cabrera ES, Villalobos-Gutiérrez C, Irausquín I, La Barbera-Sosa J,

Mesmacque G. Fatigue behavior of a 7075-T6 aluminium alloy coated with an electroless Ni-P deposit. *Int J Fat* 2006; 28:1854-1866.

[3.26] Barletta M, Costanza G, Polini R. Al_2O_3 thin coating of AA 6082 T6 components using a fast regime fluidized bed. *Thin Solid Films* 2006; 515:141-151.

[3.27] Villalobos-Gutiérrez CJ, Gedler-Chacón GE, La Barbera-Sosa JG, Pineiro A, Staia MH, Lesage J, Chicot D, Mesmacque G, Puchi-Cabrera ES. Fatigue and corrosion-fatigue behavior of an AA6063-T6 aluminum alloy coated with a WC-10Co-4Cr alloy deposited by HVOF thermal spraying, *Surf Coat Technol* 2008; 202:4572-4577.

[3.28] Reiter AE, Brunner B, Ante M, Rechberger J. Investigation of several PVD coatings for blind hole tapping in austenitic stainless steel. *Surf Coat Technol* 2006; 200:5532-5541.

[3.29] Derflinger V, Brändle H, Zimmermann H. New hard/lubricant coating for dry machining. *Surf Coat Technol* 1999; 113:286-292.

[3.30] Murakawa M, Komori T, Takeuchi S, Miyoshi K. Performance of a rotating gear pair coated with an amorphous carbon film under a loss-of-lubrication condition. *Surf Coat Technol* 1999; 120-121:646-652.

[3.31] Podgornik B, Hogmark S, Sandberg O. Influence of surface roughness and coating type on the galling properties of coated forming tool steel. *Surf Coat Technol* 2004; 184:338-348.

[3.32] Harlin P, Carlsson P, Bexell U, Olsson M. Influence of surface roughness of PVD coatings on tribological performance in sliding contacts. *Surf Coat Technol* 2006; 201:4253-4259.

[3.33] Navinšek B, Panjan P, Čekada M, Quinto DT. Interface characterization of combination hard/solid lubricant coatings by specific methods. *Surf Coat Technol* 2002; 154:194-203.

[3.34] Persson K, Gåhlin R. Tribological performance of a DLC coating in combination with water-based lubricants. *Tribol Int* 2003; 36:851-855.

[3.35] Wänstrand O, Larsson M, Hedenqvist P. Mechanical and tribological evaluation of PVD WC/C coatings. *Surf Coat Technol* 1999; 111:247-254.

[3.36] Ohana T, Nakamura T, Suzuki M, Tanaka A, Koga Y. Tribological properties and

characterization of DLC films deposited by pulsed bias CVD. *Diamond Relat Mater* 2004; 13:1500-1504.

[3.37] Zhang W, Tanaka A, Wazumi K, Koga Y, Xu BS. The effect of annealing on mechanical and tribological properties of diamond-like carbon multilayer films, *Diamond Relat Mater* 2004; 13:2166-2169.

[3.38] Yamauchi N, Okamoto A, Tukahara H, Demizu K, Ueda N, Sone T, Hirose Y. Friction and wear of DLC films on 304 austenitic stainless steel in corrosive solutions. *Surf Coat Technol* 2003; 174-175:465-469.

[3.39] Baragetti S, Lusvarghi L, Bolelli G, Tordini F. Fatigue behaviour of a 2011-T6 aluminium alloy coated with PVD WC/C, CVD DLC and PECVD SiO_x coatings. Submitted to *Surf Coat Technol*.

[3.40] Bull SJ. Failure modes in scratch adhesion testing. *Surf Coat Technol* 1991; 50(1):25-32.

[3.41] Tönshoff HK, Karpuschewski B, Mohlfeld A, Seegers H. Influence of stress distribution on adhesion strength of sputtered hard coatings. *Thin Solid Films* 1998; 332(1-2):146-150.

[3.42] Baragetti S, Lusvarghi L, Pighetti Mantini F, Tordini F. Fatigue Behaviour of Notched PVD-coated Titanium Components. *Key Engineering Materials* 2007; 348-349:313-316.

[3.43] Baragetti S, Tordini F. A Numerical Study of the Fatigue Behaviour of Notched PVD-coated Ti-6Al-4V. *Structural Durability & Health Monitoring* 2007; 3(3):165-176.

[3.44] American Society for Metals. *Metals Handbook, Properties and Selection: Stainless Steels, Tool Materials and Special-Purpose Metals*, 9th ed. Metals Park, Ohio: ASM, 1980, Vol. 3, pp. 388-391.

[3.45] Wilson AD, Leyland A, Matthews A. A comparative study of the influence of plasma treatments, PVD coatings and ion implantation on the tribological performance of Ti-6Al-4V. Surf Coat Technol 1999; 114:70-80.

[3.46] Haritos GK, Nicholas T, Lanning DB. Notch size effects in HCF behavior of Ti-6Al-4V. Int J Fat 1999; 21:643-652.

[3.47] Lanning DB, Haritos GK, T Nicholas T. Influence of stress state on high cycle

fatigue of notched Ti-6Al-4V specimens. *Int J Fat* 2005; 21:S87-S95.

[3.48] Su YL, Yao SH, Wei CS, Wu CT. Evaluation on the tension and fatigue behavior of various PVD coated materials. *Thin Solid Films* 1998; 322:218-224.

[3.49] Shiozawa K, Nishino S, Handa K. The influence of applied stress ratio on fatigue strength of TiN-coated carbon-steel. *JSME Int J - Series I* 1992; 35(3):347-353.

[3.50] Baragetti S, Terranova A, Tordini F. Contact Fatigue Behaviour of PVD-coated Spur Gears. *Key Engineering Materials* 2008; 385-387:57-60.

[3.51] Baragetti S. Thin Hard-Coated Components Fatigue Resistance: Numerical Models and Experimental Validation. *Proc ISOPE* 2007; 2894-2901.

[3.52] Stewart S, Ahmed R. Rolling contact fatigue of surface coatings - A review. *Wear* 2002; 235:1132-1144.

[3.53] Šraml M, Flašker J. Computational approach to contact fatigue damage initiation analysis of gear teeth flanks. *Int J Adv Manuf Technol* 2007; 31:1066-1075.

[3.54] Glodež S, Aberšek B, Flašker J, Ren Z. Evaluation of the service life of gears in regard to surface pitting. *Engng Fract Mech* 2004; 71:429-438.

[3.55] Suresh S. *Fatigue of Materials*, 2nd ed. Cambridge: Cambridge University Press, 2004.

4 Numerical models

In this chapter the numerical and theoretical-numerical models developed to study the fatigue and the contact fatigue behaviour of both coated and uncoated specimens and components are reported. Such models were developed by considering the experimental evidence and allowed to take into account the bulk material plasticization and the residual stress field induced by surface treatments such as coating deposition or case hardening. Some of them were conceived to enable a designer to predict the number of load cycles necessary for a crack to propagate or for initial damage to occur under fatigue or (rolling) contact fatigue. With regard to gear applications, the models were applied with good results to automotive transmission spur gears.

As already mentioned, thin hard coatings deposited by means of PVD technique are used in several mechanical applications requiring, in particular, high resistance to wear and corrosion behaviour [4.1-4.7]. By contrast, few studies on the fatigue resistance of coated components are available [4.8-4.13], even though their effect can be beneficial in case of residual surface compressive stresses [4.13, 4.14] and with an uncracked and defects-free coating. For the time being, despite the high concern in light alloys of many applications such as the automotive and the aerospace ones, only few references focused on the influence of thin hard coatings on the fatigue behaviour of such materials are available. The possibility of enhancing the mechanical resistance by means of coatings would allow to enlarge the use of light alloys such as titanium ones, not only in advanced or competition applications. In order to support this issue and to interpret and enrich the experimental results, accurate numerical studies were then carried out and will be detailed in the following. Furthermore, a powerful statistical method (DACE) was used to optimize the

coating and the deposition process parameters for components subjected to rolling contact fatigue such as gears.

4.1 A theoretical-numerical procedure to study the fatigue resistance of thin hard-coated components

The need of previewing the fatigue life of components with good reliability and saving time urges to develop suitable previsional models. A theoretical-numerical procedure for fatigue life prediction of both uncoated and thin hard-coated components was then proposed aiming to provide designers with a powerful tool to predict the fatigue behaviour of such components. Good feedback was pointed out by comparing the numerical results obtained through this method with the experimental evidence [4.8-4.11]. As regards thin hard-coated components, a prediction of the number of cycles until failure can be accurately made with the introduction of the residual stress field induced by the coating deposition process into the finite element models and the hardness values in the surface layers into the calculations. The procedure makes it possible to study the fatigue crack propagation under uniaxial stress condition such as pure bending, uniform tensile loading or combined axial and bending loads. Once the initial crack depth from the external surface of a component has been known, the calculation of the stress intensity factor, including the effects from residual stresses, and the crack propagation simulation – in a discrete way – will be possible. As a result, the evaluation of the number of cycles necessary to reach specified crack depths until component failure will be possible too. To apply the model the hypothesis of absence of coating delamination from the bulk material – quite realistic, as far as the current deposition techniques are concerned – must be assumed. This means same displacements for the nodes lying on the interface surface between the coating and the base material. A commercial code can confidently be used for the finite element models and suitable mesh refinement is advisable at the cracked area only. In [4.8] the reliability of the procedure was applied with good results to foresee the fatigue crack propagation in an electroless nickel-plated steel component, whereas in [4.9-

4.11] experimental four-point bending fatigue tests on CrN-coated steel samples made of different steel materials fitted the predictions of the model very well. In the present doctoral research studies the procedure was applied to three-dimensional FE models of spur gears used in competition applications. Before reporting the results, details of the calculation method are provided.

4.1.1 Description of the previsional procedure

Proper methods for the threshold stress intensity factor range evaluation and models for describing the crack growth rate beyond the threshold were adopted in order to develop accurate finite element models able to predict the number of load cycles necessary for a certain crack to propagate. To evaluate the threshold stress intensity factor range in the presence of a crack, microstructural fracture mechanics (MFM) was adopted. In the reference [4.15] El-Haddad et al. proposed the following relationship to calculate the threshold stress intensity factor range:

$$\Delta K_{\text{th}} = \Delta K_{\text{th,Ic}} \sqrt{\frac{a}{a + a_0}} \tag{4.1}$$

where $\Delta K_{\text{th,Ic}}$ is the threshold stress intensity factor range for long cracks expressed in MPa$\sqrt{\text{m}}$, a is the actual crack depth and a_0 is given by the following equation:

$$a_0 = \left(\frac{\Delta K_{\text{th,Ic}}}{\beta \cdot \Delta \sigma_{\text{w0}}} \right)^2 \frac{1}{\pi} \tag{4.2}$$

where $\Delta\sigma_{\text{w0}}$ is the fatigue limit of the material expressed in MPa, while β a stress intensity correction factor. The parameter a_0 in equation (4.1) represents the maximum crack depth for which short cracks are influenced by microstructural barriers. If crack depths lower than a_0 are present, microstructural barriers have an influence on the ΔK_{th} value and equation (4.1) cannot be used any more. In particular, only in the case a is not higher than

$3a_0$ to $5a_0$ this relationship can be used. Murakami and Endo [4.16] proposed a different approach to calculate the threshold stress intensity factor range. It is based on the collection of experimental data for three-dimensional cracks and short cracks:

$$\Delta K_{\text{th}} = 3.3 \cdot 10^{-3} \left(\text{HV} + 120\right)\left(\sqrt{\text{Area}}\right)^{1/3} \left(\frac{1-\text{R}}{2}\right)^{\psi} \tag{4.3}$$

$$\psi = 0.226 + \text{HV} \cdot 10^{-4} \tag{4.4}$$

where HV is the material Vickers hardness, the parameter √Area may be assumed to be equal to the crack depth expressed in μm and R is the ratio between the minimum and the maximum stress of the fatigue cycle. In this case the model applicability is limited to crack lengths within the range from $3a_0$ to $10a_0$, whereas ΔK_{th} is constant if $a > 10a_0$. The following equation [4.17] can be used to calculate the crack growth rate under an MFM regime:

$$\frac{\text{d}a}{\text{d}N} = A \cdot \Delta\gamma_{\text{p}}^{\alpha} \left(d - a\right) \tag{4.5}$$

where γ_{p} is the plastic component of the shear strain, d the distance between the microstructural barriers expressed in mm, while A and α are material constants. In order to evaluate the crack growth rate beyond the threshold, the models of Paris and Erdogan [4.18] or of Elber [4.19] can be used:

$$\frac{\text{d}a}{\text{d}N} = C \cdot \Delta K_{\text{eff}}^{m} \tag{4.6}$$

where C and m are material constants and the effective stress intensity factor range ΔK_{eff} is the same as the stress intensity factor range ΔK of the well known Paris equation, whereas in the Elber's model such a parameter allows to consider also crack closure effects decreasing the stress intensity factor range. Different and more recent fatigue crack growth rate equations – derived for spur carburized gears applications [4.20-4.22] but extendible to

every hardened component – were used to apply the theoretical-numerical model discussed in this section:

$$\frac{\mathrm{d}a}{\mathrm{d}N} = \frac{C}{\left(1 - \rho^{n}\right)}\left(\Delta K^{n} - \Delta K_{\mathrm{th}}^{n}\right) \quad \text{for} \quad \Delta K_{\mathrm{th}}^{n} \le \Delta K \le K_{C} \tag{4.7}$$

$$\frac{\mathrm{d}a}{\mathrm{d}N} = \frac{C}{1 - \rho^{n}}\left(\frac{\Delta K^{n} K_{\mathrm{Ic}}}{\Delta K_{\mathrm{Ic}}^{n} - \Delta K^{n}}\right) \quad \text{for} \quad K_{C} \le \Delta K \le K_{\mathrm{Ic}} \tag{4.8}$$

The parameters included in these two equations are calculated as follows:

$$\rho = \frac{\Delta K_{\mathrm{th}}}{K_{\mathrm{Ic}}} \tag{4.9}$$

$$K_{C} = \sqrt{\Delta K_{\mathrm{th}} K_{\mathrm{Ic}}} \tag{4.10}$$

$$A = -\frac{1}{d_{2}^{2}} \ln\left(\frac{H_{1} - H_{3}}{H_{2} - H_{3}}\right) \quad \text{for} \quad d^{*} \le d_{2} \tag{4.11}$$

$$A = -\frac{1}{\left(d_{\mathrm{c}} - d_{2}\right)^{2}} \ln\left(\frac{550 - H_{3}}{H_{2} - H_{3}}\right) \quad \text{for} \quad d^{*} > d_{2} \tag{4.12}$$

$$H = \left(H_{2} - H_{3}\right) \exp\left[-A\left(d^{*} - d_{2}\right)^{2}\right] + H_{3} \tag{4.13}$$

$$\Delta K_{\mathrm{th}} = 2.45 + 3.41 \cdot 10^{-3} \cdot H \tag{4.14}$$

$$K_{\mathrm{Ic}} = 141 - 1.64 \cdot 10^{-1} \cdot H \tag{4.15}$$

$$n = 4.31 - 8.66 \cdot 10^{-3} \cdot H + 1.17 \cdot 10^{-5} \cdot H^{2} \tag{4.16}$$

$$\mathrm{Log}\left(C\right) = -10.0 + 1.09 \cdot 10^{-2} \cdot H - 1.40 \cdot 10^{-5} \cdot H^{2} \tag{4.17}$$

where d_{c} is the thickness of the coating expressed in mm, d_2 and d^* the depth, in mm, where the hardness achieves the maximum and from the external surface, respectively, K_{Ic} the material fracture toughness in MPa√m and H_1, H_2 and H_3 the surface, the maximum and the core Vickers hardness, respectively. Therefore, if the hardness profile in the coating and in the bulk material surface layers is known, equations (4.7) and (4.8) can be extended to all hardened coated materials.

By introducing the residual stress field induced by the surface treatment into the numerical models as initial condition at the integration points of the surface layers of finite elements, as well as the mechanical properties of both the coating and the base material, the stress intensity factor for a certain modeled crack can be evaluated using the half relative displacements u of the mating flanks:

$$K_I = \frac{2E}{1+\nu}\sqrt{\frac{2\pi}{r}}\frac{u}{f(\theta)} \tag{4.18}$$

where E is the Young's modulus of the material and the parameter $f(\theta)$ is calculated as follows:

$$f(\theta) = (2\chi + 1)\sin\left(\frac{\theta}{2}\right) - \sin\left(\frac{3\theta}{2}\right) \tag{4.19}$$

$$\chi = 3 - 4\nu \quad \text{for plane strain state} \tag{4.20}$$

$$\chi = \frac{3 - \nu}{1+\nu} \quad \text{for plane stress state} \tag{4.21}$$

The relative displacement of the crack flanks is measured on the nodes near the crack tip and then ΔK is determined. By comparing the stress intensity factor range for a certain crack depth with the corresponding threshold stress intensity factor range, one can infer if the crack can propagate or not. Finally, relationships (4.7) and (4.8) allow to calculate the crack growth rate in terms of load cycles necessary for a crack to propagate, from a depth to another one, until component failure. To use these two equations, the stress intensity factor range – calculated by means of FEM models for each crack depth considering both the presence of residual stresses and the geometrical configuration of the component – and the Vickers hardness trend as a function of the depth from the external surface must be known.

4.1.2 Fatigue resistance of PVD-coated steel and titanium spur gears

Transmission spur gears for motorcycle competitions were analyzed using the reported procedure with the aim of collecting new results about the possibility of enhancing the fatigue resistance of PVD thin hard-coated components. Particular attention was paid to titanium as base material. Accurate numerical models of spur gears, both coated and uncoated, were developed in order to evaluate the crack propagation in the presence of an initial defect at tooth root [4.12]. The pinion and the driven gear – constituting the fifth speed – taken into account in the analyses are included in the gearbox shown in Figure 4.1. The values of the main parameters characterizing the selected gears were: modulus equal to 2.5 mm, tooth thickness to 13 mm and number of teeth of the pinion and of the driven gear to 23 and 22, respectively. A surface roughness of 0.8 μm was measured for both the gears. A service load of 3450 N applied on the tooth flanks of the meshing gears was considered in the analyses. Figure 4.2 shows three-dimensional solid models developed for the finite element calculations.

Figure 4.1 Gearbox including the gears analyzed [4.12].

Case hardened 15NiCr13 steel alloy was the actual material of the gears and the penetration depth of the case hardening treatment was 0.7 mm. The alpha-beta Ti-6Al-4V titanium alloy annealed at 750ºC was considered as an attractive alternative base material to study. CrN and TiN were the two PVD thin hard coatings chosen for the steel and the

titanium alloy spur gears, respectively, and the coating thickness was 5 μm in both cases. The main mechanical properties of the two base materials are listed in Table 4.1, where σ_{w0} is the fatigue limit.

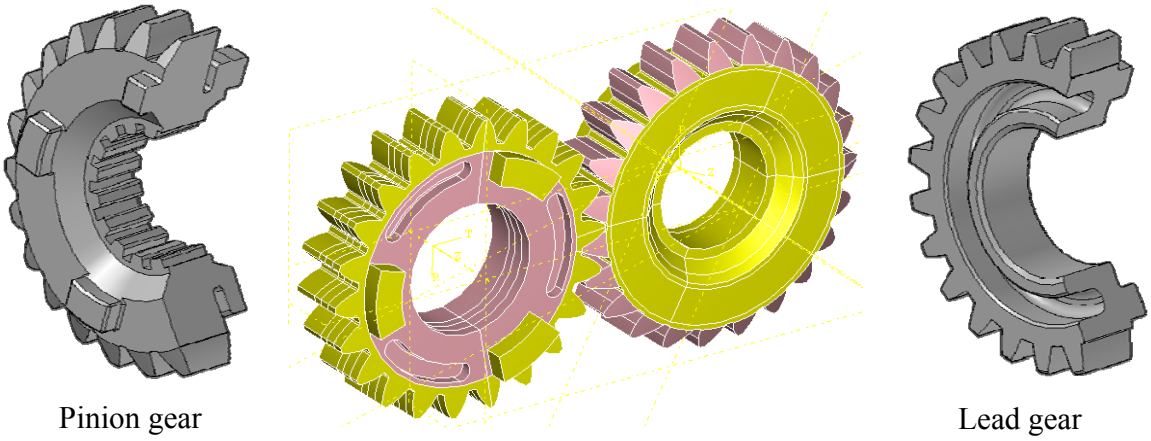

Figure 4.2 Three-dimensional pinion and driven gear models developed in [4.12].

Table 4.1 Main mechanical properties of the materials of the gears [4.12].

Material	Condition	Hardness, HV	Density, kg/m^3	*E*, MPa	*v*	A%	YS, MPa	UTS, MPa	σ_{w0}, MPa
15NiCr13	Carburized	300	7800	206000	0.28	10	883	1128	560
Ti6Al4V	Annealed	350	4500	113000	0.34	14	880	950	510

The same hardness and the same surface residual stress values were assumed in the analyses for both CrN and TiN coating, since the main goal of the research was to make a comparison between the fatigue behaviour of steel and of titanium spur gears starting from the same conditions. Furthermore, similar hardness and residual stress values can actually be shown by TiN and CrN coatings [4.23-4.26]. Therefore, a suitable surface residual stress trend and micro-hardness profile measurements in the presence of PVD CrN coatings, deposited on different steel substrates, were assumed from previous studies [4.9-4.11] and used in the calculations. Figure 4.3 shows one of the residual stress trends measured by means of X-ray diffraction in the cited references. Table 4.2 reports the hardness values – introduced into the equations – at the external surface, interface and core of both coated and uncoated steel and titanium gears.

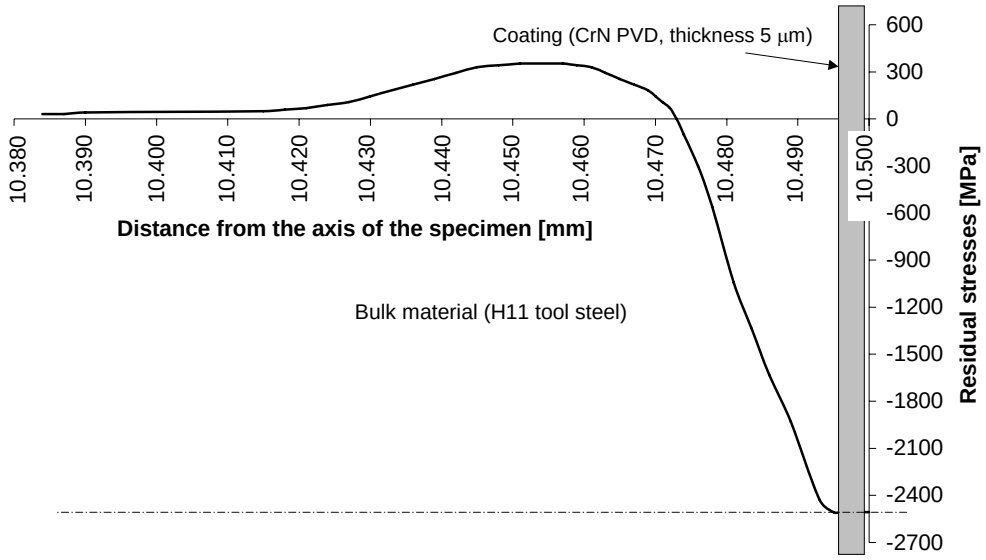

Figure 4.3 Residual stress distribution in a CrN PVD-coated steel sample with a coating thickness of 5 μm [4.10].

It is worth pointing out that the fatigue resistance of PVD-coated components is much more dependent on the residual stress values in the coating than on the stress distribution underneath [4.9, 4.10]. Therefore, the high residual compressive stress values – i.e. more than 2.4 GPa – characterizing the PVD coatings here considered make the knowledge of the trend of the residual stress field below the external surface not very important for the fatigue life prediction. As a matter of fact, the effective stress intensity factor range numerically determined at different crack depths mostly depended on the surface residual stress, since the application of different subsurface residual stress distributions did not significantly affect its value.

Table 4.2 Hardness values for the coated and the uncoated spur gears analyzed [4.12].

Material	Condition	Hardness, HV				Depth [mm] of	
		Surface	Maximum	Core	Interface	maximum hardness	interface hardness
15NiCr13	Carburized	720	760	300	550	0.2	0.5
15NiCr13	Coated	2680	2686	300	1652	0.0005	0.005
Ti-6Al-4V	Annealed	350	350	350	350	-	-
Ti-6Al-4V	Coated	2680	2686	350	1652	0.0005	0.005

The development of accurate pinion and driven gear numerical models allowed to simulate the loading condition at the base of the meshing teeth. The submodeling technique was used to simulate with good accuracy both the very low coating thickness and the presence of short cracks in the surface layers of the gear material. The mesh refinement at the crack tip was adjusted until the value of the stress intensity factor was verified not to significantly change for finite element having smaller dimensions. The value of the maximum compressive residual stress – placed at the external surface – was set at -2500 MPa for the models simulating the presence of the coating [4.10], whereas the tensile peak stress of the self-equilibrated stress distribution was placed at a depth of 0.1 mm below the external surface. The inversion point of the trend – i.e. where the residual stresses are equal to zero – was positioned at 0.04 mm underneath. The Young's modulus and the Poisson's ratio of the CrN and TiN thin hard coatings assumed in the models were, respectively, 303 GPa and 0.20 [4.10] and 600 GPa and 0.25 [4.27].

A 5 μm-deep surface crack – i.e. equal to the thickness of the coating – perpendicular to the external surface and placed at the root of the pinion meshing tooth, where the maximum bending stresses take place, was first modeled. A semi elliptical crack shape with an aspect ratio of 4:1 – i.e. the width of the crack was four times its depth – was chosen and neither the orientation of the plane on which the crack lay nor the aspect ratio were supposed to change during the propagation stage. By developing similar numerical models with cracks having greater depths, the calculation of the number of cycles necessary for a certain crack to reach the closest next depth was then allowed and a comparison, in terms of fatigue resistance, was made among the carburized steel alloy spur gear, the CrN-coated steel one and the TiN-coated titanium one. The depths of the crack modeled through the thin hard coating, perpendicular to the external surface at the root of the engaged pinion tooth, ranged from 5 to 200 μm. A hybrid non-structured mesh consisting of linear tetrahedral and hexahedral finite elements was used because of the complexity of the geometry of the spur gears. Contact elements were used on tooth flanks where the contact between the meshing teeth took place and between the crack mating surfaces to prevent them from overlapping before service load application for the presence of very high compressive residual stresses.

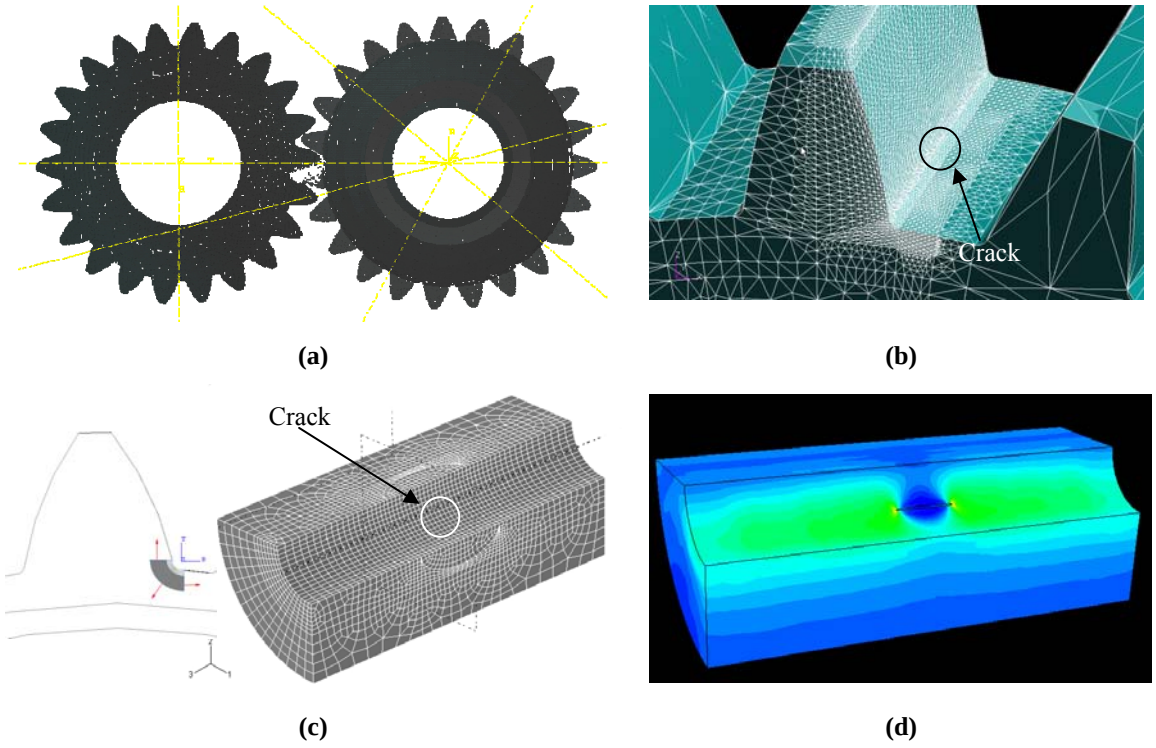

Figure 4.4 (a) Global model, (b) detail of the refined mesh at a pinion tooth root, (c) reference system and mesh of the submodel and (d) stress state around the cracked area in the submodel of one of the coated gear models [4.12].

Figures 4.4(a) and (b) show, respectively, an overview of the global model and the mesh refinement performed in the most critical areas – namely at the contact area and at the tooth root. Figures 4.4(c) and (d) show a meshed submodel and a stress contour in the same submodel after loading. A friction coefficient equal to 0.1 was adopted in the numerical models to take into account the presence of a suitable lubricant. The residual stress field induced by the coating deposition process was applied by means of the temperature gradient method, consisting of the application of a suitable temperature gradient on the element nodes from the surface to the in-depth layers so as to reproduce the desired stress profile. By assuming the plasticized area at the crack tip as limited, the base material behaviour was approximated to be linear elastic. Furthermore, this allowed to obtain conservative results for the stress intensity factor range. As already mentioned, the absence of coating-substrate delamination was assumed in the coated gear models.

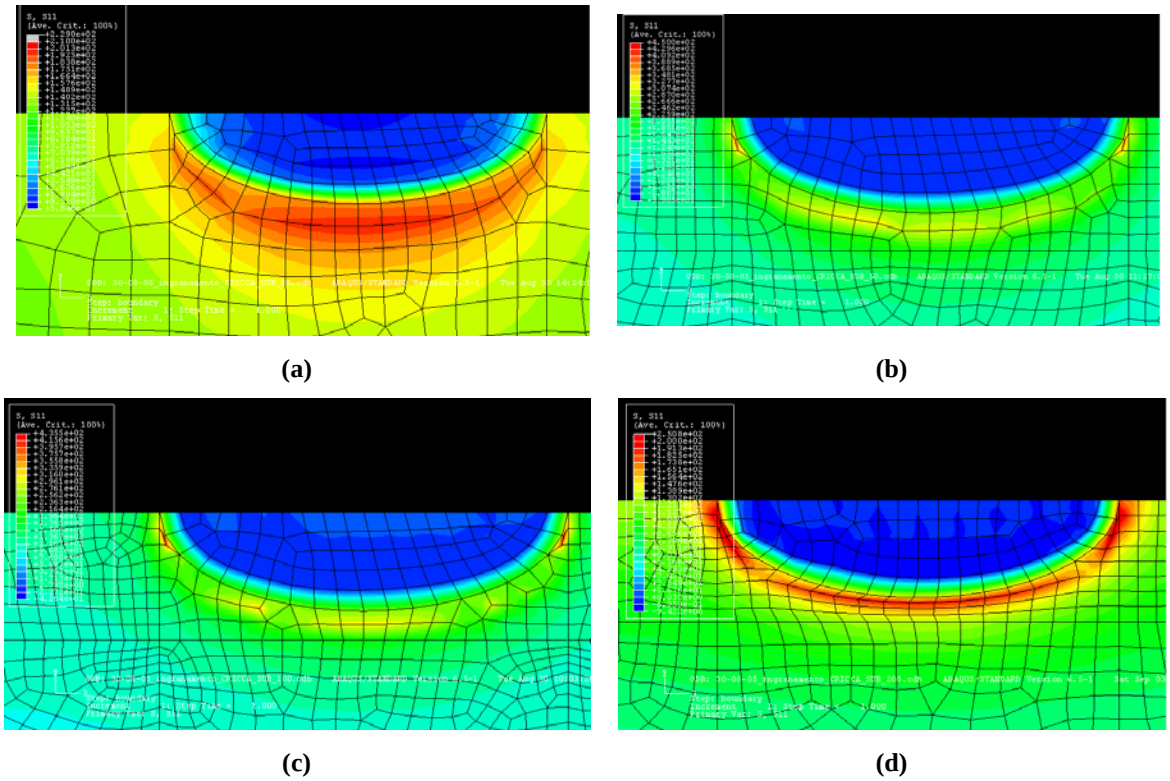

Figure 4.5 Stress contour at the crack front in the uncoated non-carburized steel gear: (a) 5-µm crack depth: ΔK_{app} = 1.86 MPa√m; (b) 50-µm: ΔK_{app} = 5.55 MPa√m; (c) 100-µm: ΔK_{app} = 6.30 MPa√m; (d) 200-µm: ΔK_{app} = 5.76 MPa√m [4.12].

Figure 4.5 shows the stress state after service load application in the uncoated non-carburized steel gear model – with the corresponding maximum values of the stress intensity factor range ΔK_{app} at the crack front reported in the caption – for different crack depths. Figure 4.6 depicts the stress state in the CrN-coated steel gear in the presence of the 100 and 200 µm-deep cracks – i.e. the deepest among the modeled ones. In particular, as regards the coated steel gear, the very high surface compressive residual stresses made it possible to observe crack opening only at depths higher than 100 µm. Table 4.3 reports the parameters, calculated with the proposed procedure, which allow to predict if crack propagation can occur at each specified crack depth for uncoated non-carburized, uncoated carburized and coated steel spur gears. One can note that in the case of untreated steel gears – i.e. both non-carburized and uncoated – only cracks having a depth lower than 5 µm cannot propagate at the applied service load. Regardless of the crack depth, among the ones analyzed, crack propagation is not expected to occur at all for the carburized uncoated

gears, whereas in the coated ones propagation could take place only with a crack depth of at least 100 μm. In fact, due to the high residual compressive stresses at the surface layers, a crack should not open until a 50-μm defect is present. Moreover, as in the carburized gears the hardened depth was greater than in the coated ones (0.5 mm for case hardening against 0.005 mm with coating deposition), despite the maximum compressive residual stresses of the carburized steel spur gears were lower than those of the coated ones, their action distributed over a deeper layer of material proved more effective in preventing crack propagation.

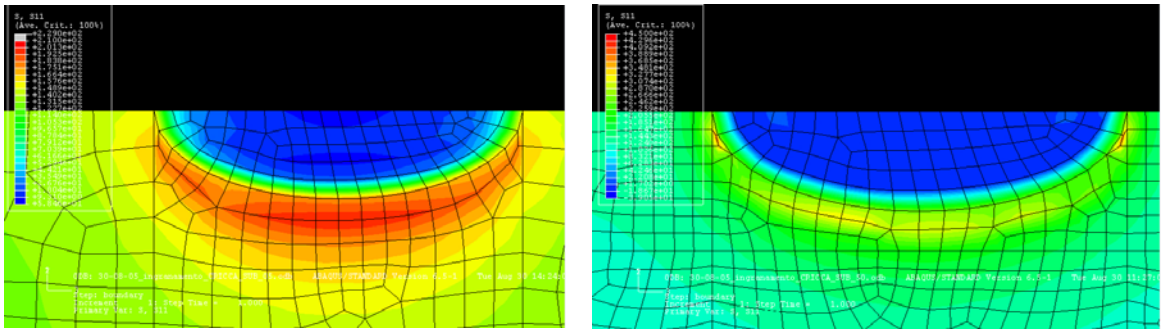

(a) **(b)**

Figure 4.6 Stress contour at the crack front in the CrN-coated steel gear: (a) 100-μm crack depth: ΔK_{app} = 5.64 MPa√m; (b) 200-μm: ΔK_{app} = 9.12 MPa√m [4.12].

Table 4.4 lists the same data reported, for the steel spur gears, in Table 4.3 for the TiN-coated titanium spur gear model and, moreover, the half relative displacement u between the crack mating surfaces and the corresponding distance r from the crack tip at which each displacement was read. A better behaviour with respect to the one of the coated steel spur gear was found, as the crack might propagate only with a defect deeper than 100 μm. Therefore, the coatings resulted to be beneficial to both steel and titanium alloy base material.

Finally, the number of cycles necessary for cracks to propagate from a specified depth to the next one for all the spur gear models analyzed are listed in Table 4.5. It is important to remark that the stress intensity factor range variation during the propagation stage was taken into account to obtain these results and, due to the fact that such a variation could not be considered with the present discrete propagation model, an average value between the

ones assumed by this parameter at each initial and final crack depth was introduced into equations (4.7) and (4.8). From the analysis of the values reported in Table 4.5 it is worth underlining that the number of cycles needed for crack growth from 100 to 200 μm for the coated titanium spur gear is remarkably higher than the one determined for the coated steel spur gear – i.e. 432220 vs. 104184 – according to the higher value of the applied stress intensity factor range for the coated steel gear with respect to the one of the coated titanium gear, namely 9.12 vs. 5.86 MPa√m. As a matter of fact, equation (4.18) confirms that the stress intensity factor range strongly depends on the elastic modulus of the base material – i.e. 206 GPa for steel and 113 GPa for titanium. A higher crack growth rate was therefore possible for the higher stress intensity factor range calculated in case of steel and so even a lower number of cycles necessary for crack propagation from 100 to 200 μm.

Table 4.3 Crack propagation predictions at specified crack depths for the uncoated non-carburized, the uncoated carburized and the coated steel spur gear. ΔK_{app} and ΔK_{th} are expressed in MPa√m [4.12].

Crack depth, μm	Non-carburized spur gear			Uncoated carburized spur gear			Coated spur gear		
	ΔK_{app}	ΔK_{th}	Propag.	ΔK_{app}	ΔK_{th}	Propag.	ΔK_{app}	ΔK_{th}	Propag.
5	1.86	2.01	No	1.86	3.87	No	0	7.62	No
25	4.32	3.44	Yes	4.32	6.24	No	0	3.44	No
50	5.55	4.34	Yes	5.55	8.05	No	0	4.34	No
100	6.30	5.46	Yes	6.30	10.55	No	5.64	5.46	Yes
200	5.76	2.99	Yes	5.76	13.73	No	9.12	3.26	Yes

Table 4.4 Crack propagation predictions at specified crack depths for the TiN-coated titanium spur gear [4.12].

Crack depth, μm	r, m	u, m	ΔK_{app}, MPa√m	ΔK_{th}, MPa√m	Propagation
5	1.09E-06	0	0	7.62	No
25	2.45E-06	0	0	3.78	No
50	1.07E-06	0	0	4.77	No
100	1.27E-06	2.89E-08	4.00	6.01	No
200	1.76E-05	1.58E-07	5.86	3.00	Yes

Table 4.5 Number of cycles to reach a 200-μm crack depth for all the spur gear models [4.12].

Crack depth, μm	Number of cycles			
	Uncoated non-carburized steel	Uncoated carburized steel	Coated steel	Coated titanium
5-25	No propagation	No propagation	No propagation	No propagation
25-50	60278	No propagation	No propagation	No propagation
50-100	86254	No propagation	49976	No propagation
100-200	106969	No propagation	104184	432220
Fatigue life	253500	-	154160	432220

4.1.3 Conclusions

The numerical results strengthened the idea that, as regards the fatigue resistance of mechanical components made of both steel and titanium alloys, thin hard coatings could be beneficial or even decisive. Also, in spite of the fact that case hardening guarantees a good effect over a greater depth than coating deposition does, coatings could really constitute an effective alternative.

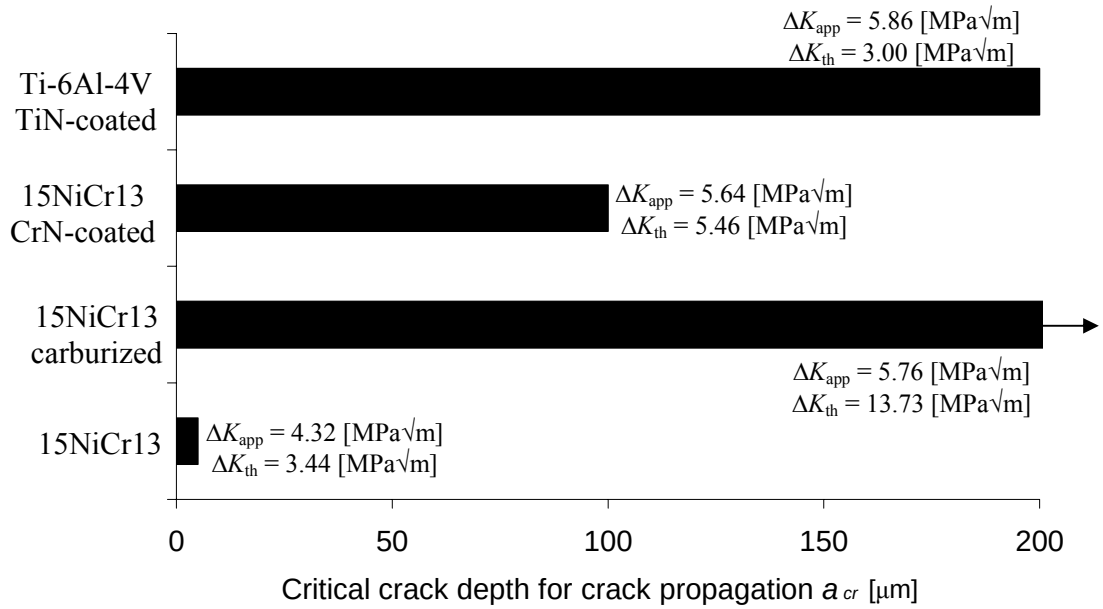

Figure 4.7 Critical crack depth for all the spur gears studied [4.12].

Figure 4.7 summarizes the results obtained by means of the reported theoretical-numerical method for all the spur gear models. It is very important to stress that the fatigue resistance of the coated titanium gear was higher than the one of the coated steel one and, moreover, it was comparable to the one of the carburized steel gear. As already stated, by using titanium alloy instead of steel as base material for gears, a considerable mass reduction would be allowed making it possible to have more power available and to reduce gas polluting emissions.

4.2 Numerical study of the fatigue behaviour of PVD-coated Ti-6Al-4V

The effect of the TiN PVD-deposited coating on the fatigue behaviour of Ti-6Al-4V titanium alloy studied through the experimental tests reported in the previous chapter was also investigated by means of numerical models. The fatigue tests were performed on coated and uncoated specimens, both smooth and with a 120° V-notch. Numerical analyses were performed in order to determine the stress distributions below the specimen surface and the stress state in the coating and to verify the influence of the variation of the coating elastic modulus on such stresses. Both the residual stress profiles induced by the coating deposition process and the plasticization of the substrate were considered and reproduced with the finite element models and the experimental results were compared with the numerical ones.

The results of this study were published on *Structural Durability & Health Monitoring*, Vol. 3, No. 3, pp. 165-176, in 2007 [4.28] and presented at the "6th International Conference on Fracture and Damage Mechanics", Madeira, Portugal, 17-19 July 2007.

4.2.1 Introduction

The Ti-6Al-4V alloy shows good fatigue behaviour and is very attractive for the low

weight-to-strength ratio. Nevertheless, its poor wear resistance often requires suitable surface treatments. The study of the influence of PVD coatings on the fatigue resistance of Ti-6Al-4V base material has not been developed enough yet. In [4.29] no significant variation in the fatigue behaviour of a TiN PA-CVD-coated titanium alloy was observed, whereas in [4.30] the influence of TiN PVD coatings on the fatigue resistance of a Ti-6Al-4V substrate was pointed out. A significant decrease in the fatigue life occurred with a coating thickness of 50 μm. This was attributed to detrimental subsurface tensile residual stresses necessary to equilibrate the compressive ones introduced in the surface layer by the deposition process. The study of the effect of the presence of notches in a Ti-6Al-4V alloy can also be important for a number of mechanical applications. The notch effect on the fatigue behaviour of the uncoated material has already been investigated [4.31-4.33] but, as far as it is known, studies on the combined effect of notches and coating have not been considered yet. Therefore, the fatigue behaviour of Ti-6Al-4V titanium alloy coated by means of a TiN PVD thin hard film was studied both experimentally (see chapter 3) and numerically. As reported in the previous chapter, rotating bending tests were carried out on both smooth and notched – coated and uncoated – specimens to evaluate the change occurring in the fatigue resistance of the coated ones [4.34].

With regard to the numerical models, several elastic-plastic FE analyses were processed to evaluate the stress distribution under the surface level of the coated specimens. The numerical results allowed the evaluation of the effect of the contemporaneous presence of residual stresses and of a notch generating stress amplification. As aforesaid, the influence of the variation of the coating elastic modulus on the stress state was also investigated through the models by choosing different values for this parameter. Moreover, the stress state data collectable with FEM models like the ones proposed could constitute a suitable input for studying the effect of internal stresses on the fatigue crack initiation at the notch tip [4.35]. Some details of the material properties and test results reported in the previous chapter, with the related comments, are recalled in the following.

4.2.2 Experimental results and discussion

Figure 4.8 shows the dimensions of the four series of hourglass-shaped specimens

machined from Ti-6Al-4V ELI ASTM F136 round bars. The 0.2 mm-deep 120° V-shaped notch – machined at the minimum cross section of one half of the specimens – is also depicted in the same figure. The material ultimate tensile strength was 895 MPa, while the yield strength was 829 MPa. A commercial TiN PVD arc-deposited coating was deposited on one half of the notched and of the smooth specimens at LAFER Spa, Piacenza, Italy, with a deposition temperature of 420°C obtaining an average thickness of 3.9 μm. Vickers microhardness (Remet HX-1000 Vickers microindenter) was evaluated on the titanium alloy bulk samples before and after the deposition to verify possible changes occurring in the mechanical properties from the heat treatment. The collected measurements suggested that no significant alterations in the substrate mechanical properties should have occurred. Rotating bending tests (R = -1) performed at a frequency of 50 Hz and at room temperature allowed to evaluate the fatigue limits at 200000 load cycles of the four series of specimens – namely smooth-uncoated, smooth-coated, notched-uncoated and notched-coated. Each test load level was set to comply with the corresponding value of the maximum bending stress at the specimen minimum cross section without notch. The fracture surfaces were analyzed by means of an SEM (FEI Quanta-200, Eindhoven, The Netherlands).

The fatigue behaviour was influenced by the presence both of the coating and of the notch: as regards the smooth specimens, fatigue limit average values of, respectively, 646 MPa for the uncoated ones and 574 MPa for the coated ones were determined, whereas in the presence of the notch the fatigue limit decreased to 327 MPa for the uncoated samples and to 281 MPa for the coated ones. Figure 4.9 shows the diagram collecting the experimental observations already reported in chapter 3. A limited difference in the fatigue behaviour between the coated and the uncoated specimens resulted from these data, as the coating produced a lowering in the average value of the fatigue limit by less than 12% for the smooth specimens and by 14% for the notched ones. Therefore, the presence of the TiN coating seemed to have a limited, but detrimental, influence on the substrate fatigue resistance. Furthermore, the similar percentages of decrease in the average fatigue limits suggested that the coating could have affected in a similar way the behaviour of the smooth and of the notched specimens.

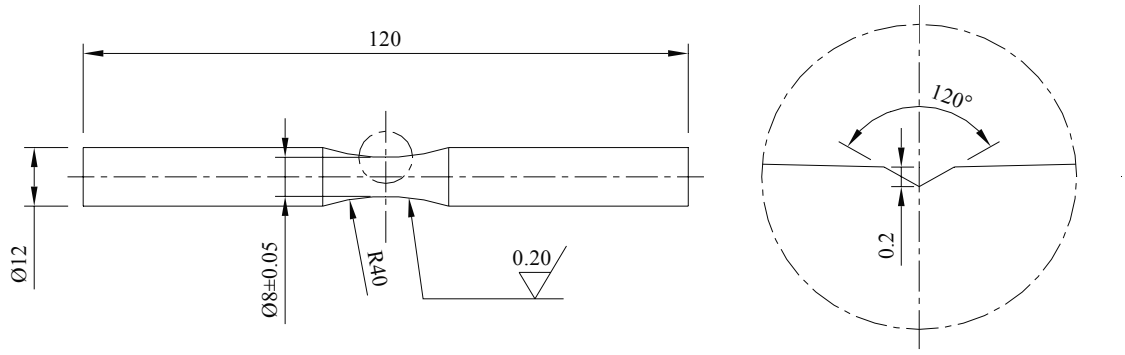

Figure 4.8 Standard specimen dimensions and a particular of the V-notch [4.28].

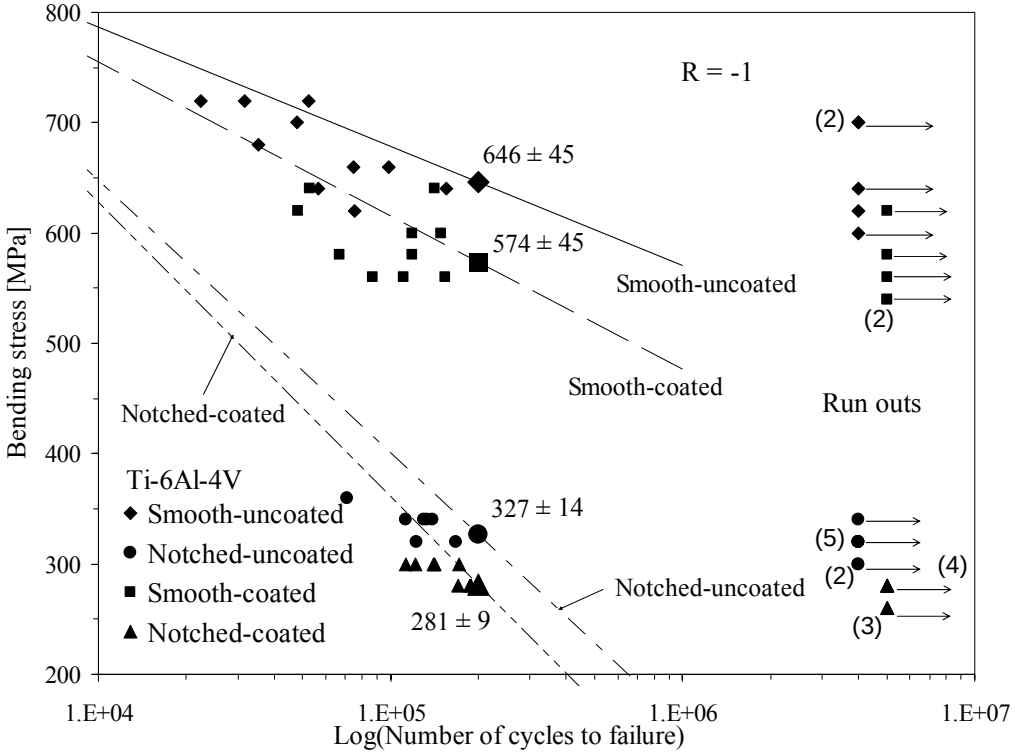

Figure 4.9 Bending stress vs. Cycles to failure diagram for the Ti-6Al-4V specimens [4.34].

4.2.3 Numerical models and discussion

The numerical evaluation of the stress distribution underneath at the minimum specimen cross section as well as the stress state in the coating was performed, in particular, to understand and interpret the experimental results. Several 3D solid models of

both the smooth and the notched specimens were then processed with the FE code ABAQUS. The submodeling technique was used for refining the calculation accuracy over the minimum specimen cross section and for specifying, by means of suitable initial conditions, the residual stress field induced by the PVD deposition process. Such a technique allows to refine the mesh by extracting a portion – i.e. a submodel – of the whole (global) model and by imposing on its boundaries the same displacements from the analysis of the global model.

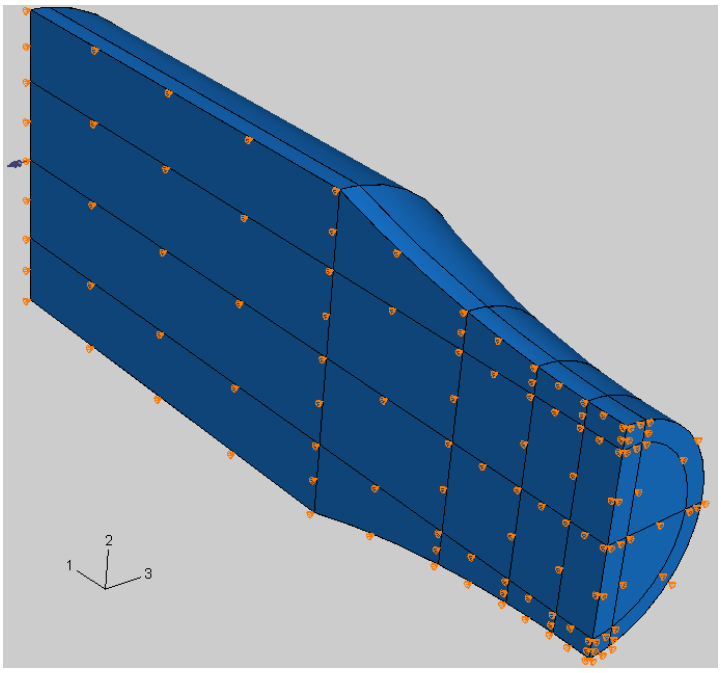

Figure 4.10 Boundary conditions and load and geometry of an FE model of a smooth specimen [4.28].

Only a quarter of the complete geometry was modelled because of the symmetry of both the specimen and the bending load. Suitable boundary conditions were imposed on the two planes of symmetry used to cut the portion of the specimen taken into account (Figure 4.10). The notch was reproduced with an adequately rounded notch tip in order to match with the corner radius of the insert used for machining. As regards the uniform bending load condition imposed along specimens in the tests, a concentrated moment applied on the neutral axis of the end free surface (left side of Figure 4.10) was used in the models. The coupling-kinematic option provided by the FE software allowed to turn the rotation produced by the moment into the corresponding translations of the nodes lying on the end

surface. The geometry of the global model of the notched-coated specimens and the embedded submodel with its location pointed at by the arrow are shown in Figure 4.11.

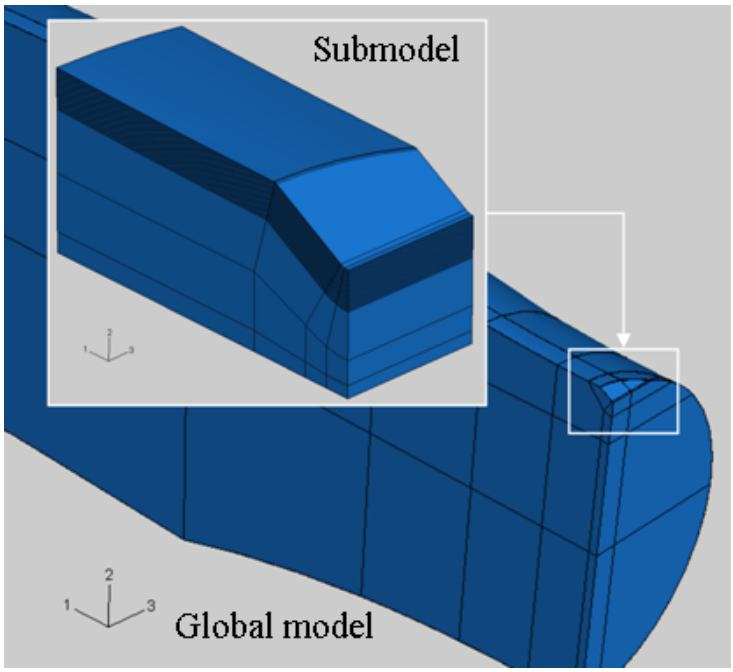

Figure 4.11 FE global model of a notched-coated specimen and particular of the related submodel [4.28].

Suitable pre-stress conditions were introduced into solid partitions, generated in the coated specimen models by offsetting the external free surface towards the in-depth layers, to impose the surface residual stress field. A higher magnification of the partitions of the submodel depicted in Figure 4.11 is shown in Figure 4.12. A proper and realistic self-equilibrated distribution of the residual stresses, similar to the earlier one used for the TiN-coated spur gear model [4.12], was assumed. It is worth recalling that the high value of the surface residual compressive stress makes it less important to know the exact trend of the residual stresses below the surface layer, as numerical simulations have demonstrated that the stress intensity factor range at different crack depths is not significantly affected by the input of different trends of residual stresses [4.9-4.11]. The high surface residual compressive stresses were reasonably assumed to be constant in the coating layer, whereas below the coating-substrate interface a steep gradient was used to drop them rapidly and reach the inversion point and the tensile peak stress. The surface residual stress in the coating was set at -2400 MPa, the inversion point was located at 0.02 mm below the

substrate surface and the maximum tensile value of 400 MPa at 0.04 mm from the same surface. Furthermore, due to the plasticization of the modeled substrate material under the combined action of the external load and the residual stresses in the areas where maximum tensile and compressive residual stresses were present, the stresses arising in the specimen plasticized areas were lower than the ones that would arise in a perfectly elastic material. Therefore, verifications of the stress self-equilibrium condition after each analysis were necessary and provided good results by comparing perfectly elastic and elastic-plastic models.

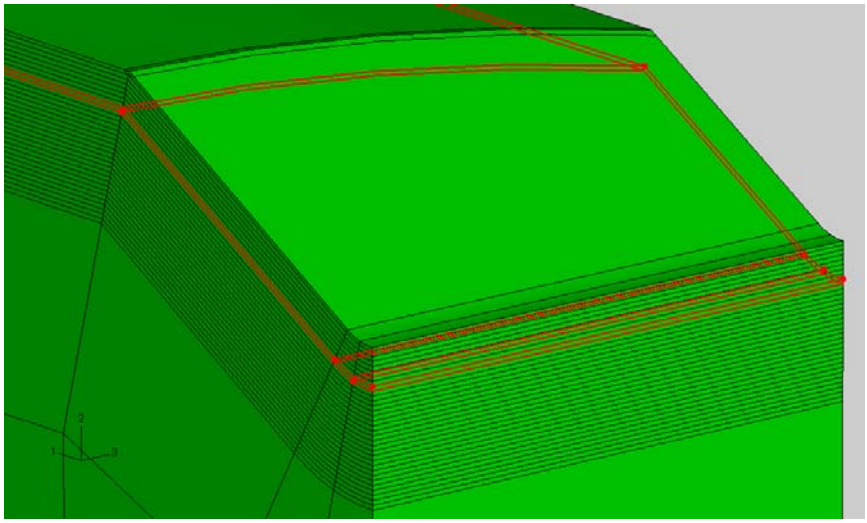

Figure 4.12 Partition in the surface layers of a notched-coated specimen submodel [4.28].

Models and submodels having more than 600000 dof were generated using eight-node C3D8 solid brick linear elements to build up the meshes. The mesh of a notched-coated specimen submodel with the visualization given by the FE code of the SS1 stress map – i.e. the stresses along the 1-direction – after loading is shown in Figure 4.13. The moment values specified in the numerical models were adjusted to produce bending stresses close to the ones occurring at the fatigue limit levels from the experimental tests on the uncoated specimens. The same bending moments were then introduced into the models for both the coated and the uncoated specimens in order to enable the comparison between the numerical results with and without the presence of the coating. Bending moments of 17 Nm for the notched specimens and of 32 Nm for the smooth ones were assumed. The bulk

material behaviour was simulated with an elastic-perfectly plastic one and the von Mises' criterion was adopted to simulate the yield condition in the analyses, whereas the coating was assumed to be perfectly elastic – with no failure criteria – to reproduce its brittle nature. Four different values of coating elastic modulus – i.e. 100, 200, 300 and 400 GPa – were investigated to verify the influence of such a parameter on the local stress state in the coating and in the bulk material. This investigation was made to evaluate the suitability of designing the best possible coating in the presence of fatigue loads and notches. The actual elastic modulus of the TiN coating analyzed should fall within the range 300-400 GPa [4.6, 4.37].

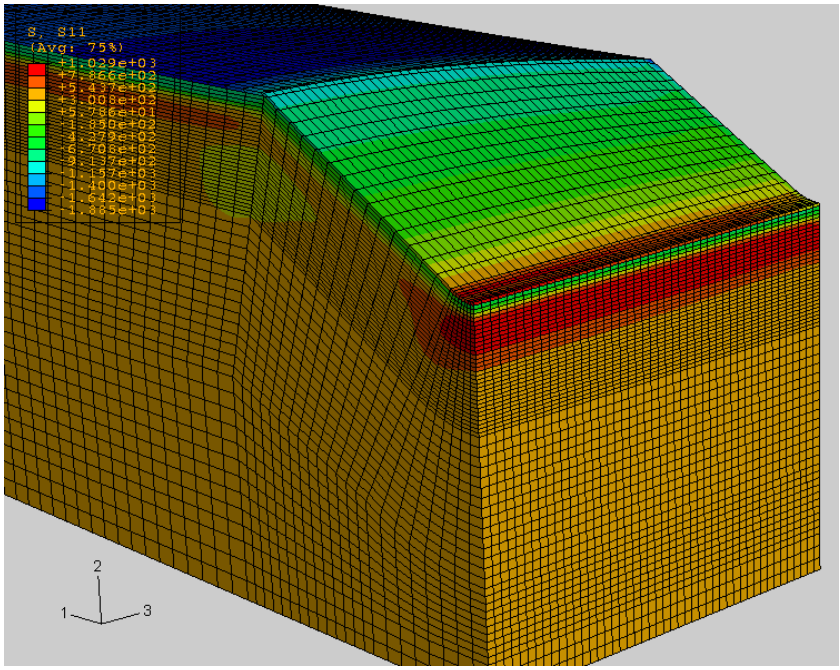

Figure 4.13 SS1 stress (MPa) map and mesh visualization in a notched-coated specimen submodel [4.28].

The main results from the FEM analyses for the smooth and the notched specimens are plotted in the diagrams shown in Figures 4.14 and 4.16, respectively, where the curves of the S11 stress component over the minimum specimen cross section are plotted vs. the depth below the external surface. The self-equilibrated residual stress profile in the unloaded condition and in the presence of the coating is also depicted on each diagram left side. Neither the highest compressive stress values nor the ones in the coating are shown in the diagrams for a better visualization. The numerical results for the smooth specimens

evidenced that each coating keeps being subjected to compressive stresses after loading, while the subsurface tensile stresses in the coated material are greater than in the uncoated one and produce a localized plasticization. Therefore, high surface compressive stresses like the ones introduced into the models would make it possible for the coating to remain under compression at the fatigue test load levels, even with the highest – and common for TiN – elastic moduli. On the other hand, the tensile stresses in the coated bulk material resulted to be higher than the ones without coating and locally approached the yield strength. Moreover, it is worth underlining that, regardless of the coating elastic modulus, the stress trends in the substrate are practically coincident and only the local stress state in the coating seems to be influenced by this parameter. Having surface compressive stresses should prevent coating from cracking and keep possible defects present before loading closed. On the contrary, the high subsurface tensile stresses – very close to the substrate surface – could justify the lowering in the fatigue limit observed for the coated specimens.

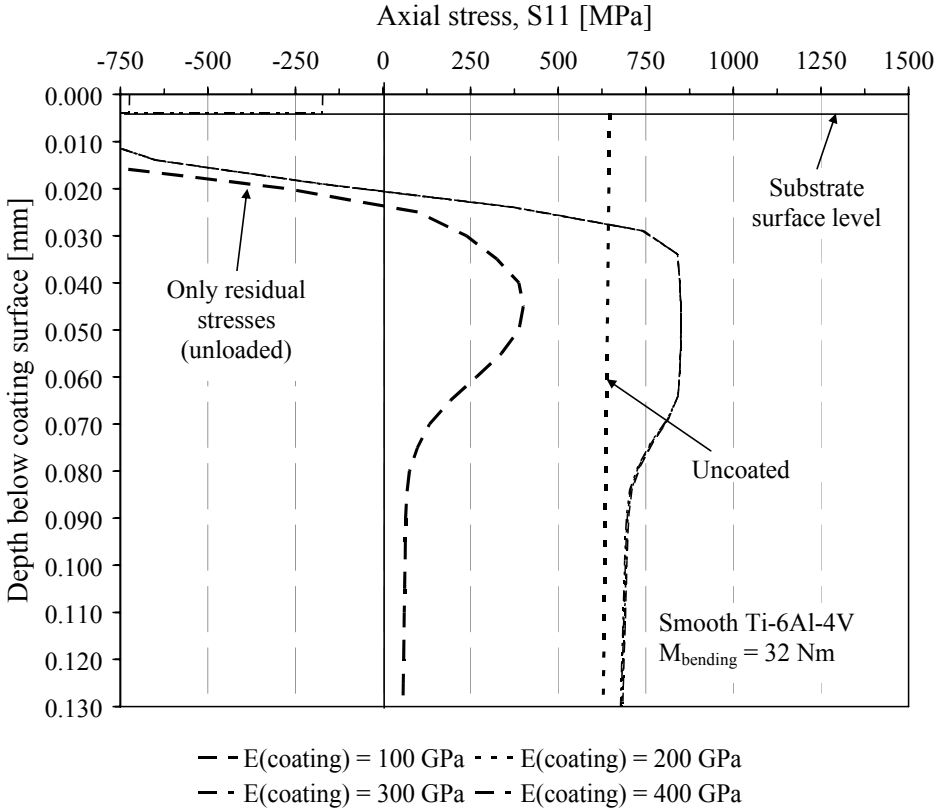

Figure 4.14 FEM results for the smooth specimens: S11 stress trends vs. depth below coating surface [4.28].

SEM micrographs of the fracture surfaces of the coated specimens confirmed that fatigue cracks initiated near and below the substrate surface level and then propagated giving rise to a net brittle fracture of the coating [4.34]. Therefore, the titanium alloy base material could have developed subsurface fatigue cracks in the area where the maximum tensile stresses took place, as pointed out with the numerical results. This behaviour could be detrimental also in case of fatigue lives exceeding 10^7 cycles [4.32], unless limiting and pushing towards the bulk material core the tensile peak stress. The superposition of the numerical stress gradient on the fracture surface of a smooth-coated specimen shown in Figure 4.15 suggests that the crack nucleation should have occurred where the calculated tensile stresses reach their maximum value (pointed at by the arrow).

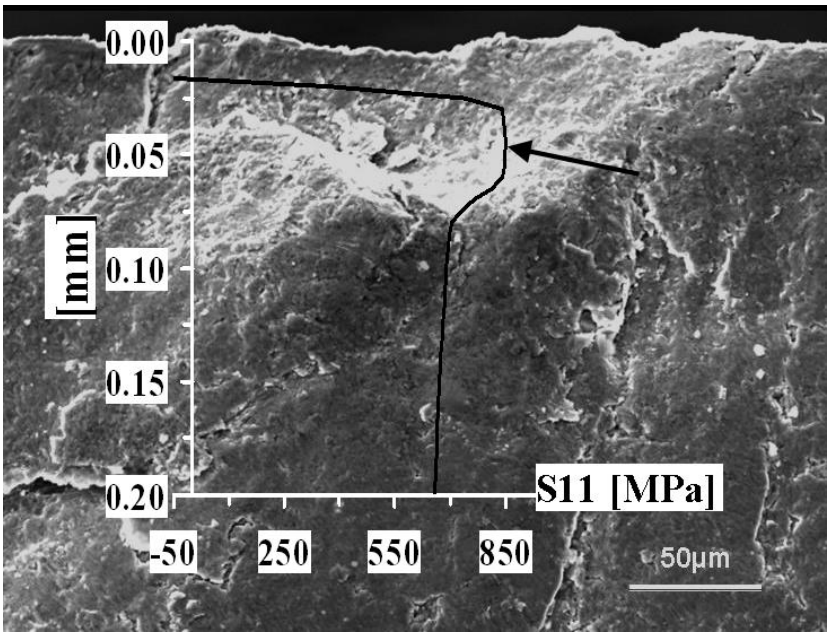

Figure 4.15 Superposition of the numerical stress gradient on a micrograph of the crack initiation site in a coated smooth specimen. The arrow points at the maximum tensile stress position in the initiation area [4.28].

Figure 4.16 summarizes the results obtained through the analyses carried out with the notched specimen models: the stress gradient of the uncoated sample is no longer linear and it is affected by the local plasticization occurring at the notch tip, whereas the trends for the substrate with different coating elastic moduli are nearly the same, analogously to the smooth specimens. In this case, the residual stresses produce a translation of the tensile peak stress below the surface level without changing its modulus. The SEM observations of

notched-coated specimen fracture surfaces showed again subsurface crack initiation in the bulk material, thus confirming the good agreement with the numerical results already noticed for the smooth specimens. The similar decrease in the fatigue resistance between smooth and notched coated specimens suggests that the position of the subsurface maximum tensile stresses could play a fundamental role in the fatigue behaviour of Ti-6Al-4V. Moreover, the stress amplification occurring at the notch tip gives rise to resultant tensile stresses in the coatings having the highest elastic moduli, even though the compressive residual stresses contribute to limit the problem. The quite high tensile stresses calculated with the 400- and 300-GPa coatings are equal to 1650 and 850 MPa, respectively, and the related computed elastic strains to 0.0022 and 0.0035. Such strain values could be close to the coating critical fracture strain [4.3, 4.38]. The stress in the coating is compressive for the elastic moduli equal to 200 and 100 GPa, showing that coatings having lower rigidity could help to prevent coating fracture under loading, provided that the residual stress distribution is similar to that of the more rigid ones.

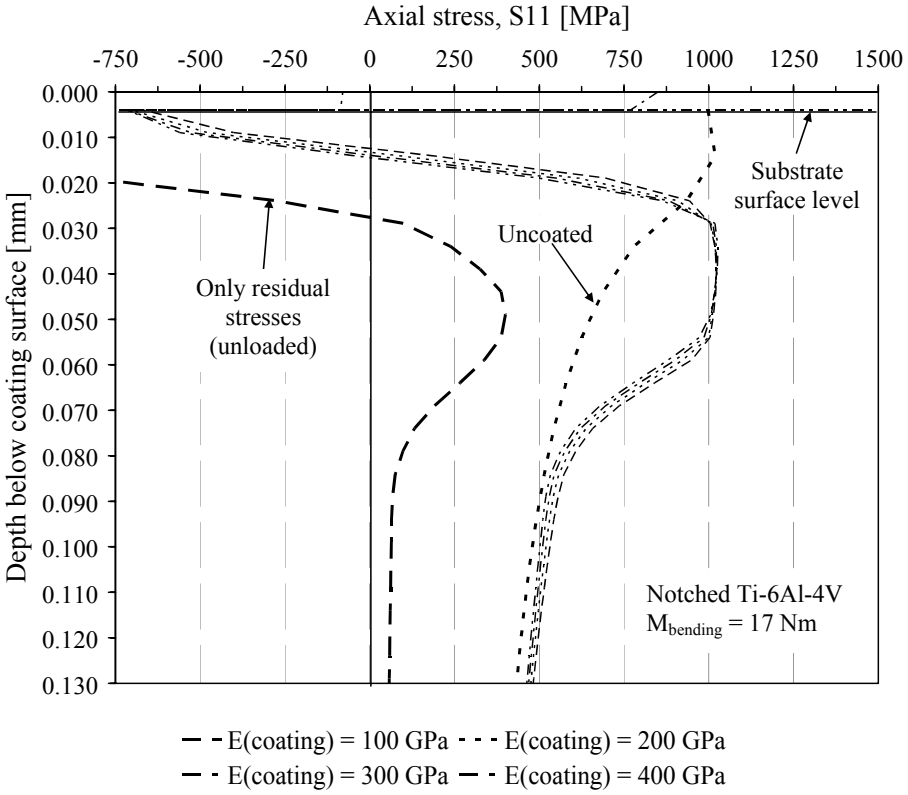

Figure 4.16 FEM results for the notched specimens: S11 stress trends vs. depth below coating surface [4.28].

The numerical results also evidenced similar stress trends between smooth and notched specimens in the bulk material after loading in the presence of the coating. On the other hand, the experimental tests pointed out that the presence of the coating was similarly detrimental – namely with similar percentages of decrease – for both the smooth and the notched specimens. The maximum tensile stresses are shifted below the surface level and generate localized plasticization for each numerical model and, due to the high surface compressive stresses which should prevent any crack nucleation in that area, an explanation for the fatigue behaviour observed with the tests could be found in the consistency between subsurface crack nucleation and the calculated resultant stress trends for both types of specimen.

4.2.4 Conclusions

The fatigue tests performed on TiN PVD-coated and uncoated, both notched and smooth, Ti-6Al-4V specimens showed that the coating was a little detrimental to the base material fatigue resistance and, furthermore, the notched and the smooth specimens had a similar reduction in the fatigue resistance – within the range 12-14%. Such behaviour was in good agreement with the finite element analyses: similar numerical resultant stress trends for both the notched-coated and the smooth-coated specimen models were obtained. The resultant tensile peak stress below the external surface could also justify the nucleation of subsurface cracks that probably occurred in the bulk material. Therefore, a remarkable benefit could be achieved with coating deposition even for notched components from the combination of the improvement in the wear resistance with a limited decrease in the fatigue behaviour.

In case of defects in the brittle TiN coating, through-thickness cracks can be easily generated. Such cracks would represent severe micro-notches for the substrate [4.38] and hence prove detrimental to its fatigue resistance. High resultant tensile stresses in the coating after loading with the highest values of coating elastic modulus – i.e. 300 and 400 GPa – were found with the numerical analyses for the notched specimens. Such stresses keep possible cracks open and make less rigid coatings be more attractive from this point of view. The resultant compressive stresses present in the softest coatings analyzed could also

prevent coating fracture from occurring. Furthermore, for fatigue lives at higher numbers of cycles – hence at lower load levels – a TiN PVD coating should be more effective, since the coating strain would be reduced – that is particularly suitable for notched components – and so even the maximum subsurface tensile stresses.

4.3 Study of the contact fatigue behaviour of coated spur gears

On top of improving surface hardness, wear, corrosion and fatigue resistance of mechanical components, as pointed out in several occasions, thin hard coatings can also be beneficial to the contact and rolling contact fatigue behaviour [4.39]. As far as it is known, there are no significant theoretical-numerical studies on the contact fatigue behaviour of PVD-coated gears considering the effect of the surface residual stresses from coating deposition and case hardening processes. Studies about the contact fatigue damage on the tooth flanks of uncoated gears are instead available [4.40, 4.41]. Models to preview the contact fatigue behaviour of coated gears were then developed and used to verify and interpret the results evidenced by the tests, reported in the previous chapter, on CrN PVD-coated spur gears made of case hardened 18NiCrMo5 steel alloy [4.42]. Several two-dimensional finite element models enabled the evaluation of the stress distribution on and below the contact surface for both coated and uncoated gears and the prediction of the number of load cycles needed for fatigue damage to appear on the tooth flanks by using the well known Coffin-Manson law [4.40]. The influence of the surface treatments on the bulk material behaviour was accurately taken into account with the models. The microscope observations carried out after the contact fatigue tests were also used in the validation of the numerical models.

The results of this study were published on *Key Engineering Materials*, Vols. 385-387, pp. 57-60, in 2008 [4.42], and presented at the "7th International Conference on Fracture and Damage Mechanics", Seoul, Korea, 9-11 September 2008.

4.3.1 Numerical models and discussion

The stress distribution on and below the contact surface for both coated and uncoated gears was numerically determined by means of the FE code ABAQUS. Several 2D models were developed and the submodeling technique was necessary to refine the calculations over the contact area. Quadrilateral CPE4 four-node bilinear plane strain elements were used to build up the meshes for the bulk material, whereas trilateral CPE3 three-node linear plane strain ones for the coating (Figure 4.17), as they evidenced better results under contact loading condition than the four-node ones. Models and submodels with more than 40000 dof were then solved at each test load level and enabled the prediction of the number of load cycles needed to fatigue damage initiation by considering a suitable cyclic softening behaviour for the base material [4.43, 4.44] and applying the Coffin-Manson equation to the numerical results [4.40]. Such a relationship between cyclic deformation amplitude and number of cycles required for fatigue damage initiation is:

$$\frac{\Delta\varepsilon}{2} = \frac{\sigma'_f}{E}\left(2N_f\right)^b + \varepsilon'_f\left(2N_f\right)^c \tag{4.22}$$

where E is the elastic modulus of the material, $\Delta\varepsilon$ the cyclic deformation amplitude, N_f the number of load cycles until initial damage, σ'_f the fatigue strength coefficient, ε'_f the fatigue ductility coefficient, b and c the strength and the fatigue ductility exponent, respectively. With regard to the 18NiCrMo5 steel alloy used as base material for the gears, the following values were used for the cited parameters: σ'_f = 1890 MPa, ε'_f = 0.848, b = -0.115 and c = -0.734 [4.43, 4.44]. A perfectly elastic material behaviour was adopted for the coating in the models, whereas an elastic-perfectly plastic one for the cylindrical roller. The surface residual stress field already used to predict the fatigue crack growth for coated gears (see earlier) was assumed to take into account the PVD process and another suitable residual stress profile was derived from the literature [4.45] to reproduce the effect of the case hardening treatment. The maximum compressive stresses at the external surface were set to -2400 MPa in the coated gear model and to -150 MPa in the uncoated one – i.e. case hardened only. The contact behaviour in the tangential direction was simulated by introducing a suitable friction factor equal to 0.5 to reproduce the unlubricated test

condition. The maximum cyclic deformations, as well as their positions over the contact area, were then determined with the numerical models.

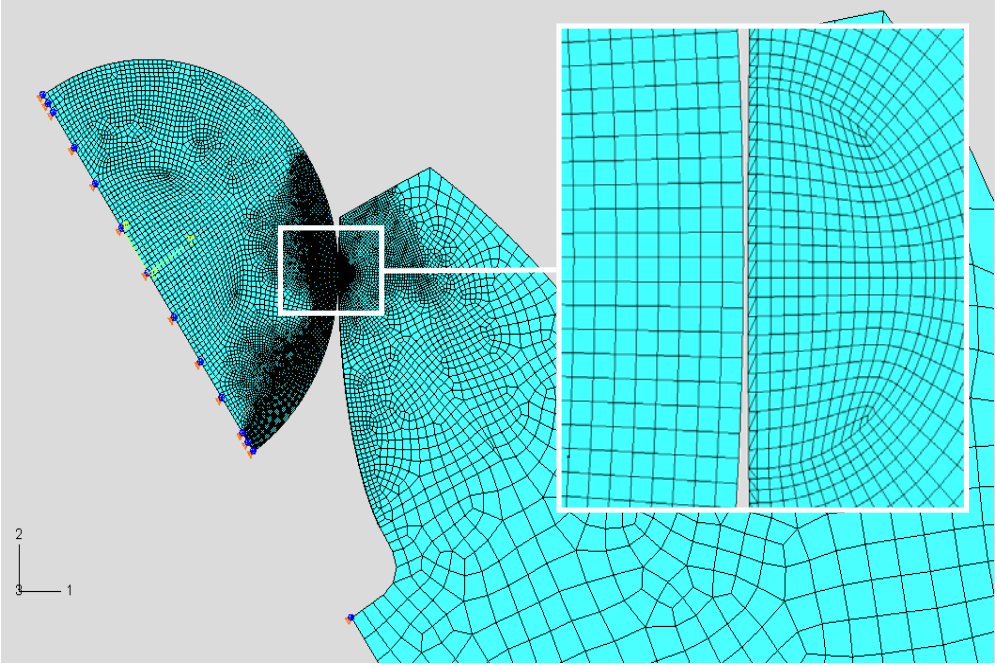

Figure 4.17 Mesh of the coated gear numerical model [4.46].

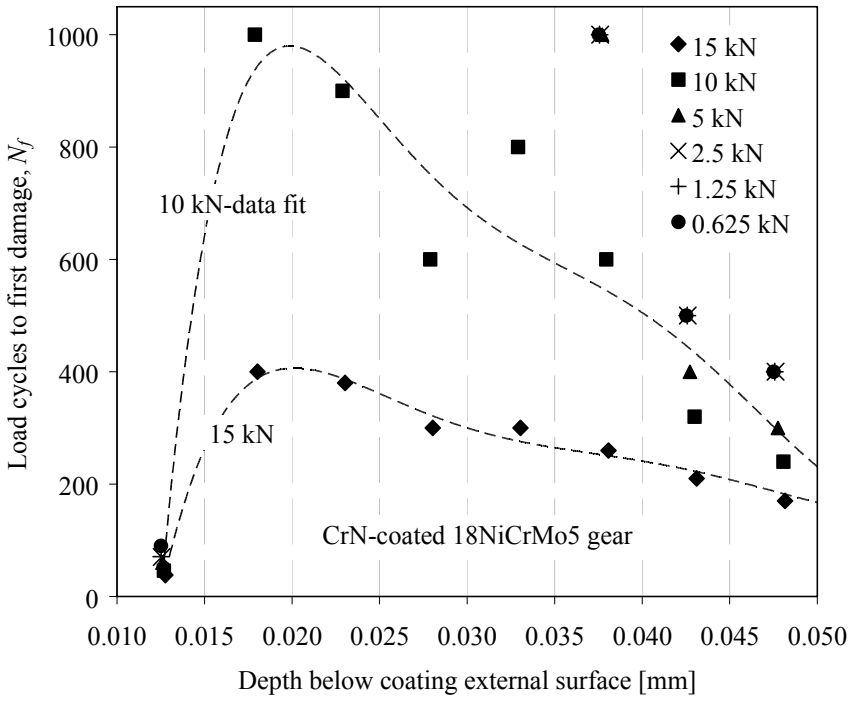

Figure 4.18 Coated gear: Load cycles until first damage vs. Depth below external surface [4.42].

The most significant results collected through the procedure are summarized in Figures 4.18 and 4.19, which show the number of cycles until first damage from the surface to the in-depth layers of the tooth, for each test load, for the coated and for the uncoated gear, respectively. The minimum value of N_f was calculated at the bulk material external surface for both the coated and the uncoated gear, showing good agreement with the test unlubricated condition. Furthermore, the number of cycles until initial damage in the uncoated gear tooth flank calculated with the load of 0.625 kN resulted greater than 10000, while at higher loads N_f was very low – namely lower than 300 – for both the coated and the uncoated gear. This was in good agreement with the experimental evidence from the contact fatigue tests (chapter 3).

4.3.2 Conclusions

A suitable theoretical-numerical procedure able to predict the number of cycles until initial contact fatigue damage in coated and uncoated gears was developed. The presence of residual stress fields induced by surface treatments was taken into account and reproduced with the models. The unsuitability for withstanding contact fatigue of the 10 μm-thick CrN PVD coating emphasized by the experimental tests (chapter 3) was confirmed using the proposed procedure. Moreover, as regards the load levels higher than 0.625 kN, both the coated and the uncoated tested gear showed damage after very low numbers of cycles and therefore confirmed the results obtained through the calculations.

The finite element analyses also showed that the maximum deformation amplitudes promoting damage initiation were at the external surface level for the uncoated gear and at the coating-bulk material interface for the coated one. This could have been due to the high friction from the unlubricated test condition. The numerical shear stress trends under the tooth flank external surface are depicted in Figures 4.20 and 4.21 for the coated and the uncoated gear, respectively. The shear stress values at the coating-substrate interface, where peaks are also achieved (Figure 4.20), and the peak values at the uncoated external surface (Figure 4.21) fitted the probable actual initial damage locations.

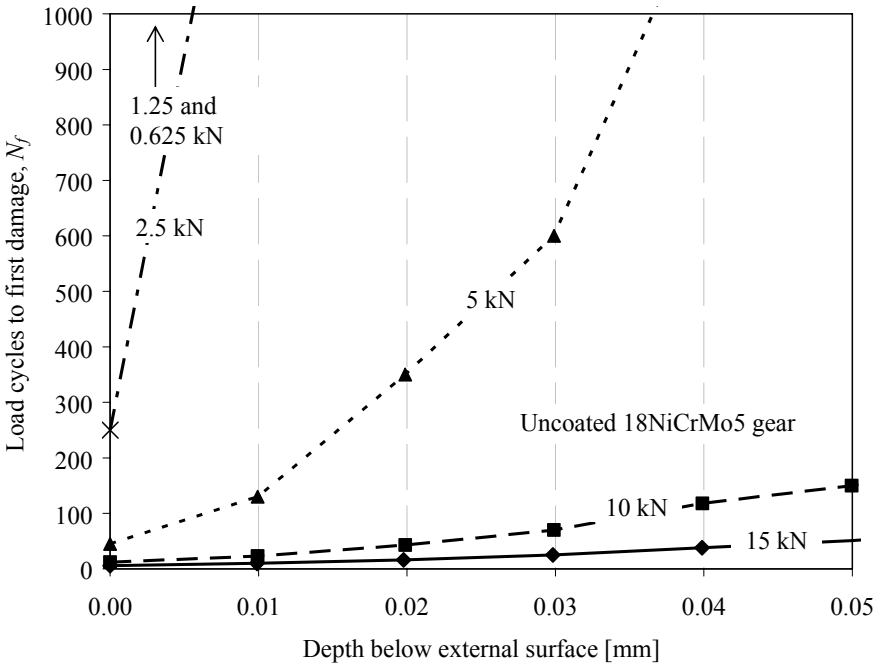

Figure 4.19 Uncoated gear: Load cycles until damage initiation vs. Depth below external surface [4.42].

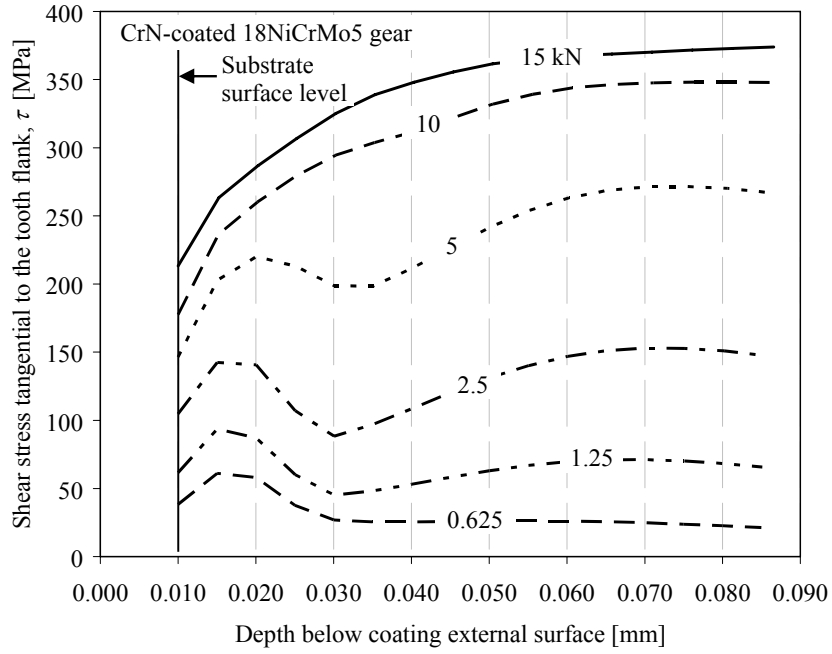

Figure 4.20 Coated gear: Shear stress vs. Depth below the external substrate surface [4.42].

The study of the influence on the contact and rolling contact fatigue behaviour of the variation of both the thickness and the elastic modulus of the coating, as well as of the

variation of the residual stress trend, constitutes a fundamental goal for further numerical analyses. The feedback from these studies could provide important guidelines for designing the best possible coating for gears or, in other words, to define the best possible characteristics which the coating should have, including the residual stress profile induced by the deposition process. Details of further studies carried out to comply with such a purpose are reported in the following section.

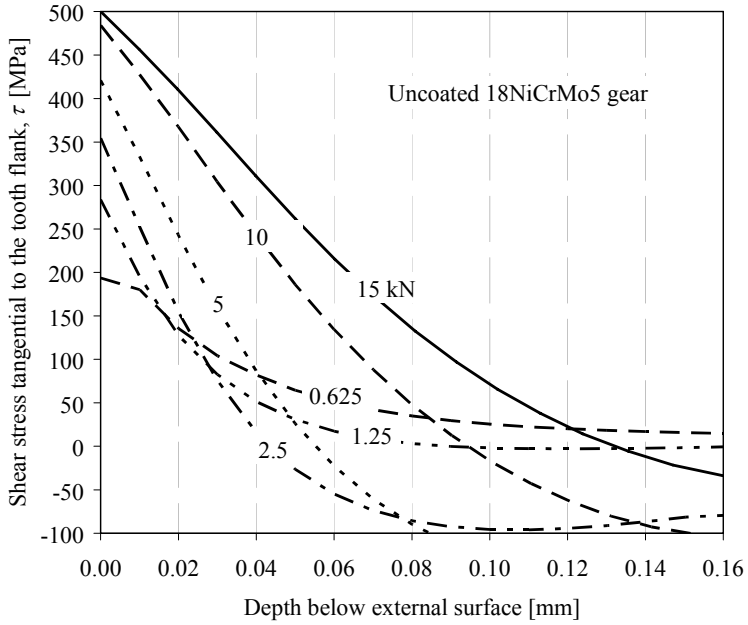

Figure 4.21 Uncoated gear: Shear stress vs. Depth below the external substrate surface [4.42].

4.4 A study of the variables affecting the fatigue and rolling contact fatigue resistance of PVD-coated spur gears

On top of the fatigue behaviour, thin hard coatings deposited with PVD technique can enhance also the contact/rolling contact fatigue resistance of mechanical components. In this section a cheap and fast procedure to evaluate the best levels of parameters characterizing coating, deposition process and bulk material is proposed. The statistical

method called Design of Experiments (DoE) was applied to the numerical results obtained through FEM models of meshing gears PVD-coated. Preliminary analyses were also performed to evaluate the fatigue behaviour of PVD-coated specimens for rotating bending tests. The same theoretical-numerical procedure explained in the previous section was used to predict the number of load cycles necessary until initial rolling contact fatigue damage. The coating elastic modulus and thickness and two parameters characterizing the trend of the residual stresses induced by the deposition process were considered among the variables affecting the fatigue and the rolling contact fatigue behaviour and different substrates, including steel, titanium and aluminium alloys, were considered. The proposed procedure could help to define the optimal coating design, especially when the replacement of traditional steels with light alloys could result in significant performance elevation.

The results of this study are were submitted for publication to the *International Journal of Fatigue* [3.47] and were presented at the "International Conference on Fatigue Damage of Structural Materials VII", Sheraton Hyannis Resort, Hyannis, Massachusetts, USA, 14-19 September 2008.

4.4.1 Introduction

As already mentioned, references dealing with the fatigue life prediction of coated components by means of suitable theoretical-numerical models are available [4.9, 4.10], but further efforts should be made to study the rolling contact fatigue behaviour of PVD-coated components such as gears. The choice of the most suitable coatings for each application is not simple and needs the assessment of the variables involving the characteristics both of the coating itself and of the bulk material. Significant systematic studies on the optimization of coating and residual stress trend parameters aiming for the maximization of the fatigue or rolling contact fatigue resistance of PVD-coated components have not been carried out yet. Bearing this consideration in mind, an advanced and powerful statistical method, namely Design of Experiments [4.48-4.52], was applied to the results obtained from three-dimensional numerical models of PVD-coated gears. Therefore, "Design of Experiments" has to be turned into "Design and Analysis of Computer Experiments" (DACE), since it is applied to numerical results. DACE made it possible to evaluate the

most attractive combination of levels assumed by the following parameters: coating thickness and elastic modulus, maximum surface compressive stress and depth below the external surface where the compressive residual stresses change into tensile. The meshing gears simulated with the numerical models are used for competitions by the Italian motorcycle racing team DUCATI CORSE srl. The procedure was also applied to models of PVD-coated standard specimens for rotating bending tests in order to find out some general feedbacks about the best combinations of levels for the variables analyzed according to the goal of improving the fatigue behaviour. Differently from the case of the meshing gears, in this case the elastic modulus of the bulk material was also considered among the variable parameters. Coating elastic moduli between 100 and 400 GPa, coating thicknesses ranging from 5 to 20 μm and steel, brass, aluminum and titanium alloy specimen base materials were considered in the analyses. Both aluminium and titanium spur gears were modeled in order to compare the traditional 16NiCr11 (UNI EN 10084) steel alloy with attractive light materials such as the Ti-6Al-4V titanium alloy and the 7075-T6 aluminium alloy. As regards Ti-6Al-4V, which is very popular in a number of applications, due to its poor wear resistance and tendency to seize when in sliding contact with itself or other metals, surface treatments such as nitriding, oxidizing or PVD coating may be necessary for enabling its use for spur gears. The cyclic behaviour of the bulk materials and the presence of the residual stress fields from coating deposition were considered and simulated with the numerical models.

To sum up, this research aimed to propose a method enabling one to design the best possible coating for a certain base material by using a powerful tool for selecting the best combination of values for the coating parameters.

4.4.2 Design and Analysis of Computer Experiments

Design and Analysis of Computer Experiments allows to manage and analyze the largest amount of numerical data about a process – a mechanical component in this case – in order to achieve its optimization in an efficient, cheap and fast way and without any need of a deep knowledge of the statistical background behind such a procedure [4.48-4.52]. By selecting parameters (variables) characterizing the process under consideration and some

levels at which they can vary, the application of this method makes it possible to choose the best combination of such levels according to a goal established at the beginning. Moreover, the application of DACE needs a very limited number of analyses (runs) out of all the possible ones. In fact, the selection of the runs is suitably arranged to take into account the whole population of possible combinations of levels. The choice of a so called "array of Taguchi" defines the series of the combinations to run. The Taguchi's $L_9(3^4)$ and $L_{16}(4^5)$ arrays were chosen for the study of the rolling contact fatigue behaviour of coated gears and of the fatigue behaviour of coated specimens, respectively. The former enables the optimization of four factors and each one has to be set at three different levels; the analysis requires only nine runs out of the possible $3^4 = 81$. Analogously, the latter enables the optimization of five factors, with each one set at four different levels, and sixteen runs have to be processed out of $4^5 = 1024$. As a result, DACE allowed to arrange and interpret suitable series of numerical results collected through FE models of the mentioned meshing gears and specimens. Some of the main parameters characterizing the coating, the residual stress profile induced by the deposition process and the base material were considered as variables in the analyses.

The following parameters were investigated for the PVD-coated specimens: coating thickness (t_{coat}) and elastic modulus (E_{coat}), base material elastic modulus (E_{bulk}); the two missing factors were not chosen so as to have two "empty columns" to verify whether parameters other than the ones first considered could be important according to another opportunity given by the method [4.51]. The levels of the parameters and the combination of such levels in each run for the coated specimens are reported in Tables 4.6 and 4.7, respectively. It is worth pointing out that the four base material elastic moduli listed in Table 4.6 were selected to reproduce steels (206 GPa), Ti-6Al-4V titanium alloy (113 GPa), aluminium alloys (70 GPa) and brass (110 GPa).

Table 4.6 Levels of the parameters chosen for the coated specimens [3.47].

Factor	Levels			
	1	2	3	4
E_{coat} [GPa]	100	200	300	400
E_{bulk} [GPa]	206	113	70	110
t_{coat} [μm]	5	10	15	20

Table 4.7 Taguchi's $L_{16}(4^5)$ array for the coated specimens [3.47].

Run no.	E_{coat}	E_{bulk}	t_{coat}	Empty 1	Empty 2
1	1	1	1	1	3
2	1	2	2	3	2
3	1	3	3	2	4
4	1	4	4	4	1
5	2	1	2	3	2
6	2	2	1	2	4
7	2	3	4	4	1
8	2	4	3	1	3
9	3	1	3	2	4
10	3	2	4	4	1
11	3	3	1	1	3
12	3	4	2	3	2
13	4	1	4	4	1
14	4	2	3	1	3
15	4	3	2	3	2
16	4	4	1	2	4

The following factors were taken into account for the gear models: coating thickness and elastic modulus, maximum residual compressive stress at the external surface ($\sigma_{res,\ sur}$), assumed to be constant in the coating, and the depth below the surface (d_{inv}) at which the compressive residual stresses turn into tensile. As a result, both the mechanical properties of the coating and the parameters determining the "shape" of the residual stress profile were supposed to be determinant variables affecting the rolling contact fatigue behaviour of coated gears. Such variables were investigated with the particular aim of pointing out guidelines defining the most advisable coating properties and residual stress profiles to induce in a coated substrate with the deposition process. No missing factors were left for empty columns in this case. Tables 4.8 and 4.9 report the array parameters with the related levels and the combination of such levels for each run, respectively. The maximum residual compressive stresses induced by coating deposition processes are fairly constant through the coating thickness and may achieve values ranging from 0.8 to 3 GPa [4.23]. Therefore, the levels for the maximum compressive stress in the coating assumed in this study are quite consistent with those ones obtainable with the current deposition technique, as well as the stress distributions underneath [4.9, 4.10]. Very thin coating thicknesses, i.e. in the

range 1-5 μm, were chosen because thicker ones would prove ineffective for rolling contact fatigue applications [4.39]. The coating Poisson's ratio was kept constant and equal to the realistic value of 0.20 [4.10]. Figure 4.22 shows an example of one of the self-equilibrated residual stress profiles assumed in the numerical models.

Table 4.8 Levels of the parameters chosen for the coated gears [3.47].

Factor	Levels		
	1	2	3
E_{coat} [GPa]	150	250	350
t_{coat} [μm]	1	3	5
$\sigma_{res,\ sur}$ [MPa]	-2500	-1750	-1000
d_{inv} [mm]	0.010	0.015	0.020

Table 4.9 Taguchi's $L_9(3^4)$ array for the coated gears [3.47].

Run no.	E_{coat}	t_{coat}	$\sigma_{res,\ sur}$	d_{inv}
1	1	1	1	1
2	1	2	2	2
3	1	3	3	3
4	2	1	2	3
5	2	2	3	1
6	2	3	1	2
7	3	1	3	2
8	3	2	1	3
9	3	3	2	1

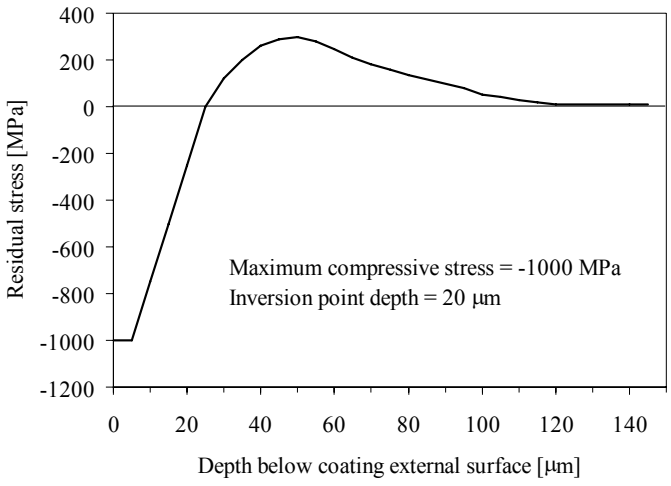

Figure 4.22 One of the residual stress trends applied in the coated gear models [3.52].

The mean square deviation (*MSD*) parameter [4.51] is a measure of the data dispersion and is used to evaluate the effects, namely the values assumed by the parameter monitored according to the goal. In this study the "smaller is better" (*S-type*) modality for the *MSD* was adopted for the coated specimens, whereas the "bigger is better" (*B-type*) one for the coated gears. In fact, the goals selected were: to minimize the maximum stress at minimum specimen cross section and to maximize the number of cycles until initial damage on gear tooth flanks. The following two equations were then used to calculate the *MSD*, depending on whether smaller is better or bigger is better modality had been adopted, respectively:

$$MSD = \frac{Y^2{}_1 + Y_2{}^2 + \ldots + Y_i^2 + \ldots + Y_n{}^2}{n} \quad \text{(smaller is better)} \tag{4.23}$$

$$MSD = \frac{\frac{1}{Y_1^2} + \frac{1}{Y_2{}^2} + \ldots + \frac{1}{Y_i^2} + \ldots + \frac{1}{Y_n{}^2}}{n} \quad \text{(bigger is better)} \tag{4.24}$$

where Y_i are the values of the effects calculated with the runs and n is the total number of samples tested in each run. Evidently, on account of the reproducibility of the numerical analyses, n was equal to 1 in this case.

Once the *MSD* has been determined, the calculation of the *S/N* ("signal to noise ratio") parameter [4.51] will be possible. It provides a measure of both the location and the dispersion of the effects as from the following equation:

$$\frac{S}{N} = -10 \cdot \mathrm{Log}(MSD) \tag{4.25}$$

Two further parameters were used, namely $(Y)'$ and $(S/N)'$, which are the mean values of, respectively, *Y* and *S/N* calculated for each single parameter assuming a certain level over the whole set of runs. The results collected by applying the previous equations allowed to evaluate the best combination of levels for the parameters investigated with the arrangement of the so called "response table". This table allows quick effect analysis by following suitable data interpretation criteria such as the rule that a parameter or a level is more significant than the others in determining the effects if its $(S/N)'$ is higher and if the

difference between maximum and minimum $(S/N)'$ for that parameter is greater than three [4.51].

4.4.3 Numerical models

In order to determine the stress and strain distributions over the minimum specimen cross section and at the contact area of the meshing tooth flanks, accurate three-dimensional models of the coated specimens and gears were developed with the finite element code ABAQUS. As usual, the hypothesis of absence of coating delamination from the base material was assumed in the models.

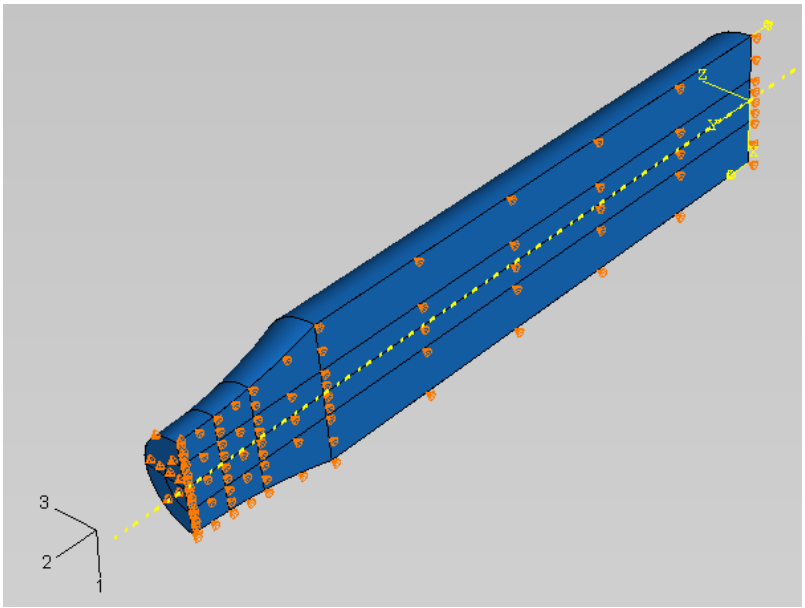

Figure 4.23 Coated specimens: geometry, boundary conditions and load application [3.47].

Standard specimens (ISO 1143) for rotating bending tests were modeled and a uniform bending load was applied to reproduce the test loading condition. The maximum axial stresses calculated over the minimum specimen cross section, as well as the stress state in the coating, were the effects monitored to apply DACE. The maximum diameter of the specimens was 12 mm, the minimum diameter over the gage length was 8 mm, the total length was 120 mm and the fillet radius of the gage length was 40 mm. Only a quarter of the whole specimen was modeled and suitable boundary conditions were imposed on the

two planes of symmetry used to cut the model to take advantage of the symmetry of both the geometry and the load (Figure 2.23). The bending load was applied by means of two concentrated forces, having the same modulus and opposite directions, positioned at the outer points of the end free surface.

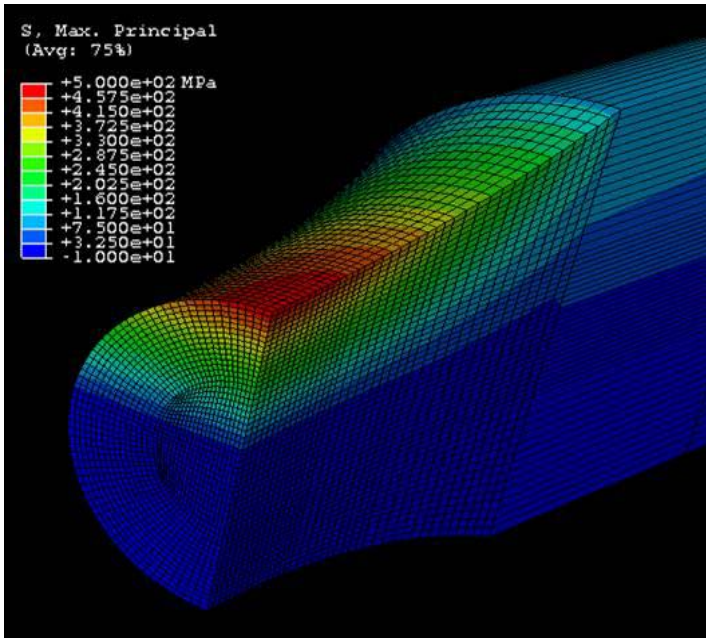

Figure 4.24 Maximum principal stress expressed in MPa and mesh visualization of a specimen model [3.47].

Suitable pre-stress conditions were assumed in the models to take into account the effect of the PVD coating deposition process over the external layers of the specimen. A realistic compressive residual stress of -2400 MPa was imposed in the coating [4.9, 4.10]. In order to limit the computational cost, no further partitions towards the in-depth layers were modeled to introduce the missing part of the self-equilibrated residual stress profile. This simplification was possible by considering the fact that, as already reminded, the fatigue resistance of PVD-coated components is mainly dependent on the residual stress value in the coating than the stress distribution underneath [4.9, 4.10]. In fact, the high residual compressive stresses – even higher than 2400 MPa in modulus – induced by the deposition of coatings such as TiN or CrN make the knowledge of the residual stress values below the external surface not very important. The load values were set to produce similar stress conditions in the different base materials to make it possible to compare the results

with one another. An elastic-perfectly plastic behaviour with a fictitious yield strength equal to 400 MPa was then assumed for all the base materials and the applied bending moment was high enough to plasticize the outer layers of the minimum specimen cross section for each substrate. Each one of the two concentrated forces generating the bending moment were then set at 1000 N and the von Mises' yield criterion was assumed. A perfectly elastic behaviour was used for the coating to comply with its brittle nature. Solid models having more than 150000 dof were generated using eight-node C3D8 solid brick linear elements to generate the meshes. The maximum principal stress map after loading for one of the models is shown in Figure 4.24.

As far as the meshing PVD-coated spur gears, the three different base materials simulated were: the 16NiCr11 (UNI EN 10084) steel alloy, the alpha-beta Ti-6Al-4V titanium alloy and the 7075-T6 aluminium alloy. The actual material of the gears analyzed, namely the pinion and the driven gear constituting the sixth speed of a DUCATI 1098 R competition motorcycle, is the first one. Due to the advantages from mass reduction, and the good results in terms of fatigue resistance which are supposed to be achievable with coated titanium spur gears (see earlier), the light alloys were studied to compare their results with the ones collected with the traditional steel. Table 4.10 lists the main properties of the three base materials.

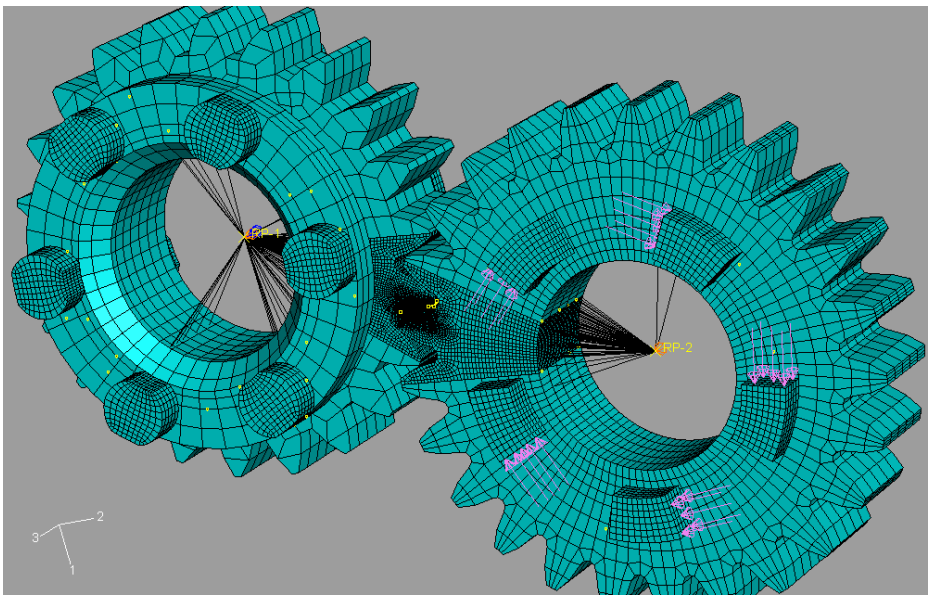

Figure 4.25 Model of the gears with the visualization of the load, boundary conditions and mesh [3.47].

Table 4.10 Main properties of the gear base materials [3.47].

Material	Density, kg/m^3	Young's modulus, MPa	Poisson's ratio	σ_Y, MPa	UTS, MPa
16NiCr11	7800	206000	0.28	785	1030-1280
Ti-6Al-4V	4500	113000	0.34	880	950
7075-T6	2810	72500	0.33	495	560

The modulus of the gears was 2.5 mm, the tooth thickness 13 mm, the number of teeth and the pitch diameter of the pinion gear were 25 and 64.89 mm, respectively, while 22 and 57.10 mm were the values of the same parameters for the driven gear. A three-dimensional FE solid model of the gears showing their geometry, the boundary conditions and how the load was applied to the pinion gear is depicted in Figure 4.25. The gears were positioned so that the contact between the meshing teeth was at the outer point of single teeth pair engagement, namely the most critical contact loading condition. To concentrate the constraints from the internal cylindrical surfaces to the corresponding reference points placed on the gear axis of rotation, the coupling-kinematic option was used (Figure 4.25). The rotation of the pinion around its axis was left unconstrained to enable the application of the service load by distributing suitable pressures, whereas the driven gear was fully constrained. A resulting torque of 244 Nm was applied in the models considering the maximum service load transmitted during a race. Tied connections were used to limit the number of degrees of freedom of the global models. Contact elements were placed over the contact area between the meshing tooth flanks of the pinion and of the driven gear and a friction coefficient equal to 0.1 was used for simulating the lubricated service condition in the case of PVD coated gears. Variations within a range of ±30% for such a coefficient should not cause any significant modification in the peak stress and strain values [4.12].

The submodeling technique was used for improving the accuracy of the calculations over the contact area of the meshing tooth flanks. The residual stress distributions defined as from the combinations included in the runs were specified in the models by using suitable pre-stress initial conditions applied to thin solid partitions generated in the surface layers. In Figure 4.26 the geometry of the submodel embedded in the driven gear global model, its location along the tooth thickness pointed at by the arrow and the solid partitions are shown. The submodel was positioned where the maximum stresses and deformations took place underneath from the numerical analyses. The realistic non-uniform distribution

of the contact load along the tooth thickness is clearly evident by looking at the equivalent von Mises' stress map in the titanium driven gear model depicted in Figure 4.27. Eight-node C3D8 solid brick linear elements were used to built up the meshes of the base material, while four-node M3D4 shell elements with membrane behaviour were chosen for the coating. Models and submodels having up to 750000 degrees of freedom were then processed.

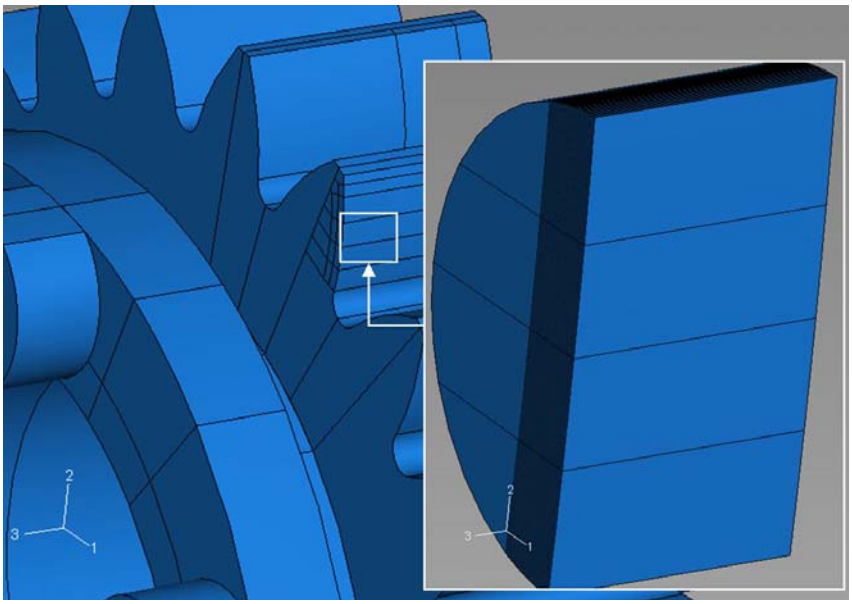

Figure 4.26 Submodel with the indication of its location and the visualization of the solid partitions [3.47].

The numerical results provided the data necessary to foresee the number of load cycles until damage initiation on the tooth flanks from rolling contact fatigue. Proper cyclic behaviours were used in the models for the base materials, namely softening ones for the 16NiCr11 steel alloy and the 7075-T6 aluminium alloy and a hardening one for the Ti-6Al-4V titanium alloy [4.43, 4.44, 4.54]. The Ramberg-Osgood equation was applied using the material parameters reported in Table 4.11:

$$\varepsilon = \frac{\sigma}{E} + \alpha \frac{\sigma_Y}{E} \left(\frac{\sigma}{\sigma_Y} \right)^{\frac{1}{n}} \tag{4.26}$$

where E and σ_Y are the elastic modulus and the yield stress of the base material,

respectively.

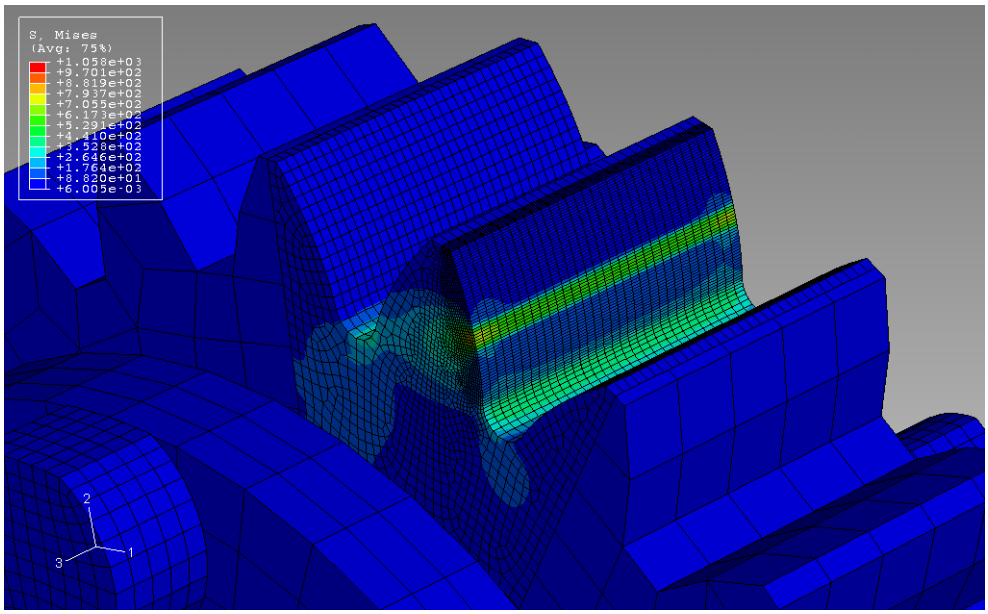

Figure 4.27 Equivalent Mises' stress (values in MPa) in a coated titanium driven gear model [3.47].

As in the previous section, the Coffin-Manson relationship (equation (4.22)) [4.40, 4.53] between deformation amplitude and number of cycles necessary for fatigue damage initiation was then applied to the numerical results to calculate the number of cycles until initial damage for the coated gears. Due to the complexity of the contact loading condition between tooth flanks involving triaxial stress and strain states, in spite of being written for uniaxial loads, the Coffin-Manson equation was used anyhow with the uniaxial strain components replaced with the equivalent von Mises' ones.

Table 4.11 Parameters of the gear base materials included in equations (4.22) and (4.26).

Parameter	Material		
	16NiCr11	Ti-6Al-4V	7075-T6
α	25	0.770	0.30
n	0.18	0.20	0.06
σ'_f	1890	2030	1466
ε'_f	0.848	0.841	0.262
b	-0.115	-0.104	-0.143
c	-0.734	0.688	-0.619

4.4.4 Results and discussion

Table 4.12 reports the best combination of levels for the specimen parameters according to the goal of minimizing the maximum stresses over the minimum cross section. Such a combination optimized the stress state both in the coating and in the base material at the interface and included the most rigid base material and the softest and thickest coating. Therefore, the analyses showed that a thick and soft coating on a steel substrate could prove effective in presence of fatigue. Apart from the coating thickness value of 20 μm, which, due to the need of preventing fracture and/or delamination, is quite unusual for the current applications, the good fatigue behaviour in presence of a soft coating could represent an important outcome for designers. In fact, provided that the residual stress profile is similar to the ones of the more rigid coatings deposited with the current PVD techniques [4.6, 4.37], a softer coating would make it possible to limit the stress values after loading, preventing itself from fracturing or delaminating [4.28]. Also, no significant variations in both $(Y)'$ and $(S/N)'$ parameters were observed, suggesting that no further influencing variables had to be considered in the analyses.

Table 4.12 Best combination for the coated specimen parameters [3.47].

Factor	Best level	Value
E_{coat} [GPa]	1	100
E_{bulk} [GPa]	1	206
t_{coat} [μm]	4	20

As regards the coated gear models, the parameter monitored for the application of DACE was the number of cycles until initial damage N_f from the external contact surface to the in-depth layers and the *B-type* modality was used. The minimum N_f calculated with the theoretical-numerical procedure was nearly the same and occurred at the same depth – i.e. 0.15 mm – below the external surface in all the runs for each one of the three gear base materials. Such a depth was below the layers where the residual stresses assume high values. As a result, it was inferred that the rolling contact fatigue behaviour could not be influenced by the presence of residual stresses from coating deposition process.

Table 4.13 Titanium gear response table: Y is the minimum N_f where there are high residual stresses [3.47].

Run no.	Y	MSD	S/N		Level	$(Y)'$	$(S/N)'$	$\Delta(S/N)'$
1	103000	9.43E-11	100.26		1	114667	101.16	
2	115000	7.56E-11	101.21	E_{coat}	2	124000	101.84	1.22
3	126000	6.30E-11	102.01		3	132333	102.38	
4	113000	7.83E-11	101.06		1	109667	100.79	
5	121000	6.83E-11	101.66	t_{coat}	2	123667	101.83	1.97
6	138000	5.25E-11	102.80		3	137667	102.76	
7	113000	7.83E-11	101.06		1	125333	101.89	
8	135000	5.49E-11	102.61	$\sigma_{res,\ sur}$	2	125667	101.91	0.338
9	149000	4.50E-11	103.46		3	120000	101.57	
					1	124333	101.79	
				d_{inv}	2	122000	101.69	0.201
					3	124667	101.89	

Table 4.14 Aluminium gear response table: Y is the minimum N_f where there are high residual stresses [3.47].

Run no.	Y	MSD	S/N		Level	$(Y)'$	$(S/N)'$	$\Delta(S/N)'$
1	2350	1.81E-07	67.42		1	2657	68.45	
2	2650	1.42E-07	68.46	E_{coat}	2	2917	69.22	1.48
3	2970	1.13E-07	69.46		3	3182	69.93	
4	2470	1.64E-07	67.85		1	2447	67.77	
5	2880	1.21E-07	69.19	t_{coat}	2	2910	69.25	2.81
6	3400	8.65E-08	70.63		3	3398	70.58	
7	2520	1.57E-07	68.03		1	2983	69.38	
8	3200	9.77E-08	70.10	$\sigma_{res,\ sur}$	2	2982	69.32	0.49
9	3825	6.84E-08	71.65		3	2790	68.89	
					1	3018	69.42	
				d_{inv}	2	2857	69.04	0.38
					3	2880	69.14	

In order to study the influence on the rolling contact fatigue behaviour of the four mentioned parameters – concerning both the coating properties and the residual stress distribution – the "local" minimum N_f in the depth range where the residual stresses assume significant values was observed. Tables 4.13, 4.14 and 4.15 list the values of this effect for all the runs and the data necessary for the evaluation of the influence of each single parameter on the effects for the three base materials. The rather low N_f values for 16NiCr11 and 7075-T6 base materials were probably due to the softening behaviour of these alloys

and to the fact that in the numerical models no hardening treatment was simulated.

Table 4.15 Steel gear response table: Y is the minimum N_f where there are high residual stresses [3.47].

Run no.	Y	MSD	S/N		Level	$(Y)'$	$(S/N)'$	$\Delta(S/N)'$
1	1670	3.59E-07	64.45		1	1733	64.77	
2	1740	3.30E-07	64.81	E_{coat}	2	1748	64.85	0.33
3	1790	3.12E-07	65.06		3	1801	65.11	
4	1703	3.45E-07	64.62		1	1700	64.61	
5	1757	3.24E-07	64.90	t_{coat}	2	1774	64.98	0.53
6	1785	3.14E-07	65.03		3	1808	65.14	
7	1728	3.35E-07	64.75		1	1760	64.91	
8	1826	3.00E-07	65.23	$\sigma_{res,\ sur}$	2	1764	64.93	0.03
9	1850	2.92E-07	65.34		3	1758	64.90	
					1	1759	64.90	
				d_{inv}	2	1751	64.86	0.11
					3	1773	64.97	

The best combination for all the models was the one of the ninth run, with the variables at the following levels: coating elastic modulus and thickness equal to 350 GPa and 5 μm, maximum compressive surface stress equal to -1750 MPa and inversion point for residual stresses located at 0.010 mm below the external surface. By means of DACE it was hence demonstrated that a thick and rigid coating could prove effective against rolling contact fatigue and that the influence of the coating parameters, i.e. thickness and elastic modulus, can be much greater than that of the residual stress parameters – especially for light materials, as from the differences in the $(S/N)'$ values reported in Tables 4.13 and 4.14. These results strengthened the idea about the negligible effects of the variation in the residual stress profile on the rolling contact fatigue behaviour of coated gears. It is also worth pointing out that a hardened substrate is advisable to support such a thick coating having at least a three times higher elastic modulus. Furthermore, fracture or delamination from contact or rolling contact fatigue can occur in the presence of the thickest coating [4.39]. Therefore, significant further efforts should be made by the current deposition technique to achieve acceptable performances for a coating having properties like the ones determined through DACE.

4.4.5 Conclusions

The objective of the study presented in this section was to investigate, with the advanced, fast and cheap DACE, the influence of certain parameters on the fatigue and the rolling contact fatigue behaviour of PVD-coated mechanical components. The developed procedure could constitute a powerful tool to define the best combination of levels for such parameters characterizing both coating and bulk material. The results showed that soft coatings, with residual stresses similar to those of the more rigid deposits available on the market, can prove effective for the fatigue resistance. The steel substrate resulted to be the best material from this point of view, even though the study reported in the first section of the chapter proved that coated titanium could show performances comparable with the ones of case hardened traditional construction steels [4.12]. With regard to the coated gears, the minimum number of cycles until initial damage was not influenced by the parameters taken into account with DACE and occurred at the same depth for all the base materials. In fact, at such a depth – namely about 0.15 mm below the external surface – the residual stresses induced by the deposition process assume negligible values. As a result, the damage from rolling contact fatigue could not be significantly affected by coating deposition processes. The analysis of the effects in the substrate surface layers, where the residual stresses are significant, showed that the best combination for retarding damage initiation on tooth flanks is the one including the thickest and most rigid coating for all the gear base materials. Furthermore, the coating elastic modulus and thickness had a high influence on the effects, particularly for the light base materials. A low influence on the results was found, instead, for the parameters characterizing the residual stress trends. The aluminium and, in particular, the titanium option could then be taken into account more and more seriously and developed with further research studies in the future. Many technological applications could take advantage from the opportunity of lowering the mass of components by using suitably coated light alloys. Also, the conflicting feedbacks in terms of coating elastic modulus between the results from the specimen and from the meshing gear models suggest that suitable compromises could be advisable for this parameter in applications requiring good resistance to both fatigue and rolling contact fatigue.

References

[4.1] Merlo AM. The contribution of surface engineering to the product performance in the automotive industry. *Surf Coat Technol* 2003; 174-175:21-26.

[4.2] Su YL, Yao SH, Wei CS, Kao WH, Wu CT. Comparison of wear, tensile, and fatigue properties of PVD coated materials. *Mater Sci Technol* 1999: 15(1):73-77.

[4.3] Su YL, Yao SH, Wei CS, Kao WH, Wu CT. Influence of single- and multilayer TiN films on the axial tension and fatigue performance of AISI 1045 steel. *Thin Solid Films* 1999:338:177-184.

[4.4] Vetter J, Barbezat G, Crummenauer J, Avissar J. Surface treatment selections for automotive applications. *Surf Coat Technol* (2005); 200:1962-1968.

[4.5] Guu YH, Hocheng H. Improvement of fatigue life of electrical discharge machined AISI D2 tool steel by TiN coating. *Mater Sci Eng* 2001; A318:155-162.

[4.6] Mendibide C, Steyer P, Fontaine J, Goudeau P. 4124 Improvement of the tribological behaviour of PVD nanostratified TiN/CrN coatings – An explanation. *Surf Coat Technol* 2006; 201:4119-4124.

[4.7] PalDey S, Deevi SC. Single layer and multilayer wear resistant coatings of (Ti,Al)N: a review. *Mater Sci Eng* 2003; A342:58-79.

[4.8] Baragetti S, La Vecchia GM, Terranova A. Analysis of fatigue crack propagation in nickel-plated components. *Int J Fat* 2001; 23:S395-S404.

[4.9] Baragetti S, La Vecchia GM, Terranova A. Fatigue behaviour and FEM modelling of thin-coated components. *Int J Fat* 2003; 25:1229-1238.

[4.10] Baragetti S, La Vecchia GM, Terranova A. Variables affecting the fatigue resistance of PVD-coated components. *Int J Fat* 2005; 27(10-12):1541-1550.

[4.11] Baragetti S, Gelfi M, La Vecchia GM, Lecis N. Fatigue resistance of CrN thin films deposited by arc evaporation process on H11 tool steel and 2205 duplex stainless steel. *Fat Fract Engng Mater Struct* 2005; 28(7):615-621.

[4.12] Baragetti S, Fatigue resistance of steel and titanium PVD coated spur gears, *Int J Fat* 2007; 29:1893-1903.

[4.13] Su YL, Yao SH, Wei CS, Wu CT, Kao WH. Evaluation on wear, tension and fatigue behaviour of various PVD coated materials. *Materials Letters* 1998; 35:255-260.

[4.14] Kim KR, Suh CM, Murakami RI, Chung CW. Effect of intrinsic properties of ceramic coatings on fatigue behaviour of Cr-Mo-V steels. *Surf Coat Technol* 2003; 171:15-23.

[4.15] El-Haddad MH, Smith KN, Topper TH. Fatigue crack propagation of short cracks. *ASME J Engng Mater Technol* 1979; 101:42-46.

[4.16] Murakami Y, Endo M. Effects of defects, inclusions and inhomogeneities on fatigue strength. *Int J Fat* 1994; 16:519-533.

[4.17] Miller KJ. The short crack problem. *Fat Fract Engng Mater Struct* 1982; 5(3):223-232.

[4.18] Paris PC, Erdogan FJ. A critical analysis of crack propagation laws. *Basic Engng* 1963; 85:528-534.

[4.19] Elber W. Fatigue crack closure under cyclic tension. *Engng Fract Mech* 1970; 2:37-45.

[4.20] Inoue K, Lyu S, Deng G, Kato M. Fracture mechanics based evaluation of the effect of the surface treatments on the strength of carburized gears. *Proc VDI Berichte* 1996; 1320:357-369.

[4.21] Inoue K, Kato M, Yamanaka M. Fatigue strength and crack growth of carburized and shot peened spur gears. *Proc Power Transmission Engineering Conf (ASME)* 1989; 663-668.

[4.22] Kato M, Deng G, Inoue K, Takatsu N. Evaluation of the strength of carburized spur gear teeth based on fracture mechanics. *JSME Int J-Series C* 1993; 36(2):233-240.

[4.23] Djouadi MA, Nouveau C, Banakh O, Sanjinés R, Lévy F, Nouet G. Stress profiles and thermal stability of Cr_xN_y films deposited by magnetron sputtering. *Surf Coat Technol* 2002; 151-152:510-514.

[4.24] Ejiri S, Sasaki T, Hirose Y. X-ray stress measurement for TiN films evaporated by PVD. *Thin Solid Films* 1997; 307:178-182.

[4.25] Murotani T, Hirose H, Sasaki T, Okazaki K. Study on stress measurement of PVD-coating layer. *Thin Solid Films* 2000; 377-378:617-620.

[4.26] Suh CM, Hwang BW, Murakami RI. Behaviours of residual stress and high-temperature fatigue life in ceramic coatings produced by PVD. *Mater Sci Engng* 2003; A343:1-7.

[4.27] Internet web site www.matweb.com.

[4.28] Baragetti S, Tordini F. A Numerical Study of the Fatigue Behaviour of Notched PVD-coated Ti-6Al-4V. *Structural Durability & Health Monitoring* 2007; 3(3):165-176.

[4.29] Wilson AD, Leyland A, Matthews A. A comparative study of the influence of plasma treatments, PVD coatings and ion implantation on the tribological performance of Ti-6Al-4V. *Surf Coat Technol* 1999; 114:70-80.

[4.30] Kolkman HJ. Effect of TiN/Ti gas turbine compressor coatings on the fatigue strength of Ti-6Al-4V base metal. *Surf Coat Technol* 1995; 72:30-36.

[4.31] Lanning DB, Haritos GK, Nicholas T. On the use of critical distance theories for the prediction of the high cycle fatigue limit stress in notched Ti-6Al-4V. *Int J Fat* 1999; 27:45-57.

[4.32] Haritos GK, Nicholas T, Lanning DB. Notch size effects in HCF behavior of Ti-6Al-4V. *Int J Fat* 1999; 21:643-652.

[4.33] Lanning DB, Haritos GK, T Nicholas T. Influence of stress state on high cycle fatigue of notched Ti-6Al-4V specimens. *Int J Fat* 2005; 21:S87-S95.

[4.34] Baragetti S, Lusvarghi L, Pighetti Mantini F, Tordini F. Fatigue Behaviour of Notched PVD-coated Titanium Components. *Key Engineering Materials* 2007; 348-349:313-316.

[4.35] Kujawski D, Stoychev S. Internal stress effects on fatigue crack initiation at notches. *Int J Fat* 2007; 29:1744-1750.

[4.36] Bemporad E, Sebastiani M, De Felicis D, Carassiti F, Valle R, Casadei F. Production and characterization of duplex coatings (HVOF and PVD) on Ti-6Al-4V substrate. *Thin Solid Films* 2006; 515:186-194.

[4.37] Puchi-Cabrera ES, Matínez F, Herrera I, Berríos JA, Dixit S, Bhat D. On the fatigue behavior of an AISI 316L stainless steel coated with a PVD TiN deposit. *Surf Coat Technol* 2004; 182:276-286.

[4.38] Shiozawa K, Nishino S, Handa K. The influence of applied stress ratio on fatigue-strength of TiN-coated carbon-steel. *JSME Int J - Series I* 1992; 35(3):347-353.

[4.39] Stewart S, Ahmed R. Rolling contact fatigue of surface coatings - A review. *Wear* 2002; 235:1132-1144.

[4.40] Šraml M, Flašker J. Computational approach to contact fatigue damage initiation analysis of gear teeth flanks. *Int J Adv Manuf Technol* 2007; 31:1066-1075.

[4.41] Glodež S, Aberšek B, Flašker J, Ren Z. Evaluation of the service life of gears in regard to surface pitting. *Engng Fract Mech* 2004; 71:429-438.

[4.42] Baragetti S, Terranova A, Tordini F. Contact Fatigue Behaviour of PVD-coated Spur Gears. *Key Engineering Materials* 2008; 385-387:57-60.

[4.43] American Society for Metals. *Metals Handbook, Properties and Selection: Stainless Steels, Tool Materials and Special-Purpose Metals*, 9th ed. Metals Park, Ohio: ASM, 1980, Vol. 3, pp. 388-391.

[4.44] Higashida Y, Burk JD, Lawrence FV. Strain-controlled fatigue behaviour of ASTM A36 and A515, grade F steels and 5083-0 aluminium weld materials. *Weld Res Suppl* 1978; 5083:334s-344s.

[4.45] MackAldener M, Olsson M. Tooth Interior Fatigue Fracture - computational and material aspects. *Int J Fat* 2001; 23:329-340.

[4.46] Baragetti S, Tordini F, Surface Treatment Effects on Bulk Material Fatigue Resistance, in: *Bulk Materials: Research, Technology and Applications* (book). NY: Nova Science Publishers; in course of publication.

[4.47] Baragetti S, Tordini F. Variables affecting the fatigue and rolling contact fatigue resistance of PVD-coated spur gears. Submitted to *Int J Fat*.

[4.48] Sacks J, Welch WJ, Mitchell TJ, Wynn HP. Design and analysis of computer experiments. *Statist Sci* 1989; 4(4):409-35.

[4.49] Currin C, Mitchell T, Morris M, Ylvisaker D. Bayesian prediction of deterministic functions, with applications to the design and analysis of computer experiments. *J Amer Statist Assoc* 1991; 86:953-963.

[4.50] Drignei D. The computational order of a DACE dynamical model. *Computational Statistics & Data Analysis* 2007; 51:3654-3665.

[4.51] Condra LW. *Reliability Improvement with Design of Experiments*. New York: Marcel Dekker Inc.; 1993.

[4.52] Montgomery DC. *Design and Analysis of Experiments*, 4th ed. New York: John Wiley & Sons; 1997.

[4.53] Salerno G, Magnabosco R, de Moura Neto C. Mean strain influence in low cycle

fatigue behaviour of AA7175-T1 aluminum alloy. *Int J Fat* 2007; 29:829-835.

[4.54] Madge JJ, Leen SB, Shipway PH. The critical role of fretting wear in the analysis of fretting fatigue. *Wear* 2007; 263:542-551.

5 Concluding remarks

In this thesis the results collected during three years of doctoral research activity are reported. These studies were conducted to understand and predict the effects of thin hard coatings deposited by means of PVD and CVD techniques on mechanical components. A wide range of different coatings and base materials were investigated with experimental, numerical and statistical methods. Base materials ranging from traditional construction steels to light alloys for advanced applications or competitions were taken into account. Particular concern was given to the fatigue and (rolling) contact fatigue behaviour of thin hard-coated specimens and components, pointing out that the surface residual stresses induced by the deposition process is supposed to represent one of the most important factors determining the enhancement (or the worsening) of the substrate fatigue resistance. The tendency of the presence of high compressive surface residual stresses of proving effective against fatigue was confirmed by the outcomes collected. In fact, such compressive stresses are expected to prevent crack nucleation and propagation both in the coating and in the base material. From this point of view, good results were observed for coated light materials such as aluminium and titanium alloys. A huge progress from lightening mechanical components in order to have more power available and less fuel consumption could then take place for many applications.

The choice of the most effective coating for each substrate is not trivial, as emphasized by the experimental evidence reported and discussed in this work. In fact, a wide range of substrate-coating combinations should be tested to determine the best solution for each application. In some cases the coating was observed to be little detrimental to the fatigue resistance of the base material, such as for 39NiCrMo3 coated with SiO_x and for Ti-6Al-4V

coated with TiN. If one considers the enhancement in the corrosion resistance or in the tribological properties which is possible in the presence of these coatings, the limited decrease in the fatigue resistance can be evaluated rather satisfying anyhow. The best results in terms of fatigue resistance were displayed by the PVD-deposited WC/C coating on 2011-T6 aluminium alloy. Experimental contact fatigue tests were also carried out on coated and uncoated transmission spur gears made of 18NiCrMo5 steel alloy with the particular aim of validating a suitable theoretical-numerical procedure developed for predicting the number of load cycles until first damage on tooth flanks. Such tests confirmed that a 10 μm-thick PVD-deposited CrN coating is unsuitable for meshing gear applications. SEM analyses also evidenced that the coating deposition may not affect the contact fatigue behaviour of the base material.

With regard to the numerical studies, accurate three-dimensional finite element models were developed to analyze and interpret the results from fatigue tests on Ti-6Al-4V specimens. The similar fatigue behaviour in the presence of the TiN PVD coating between notched and smooth specimen was studied numerically with good outcomes and the influence of the variation of the coating elastic modulus was considered too. Soft coatings resulted to be more effective with respect to the fatigue resistance. Furthermore, a suitable and reliable theoretical-numerical procedure was developed to evaluate the number of cycles until failure for coated components by simulating discrete crack propagation. This procedure was applied to models of PVD-coated transmission spur gears for high speed racing motorcycles and allowed to point out that PVD thin hard coatings can prove effective in enhancing the fatigue resistance of both steel and titanium gears. Also, the fatigue resistance of the coated titanium gear was higher than the one of the coated steel gear and comparable with the one of the carburized (uncoated) steel gear. Therefore, the use of suitably coated titanium instead of steel for gears could be advisable and would enable considerable mass reduction. During the doctoral researches, several FE models of gears were developed and enabled the definition of a procedure able to predict the number of cycles necessary to damage initiation on tooth flanks under rolling contact fatigue. Such a procedure provided results in good agreement with the experimental contact fatigue tests previously mentioned. The advanced, fast and cheap statistical DACE method was also used to study variables supposed to affect the fatigue and the rolling contact fatigue

behaviour of PVD-coated components. As far as the fatigue resistance is concerned, the analyses showed that soft coatings could prove effective. The study of the rolling contact fatigue behaviour of coated gears confirmed that the damage could not be significantly affected by the coating deposition process. By applying DACE the best combination of variable levels for retarding damage in the substrate layers characterized by the presence of high residual stresses was the one including the thickest and most rigid coating for all the base materials studied. Furthermore, the parameters related to the coating – i.e. elastic modulus and thickness – had a higher influence on the results than the one of the parameters related to the residual stress trends, particularly in case of light base materials. The conflicting results for the coating elastic modulus between the analyses on specimens and on meshing gears suggest that suitable compromises may be advisable for this parameter in applications requiring good resistance to both fatigue and rolling contact fatigue. The proposed procedures could constitute powerful tools and provide useful guidelines for designers in order to define the best combination of property levels for coatings and bulk materials and to foresee the service life of components.